AFOSR TR—80—0441

UILU-ENG-80-2540

# LEVEL

## OPTICALLY PUMPED FAR INFRARED MOLECULAR LASERS

ADA086495

Paul D. Coleman
Electro-Physics Laboratory
Electrical Engineering Department
University of Illinois
Urbana, Illinois 61801

DTIC
ELECTE
JUL 7 1980

C

Final Report for the Period
1 Feb 76 - 31 Jan 80
Grant AFOSR-76-2988

2301

A1

Approved for public release; distribution unlimited

April 1980

138

DDC FILE COPY

80 7 2 109

| REPORT DOCUMENTATION PAGE | READ INSTRUCTIONS BEFORE COMPLETING FORM |
|---|---|

| 1. REPORT NUMBER AFOSR-TR- 80-0441 | 2. GOVT ACCESSION NO. AD-A086495 | 3. RECIPIENT'S CATALOG NUMBER |
|---|---|---|

| 4. TITLE (and Subtitle) OPTICALLY PUMPED FAR INFRARED MOLECULAR LASERS | 5. TYPE OF REPORT & PERIOD COVERED Final 2-1-76/1-31-80 |
|---|---|
| | 6. PERFORMING ORG. REPORT NUMBER UILU-ENG-80-2540 |

| 7. AUTHOR(s) Paul D. Coleman | 8. CONTRACT OR GRANT NUMBER(s) AFOSR 76-2988 |
|---|---|

| 9. PERFORMING ORGANIZATION NAME AND ADDRESS Electrical Engineering Department University of Illinois Urbana, Illinois 61801 | 10. PROGRAM ELEMENT, PROJECT, TASK AREA & WORK UNIT NUMBERS 61102F 2301-A1 |
|---|---|

| 11. CONTROLLING OFFICE NAME AND ADDRESS AFOSR/NP Building 410, Bolling Air Force Base Washington, D.C. 20332 | 12. REPORT DATE April 1980 |
|---|---|
| | 13. NUMBER OF PAGES 136 |

| 14. MONITORING AGENCY NAME & ADDRESS(If different from Controlling Office) | 15. SECURITY CLASS. (of this report) Unclassified |
|---|---|
| | 15a. DECLASSIFICATION/DOWNGRADING SCHEDULE |

16. DISTRIBUTION STATEMENT (of this Report)

Approved for public release; distribution unlimited.

17. DISTRIBUTION STATEMENT (of the abstract entered in Block 20, if different from Report)

18. SUPPLEMENTARY NOTES

19. KEY WORDS (Continue on reverse side if necessary and identify by block number)

Optically Pumped FIR Lasers
Molecular Gas Lasers
Far IR Technology
Density Matrix Laser Analysis

20. ABSTRACT (Continue on reverse side if necessary and identify by block number)

This report summarizes studies on optically pumped far infrared molecular gas lasers for the period 1 February 1976 to 31 January 1980 with detailed descriptions of work done during the period 1 February 1979 to 31 January 1980. The research has been concerned with the general subjects of far infrared integrated optics and technology, the discovery of new optically

DD FORM 1473 1 JAN 73    EDITION OF 1 NOV 68 IS OBSOLETE

pumped molecular laser systems, and the study and analysis of nonlinear processes (Raman and hyper-Raman) that can occur in optically pumped systems.

The theoretical density matrix analysis of the gain spectra of nonlinear systems and the first detailed experimental measurements of these systems are presented. It is demonstrated that third and fifth order nonlinear processes can exceed first order laser processes.

An experimental study of the generation of a 22.653 GHz signal (the largest wavelength yet reported) in optically pumped $NH_3$ is described. The frequency tunability and single shot spectral characteristics of the signal were measured with precision.

A single laser pump in a four-level system can yield two laser signals, which in the linear case are not coupled together. However, with stronger pumping, nonlinear effects can couple the two laser signals with the result that the behavior of one laser signal is determined by the other and vice versa. The self-consistent analysis of this problem is described.

# TABLE OF CONTENTS

# OPTICALLY PUMPED FAR INFRARED MOLECULAR LASERS

## I. INTRODUCTION - P. D. Coleman

The objective of grant AFOSR 76-2988 was the study of optically pumped far infrared molecular lasers, including nonlinear Raman and hyper-Raman processes, and associated technology.

The waveglength range from approximately 20 to 1,000 μm remains an unsolved coherent source problem with respect to prime, practical sources. There are no counterparts in the far infrared of devices like IMPATTs, magnetrons, laser diodes, gyrotrons, etc.

While in principle, megavolt electronics sources like free electron lasers, can reach into the far IR, and tubes like the carcinotron can be extended to around 1,000 GHz, the only proven, high spectral quality, modest technology, coherent source available to all researchers in the area, is the optically pumped molecular gas laser. Its one flaw is that it is not a prime source, but a frequency translator in that it is a laser pumped laser, subject to the Manley-Rowe restriction.

As a quantum system, molecules are ideal in that they possess all of the far infrared frequencies of interest. The problem is that it has not been discovered how to efficiently excite them from a DC energy source.

In spite of the Manley-Rowe limitations, the optically pumped molecular gas laser has done more by far than any other

2

device in opening the far IR region for development and
practical application.  It was the aim of this grant to con-
tribute to this development.

II.  SUMMARY OF ACCOMPLISHMENTS - P. D. Coleman

The research accomplishments of this grant were associated with four topics:

1)  Far infrared integrated optics

2)  Far infrared technology

3)  New optically pumped systems

4)  Nonlinear studies and analysis

One of the first achievements of the grant was the first demonstration of waveguide propagation in single crystal ($\alpha-SiO_2$) quartz waveguide in the far IR ($\lambda=496.1\mu m$), the evaluation of waveguide attenuation, prism and grating couplers.  This work was documented in the annual grant reports, the IEEE Journal of Quantum Electronics paper, "Far IR Guided Wave Optics Experiments with Anisotropic Crystal Quartz Waveguides", in May 1977 and the Ph.D. thesis of E. J. Danielewicz.  This study identified and solved a number of the problems unique to integrated optics in the far IR.

In the area of far infrared technology, the specific accomplishments were:

1)  Study and evaluation of the optical properties of materials useful in the far IR,

2)  Analysis of prism and grating couplers for far IR dielectric waveguides,

3)  First use of metal-mesh hybrid mirrors for output couplers for far IR resonators,

4

4)  The first demonstrated use of capillary, dielectric
tube waveguides for high power, optical pumping of nonlinear
systems,

5)  The first designs of triple resonant (IR-FIW-MW) re-
sonators for optically pumped systems,

6)  Development of laboratory built $CO_2$ pump lasers with
output capabilities to 5 joules,

7)  Contributor to the use of SAW-RAC devices for the
single shot spectral measurement of far IR lasers,

8)  Optically pumped molecular lasers at 22.65 GHz.

In the area of new optically pumped systems, lasing was
discovered in $PH_3$ and all lasing lines assigned, hot band lasing
in $NH_3$ extended and explored, and the first lasing line assign-
ment in the important molecule $CH_3OH$ made in December 1976.

For the past two years (1978-80), extensive work has been
pursued of high level, *two-photon pumping* of molecular gases
to evaluate nonlinear behavior (Raman, hyper-Raman, para-
metric) of the system.  This has been a combination experiment-
analytical study of the quantum systems.

Computer programming of the density matrix equations for
three- and four-level systems, has permitted the evaluation
of highly nonlinear gain spectra of optically pumped molecular
gases on a short time and modest cost scale.  Given the basic
spectroscopic molecular data, most of the far IR molecular
laser systems can now be readily analyzed in detail  An

experimental verfication of calculations made on $NH_3$ has been made. This work has been documented in two papers, "Stimulated Hyper-Raman Scattering in a Molecular Gas", IEEE J. Quan. Electron., March 1980, and "Gain/Absorption Spectra of Several Optically Pumped $NH_3$ Systems", to appear in IEEE J. Quan. Electron., and the Ph.D. thesis of K. J. Kim.

III.  CALCULATED-EXPERIMENTAL EVALUATION OF THE GAIN/ABSORPTION
      SPECTRA OF SEVERAL OPTICALLY PUMPED $NH_3$ SYSTEMS - K. Kim

Introduction

The semiclassical analysis of a laser system based on the
density matrix equations to calculate the electric polarization
$\bar{P}$ and Maxwell's equations to calculate the fields, is capable
of describing all the coherent interactions of the system.  The
practical problem is that the density matrix equations are
difficult to solve in closed form for highly nonlinear processes
and computer solutions of the equations can become expensive
even with approximations.  Agreement between calculations and
experimental data will then depend upon the approximations
and/or restrictive conditions that have been made.

Given the typical approximations, it is the objective of
this paper to experimentally measure in detail the gain spectra
curves (essentially the complex electric susceptibility) and
compare the data with computer calculations to evaluate the
validity of the approximations.

Optically pumped FIR molecular lasers were first analyzed
by means of rate equations [1-5], which have limited generality.
Density matrix analysis of masers [6-8] was used in the late
1950's and later applied to FIR molecular lasers [9-12] in
the 1970's.  A limited amount of work [13-15], using a Fabry-
Perot interferometer, has been done to measure the gain spectra
of optically pumped molecular.lasers and compare the results

with density matrix analysis. This Fabry-Perot technique is tedious to apply and it has difficulties in measuring finer details, such as M-splittings, of the spectra.

A gain spectra measurement can be a somewhat routine problem if a suitable, frequency tunable, coherent, probe source exists in the frequency range of interest. The lack of such sources in the FIR is one reason one employs a Fabry-Perot interferometer. However, if one would consider an optically pumped molecular gas system where the one or more pairs of energy levels had transitions in the microwave region (i.e., up to 100 GHz), the spectra measurement problem would be greatly simplified, thanks to the availability of tunable sources.

The $NH_3$ molecule is an excellent candidate to verify density matrix equation calculations since it can be readily pumped with a $CO_2$ laser and it has many ga$\leftrightarrow$gs transitions in the 8-40 GHz range [16]. The spectroscopy, frequency off-sets, matrix elements, $T_1$'s and $T_2$'s are well known so that calculations with no free parameters can be made.

In this paper, three $NH_3$ systems were chosen for study: two two-photon, three-level systems, both have a gain spectrum with different M degeneracies, and a three-photon, four-level system having an absorption spectrum, which can be accessed with an 18-26 GHz tunable BWO probe source. This choice permits accurate measurements of the M-splittings, AC Stark shifts, absolute gains and spectral line widths to compare with

8

calculations.   Agreement with calculations and experimental data for these fine details, builds confidence that subsequent calculations of laser output power versus pump power, gain saturation, optimum pressure, etc. will also agree with experimental data.   One example will be given to substantiate this point.

## Density Matrix Analysis

The density matrix equations, used in the computer calculations, were taken in the form

$$\frac{\partial \rho_{nn}}{\partial t} + \frac{\rho_{nn} - \rho_{nn}^e}{(T_1)_{nn}} = \frac{1}{ih} \sum_k \left[ H'_{nk}\rho_{kn} - \rho_{nk}H'_{kn} \right] \tag{1}$$

and

$$\frac{\partial \rho_{nm}}{\partial t} + \left[ \frac{1}{(T_2)_{nm}} - i\Omega_{mn} \right] \rho_{nm} = \frac{1}{ih} \sum_{\substack{k \\ n \neq m}} \left[ H'_{nk}\rho_{km} - \rho_{nk}H'_{km} \right] \tag{2}$$

where $H'_{nk} = -(\overline{\mu} \cdot \overline{E})_{nk}$ is the interaction matrix element, $\overline{\mu}$ the electric dipole element and $\overline{E}$ the total electric field.

The electric polarization $\overline{P}$ is given by the expression

$$\overline{P} = N \ Trace(\overline{\mu}\tilde{\rho}) = \epsilon_o \chi_e \overline{E} \tag{3}$$

where N is the molecular density and $\chi_e$ the complex susceptibility.

The approximations used were the following:

1) Steady state (laser pulses longer than the relaxation times).

2) Homogeneous linewidths.

3) Simple relaxation terms $T_1$ and $T_2$ for each level.

4) M-changing collisons neglected.

5) Pump laser linewidths $\Delta\nu_L$ smaller than $1/T_1$ and $1/T_2$.

6) Plane wave electric fields.

10

The $NH_3$ molecular data used for the relaxation times were

$$T_2 = T_{1G} = 1.326 \times 10^{-8} \text{ sec-torr,}$$

$$T_{1\nu_2} = T_{12\nu_2} = 9.0946 \times 10^{-8} \text{ sec-torr,}$$

and for the matrix elements, the values taken were

| | |
|---|---|
| $Ga \leftrightarrow \nu_2 s$ | $\mu_{ij} = 0.23$ debye |
| $\nu_2 s \leftrightarrow 2\nu_2 a$ | $\mu_{ij} = 0.27$ debye $= 9.0 \times 10^{-31}$ coul-meters |
| $Gs \leftrightarrow Ga$ | $\mu_{ij} = 1.475$ |
| $\nu_2 s \leftrightarrow \nu_2 a$ | $\mu_{ij} = 1.25$ |
| $2\nu_2 s \leftrightarrow 2\nu_2 a$ | $\mu_{ij} = 0.83$ |

For parallel field polarizations, the change in $\mu^2$ with quantum numbers JKM is given by the expression

$$\mu^2 = \mu_{ij}^2 \frac{K|M|}{J(J+1)} \tag{4}$$

while for perpendicular polarizations, the expression for $\mu^2$ is

$$\mu^2 = \mu_{ij}^2 \frac{K}{J(K+1)} \left( \frac{J(J+1) - M^2}{2} \right)^{\frac{1}{2}} \tag{5}$$

In the case of a two-photon, three-level system, the solution of Eq. (3), for the imaginary part $\chi_e''$ of the susceptibility, will be of the form

$$\chi_e'' = a(\rho_{00}^0 - \rho_{11}^0) + b(\rho_{00}^0 - \rho_{22}^0) \tag{6}$$

while for a three-photon, four-level system, $\chi_e''$ will be of the form

$$\chi_e'' = a(\rho_{00}^{0}-\rho_{11}^{0}) + b(\rho_{00}^{0}-\rho_{22}^{0}) + c(\rho_{00}^{0}-\rho_{33}^{0}) \tag{7}$$

where $^0$ means steady state values, and a, b, c are complicated resonance expressions.

The first term in the equations is the linear (laser) term, the second term is the third order nonlinear (Raman) term, and the third term is the fifth order nonlinear (hyper-Raman) term. This results in the gain or absorption spectra having either two or three resonant peaks, each with possible M-splittings.

The experimental problem is to measure the frequency locations of the gain peaks, the gain peak values, and the widths of the gain peaks. Agreement with calculated data would check the validity of the approximations made in using the density matrix equations.

## Experimental IR-MW Configuration

The $NH_3$ systems to be studied require a test cell that can accommodate one or two $CO_2$ laser signals plus an 18-26 GHz microwave probe signal. No intentional feedback is provided for any $CO_2$ or FIR signals that may be present.

A test cell, made from K-band (RG53/U) waveguide as shown in Fig. 1, can serve as a rather general diagnostic setup for a variety of IR-MW experiments. The waveguide is terminated with two KCl Brewster windows for introduction of the $CO_2$ laser signals, either in parallel or counter propagating.

Two 45° waveguide joints using #28 wire allow the microwave probe signals and $CO_2$ signals to pass through the cell independently. A Watkins-Johnson WJ2022 BWO was used for the microwave probe source and a matched microwave Schottky diode was used for the detector.

The 18-26 GHz microwave probe signals were well matched, resulting in a single pass through the system. Reflections at $CO_2$ and FIR frequencies would appear to be small, so that in general only signals with rather high gains would be expected to be generated.

13
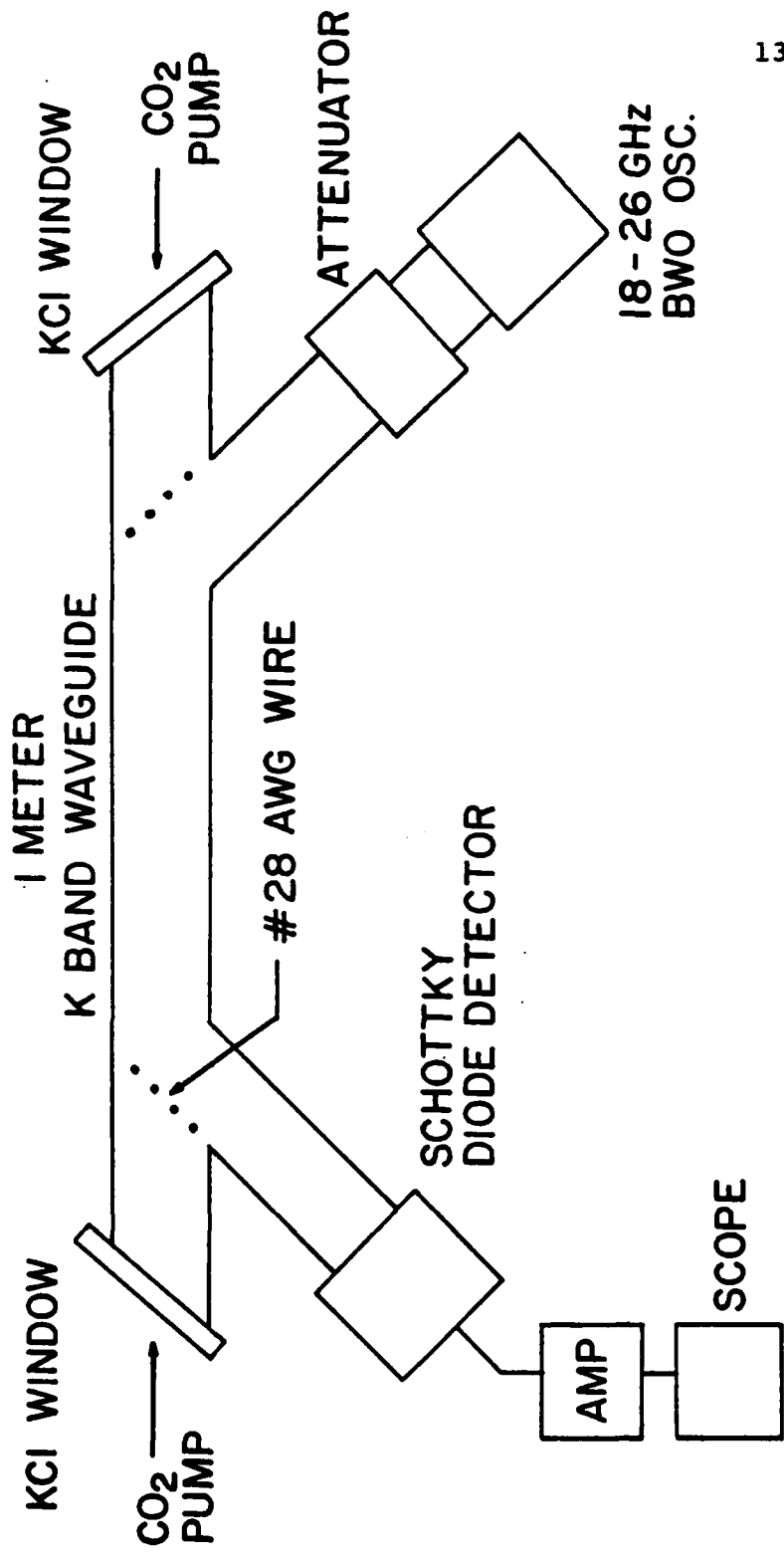


Figure 1. Schematic diagram of IR-MW apparatus for gain spectra measurements.

## Two-Photon, Three-Level Gain Experiment gs(5,4)

The first two-photon, three-level gain experiment studied was that shown in Fig. 2a). Here the gs(5,4) to $\nu_2a(5,4)$ transition in $NH_3$ is pumped by the $R(6)_{10}$ laser line of $CO_2$, which is only 0.544 GHz off resonance, and the gs(5,4) to ga(5,4) transition probed with the microwave source.

The calculated gain spectra, for parallel and perpendicular pump-signal polarizations, are given in Figs. 3 and 4. The two peaked (with M-splittings) gain spectra curves are symmetric about the $(\nu_s - \nu_{21})$ values of 0 and -0.544 GHz. To a first approximation the frequency separation of the various M peaks is the *Rabi frequency* $\mu E/h$, *i.e.*, for $|M| = 1$, the Rabi frequency is 0.63 GHz versus the calculated value (22.68-22.08) of 0.60 GHz. Above each M gain peak is written the calculated value of the frequency, which is to be compared to the experimental value.

Oscilloscope traces of the "Raman" signal at 22.03 GHz and "laser" signal at 22.72 GHz, along with the single mode $R(6)_{10}$ $CO_2$ signal, are displayed in Fig. 5 for the case of perpendicular polarization. Allowing for the 50 MHz amplifier used with the Schottky diode detector, the widths of the various signals are essentially equal with no time delays.

In Fig. 6 is plotted the calculated peak signal gain frequency versus the peak $CO_2$ $R(6)_{10}$ pump intensity in kilowatts/cm$^2$

15

$g_s = a(n_2 - n_1) + b(n_2 - n_3)$

LASER        RAMAN

a)

$\nu_2 a(5,4)$ ———————— 3

$\nu_p$ | R(6)$_{10}$

$ga(5,4)$ ———————— 2

$\nu_s$

$gs(5,4)$ —————— $\Delta\nu$ —— 1

$\nu_{21} = 22.653$ GHz

$\Delta\nu = 0.544$

$(\nu_{21} - \Delta\nu) = 22.109$

$2J + 1 = 11$

b)

$\nu_2 a(2,2)$ ———————— 3

$\nu_p$ | R(8)$_{10}$

$ga(2,2)$ ———————— 2

$\nu_s$

$gs(2,2)$ —————— $\Delta\nu$ —— 1

$\nu_{21} = 23.723$ GHz

$\Delta\nu = 0.926$

$(\nu_{21} - \Delta\nu) = 22.797$

$2J + 1 = 5$
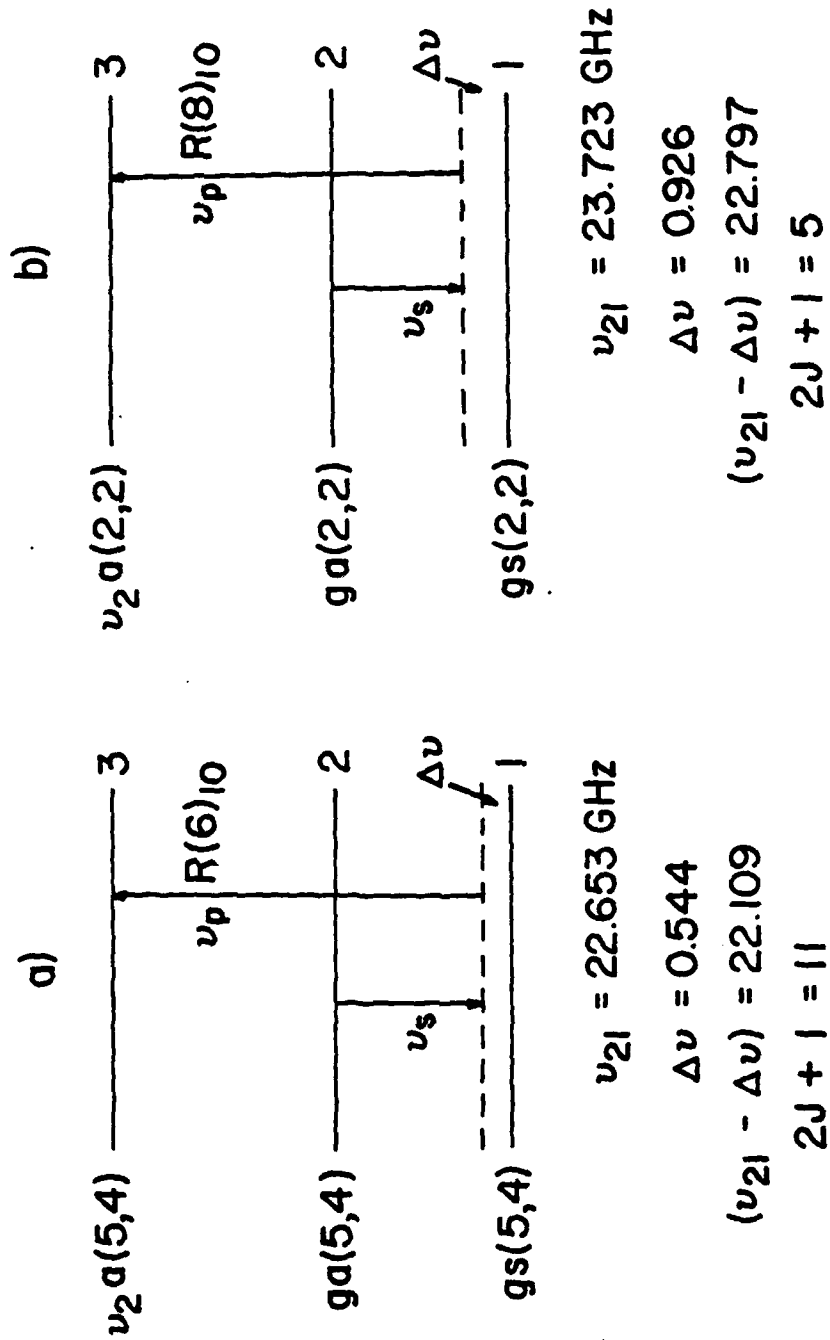
Figure 2. Two-photon, three-level experiments.
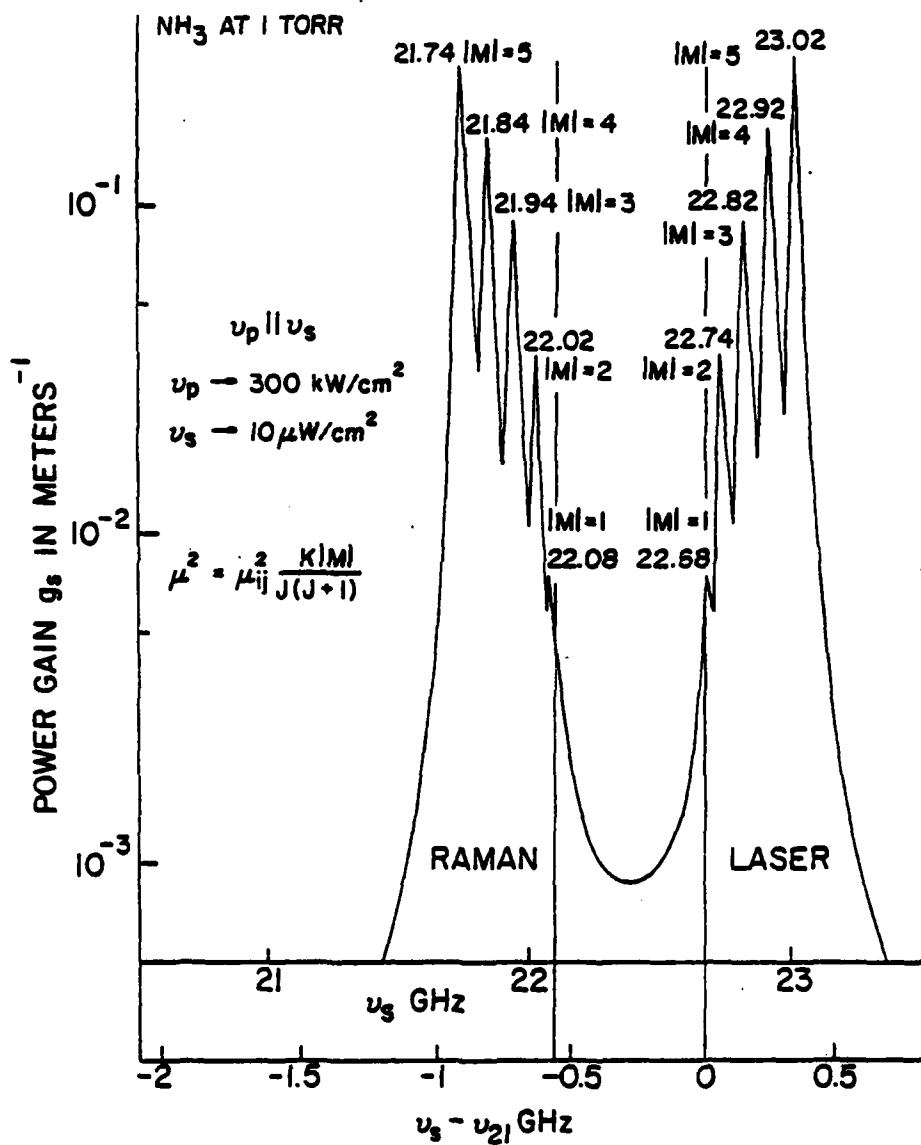
Figure 3. Calculated gain spectrum showing M-splitting (Experiment #1).

17
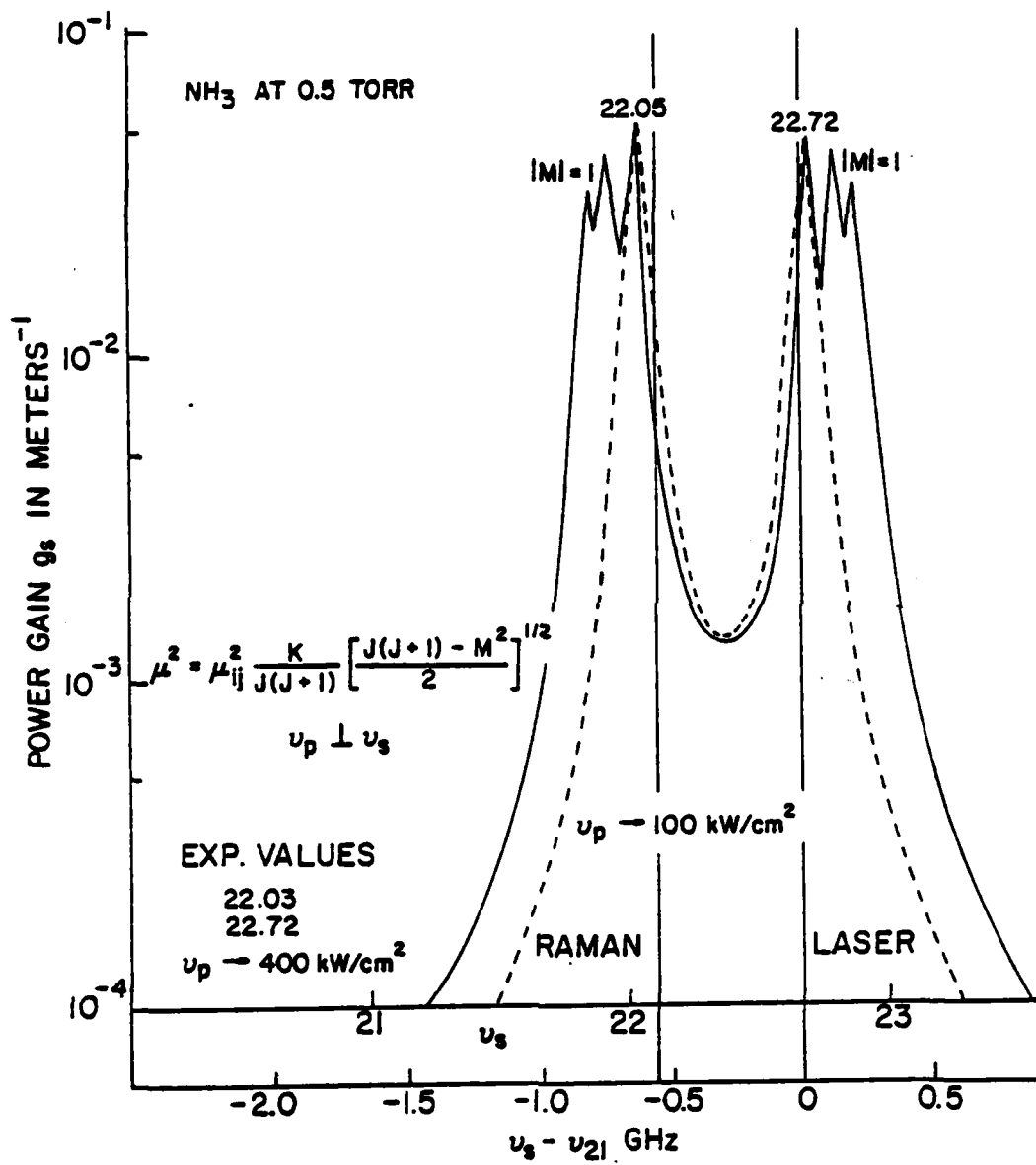


Figure 4.  Calculated gain spectrum (Experiment #1).
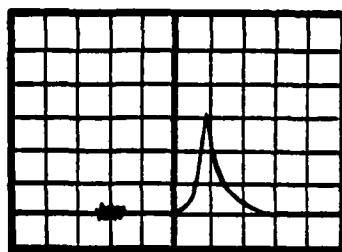
$CO_2$ $R(6)_{10}$ SIGNAL

0.5 $\mu$sec/div.

$NH_3$ at 0.5 torr
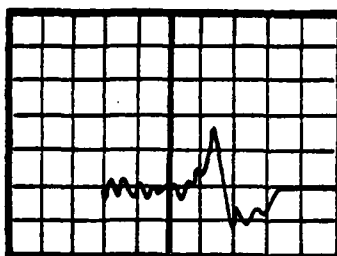
RAMAN SIGNAL
at 22.03 GHz

50 MHz AMP.

$\upsilon_p \perp \upsilon_s$

$R(6)_{10} \sim 100 \text{ kW/cm}^2$
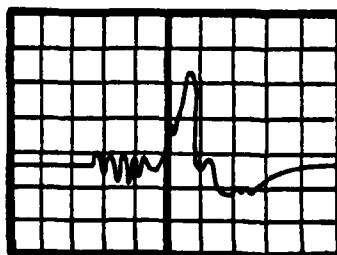
"LASER" SIGNAL
at 22.72 GHz

Figure 5. Temporal characteristics of signals (Exp. #1).
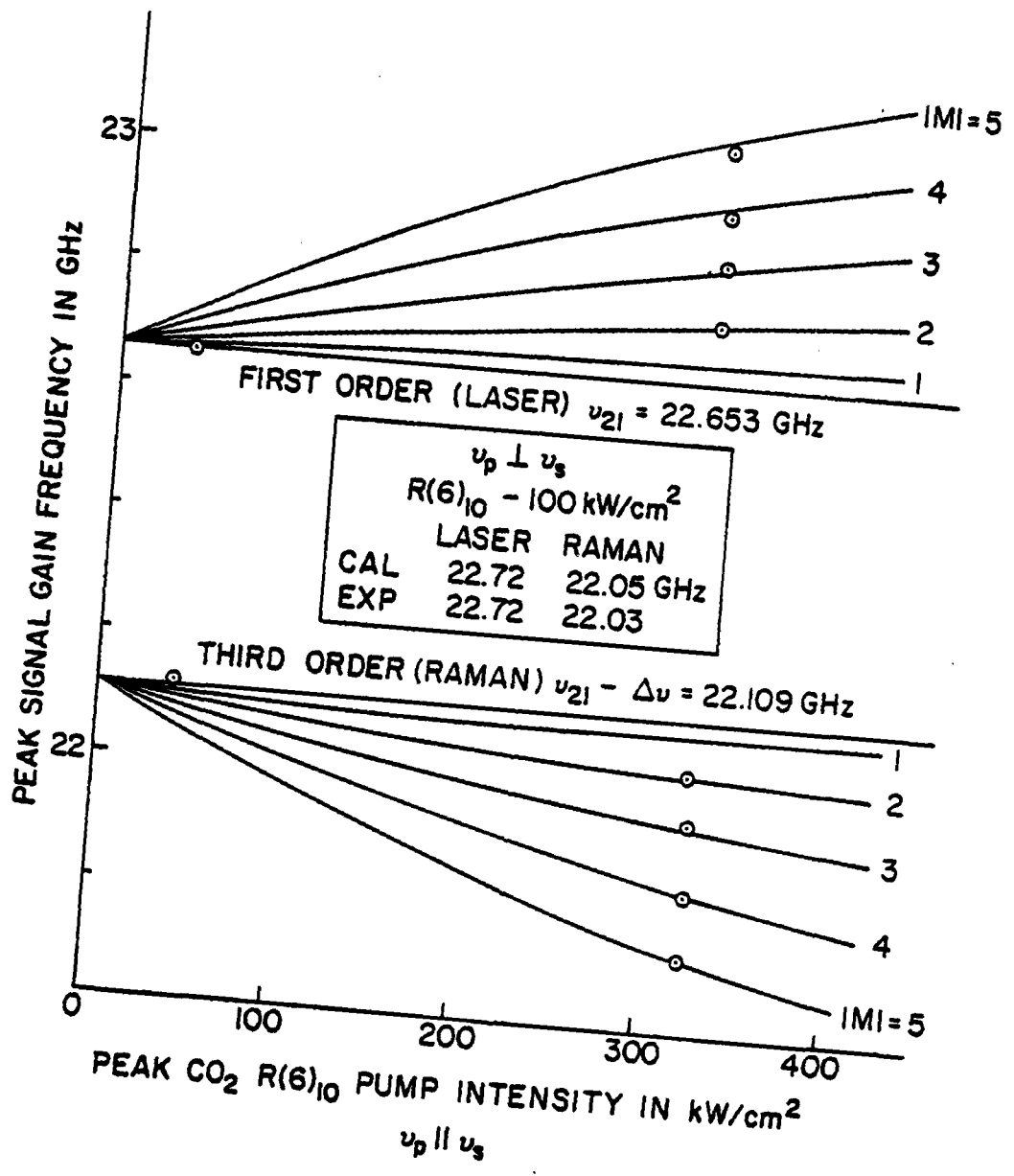
Figure 6.  M-splittings of gain frequency peaks with pump intensity for gain experiment gs(5,4).

for the various values of $|M|$ and the experimental data at fixed $CO_2$ pump intensity superimposed. It is seen that the agreement is excellent for a $CO_2$ pump intensity of 323 $kW/cm^2$, with the exception of the two points for $|M| = 1$ which agrees well for a pump intensity of the order of 40 $kW/cm^2$. The last two data points probably correspond to pump intensities in the tail of the $CO_2$ pump pulse.

The case of pump and signals fields perpendicularly polarized, the gain spectrum curves are not M-split for a pump intensity of 100 $kW/cm^2$, but the gain peaks are displaced from 22.653 and 22.109 GHz, as seen from Fig. 4. The calculated values were 22.72 and 22.05 versus the measured values of 22.72 and 22.03 GHz shown in the insert of Fig. 6.

The gain peaks for the perpendicularly polarized case were not M-split to an appreciable extent for calculated pump intensities up to 400 $kW/cm^2$ and were difficult to resolve experimentally at the lower intensities that were used. Hence only two measured values are listed.

Two-Photon, Three-Level Gain Experiment (gs(2,2)

In this experiment, the two-photon, three-level system studied was that shown in Fig. 2b) where the gs(2,2) to $\nu_2 a(2,2)$ transition in $NH_3$ is pumped by the $R(8)_{10}$ laser line of $CO_2$, which is 0.926 GHz off resonance. These conditions lead to a calculated gain spectrum displayed in Fig. 7, where the gain peaks are M-split symmetrically above 23.723 and below 22.797 GHz.

The calculated peak gain frequencies versus $CO_2$ pump intensity curves are presented in Fig. 8 with the experimental data corresponding to a $CO_2$ pump intensity of 200 kW/cm$^2$ plotted on the curves.

The FWHM peaks of the M-split calculated gain peaks is 24 MHz, the $(\pi T_2)^{-1}$ value, while the experimental curves are much broader ($\sim$ 90 MHz), reflecting the Doppler broadened (FWHM) linewidth [17] of 90 MHz for $NH_3$ at 300°K and 10 μm wavelength, which was neglected in the calculations. This Doppler broadening results in the M-split gain curves, in practice, not to be as sharp as depicted, have less deep "valleys" and probably not as large a peak gain. The experimental gain data was not absolute values but arbitrary units partially fitted to the curves.

The assumption of plane electromagnetic waves is not fulfilled in the microwave guide. Hence the transverse spacial variation of the various fields must also contribute to the broadening of the gain peaks. Considering these facts, the agreement of the data with calculations appears good.
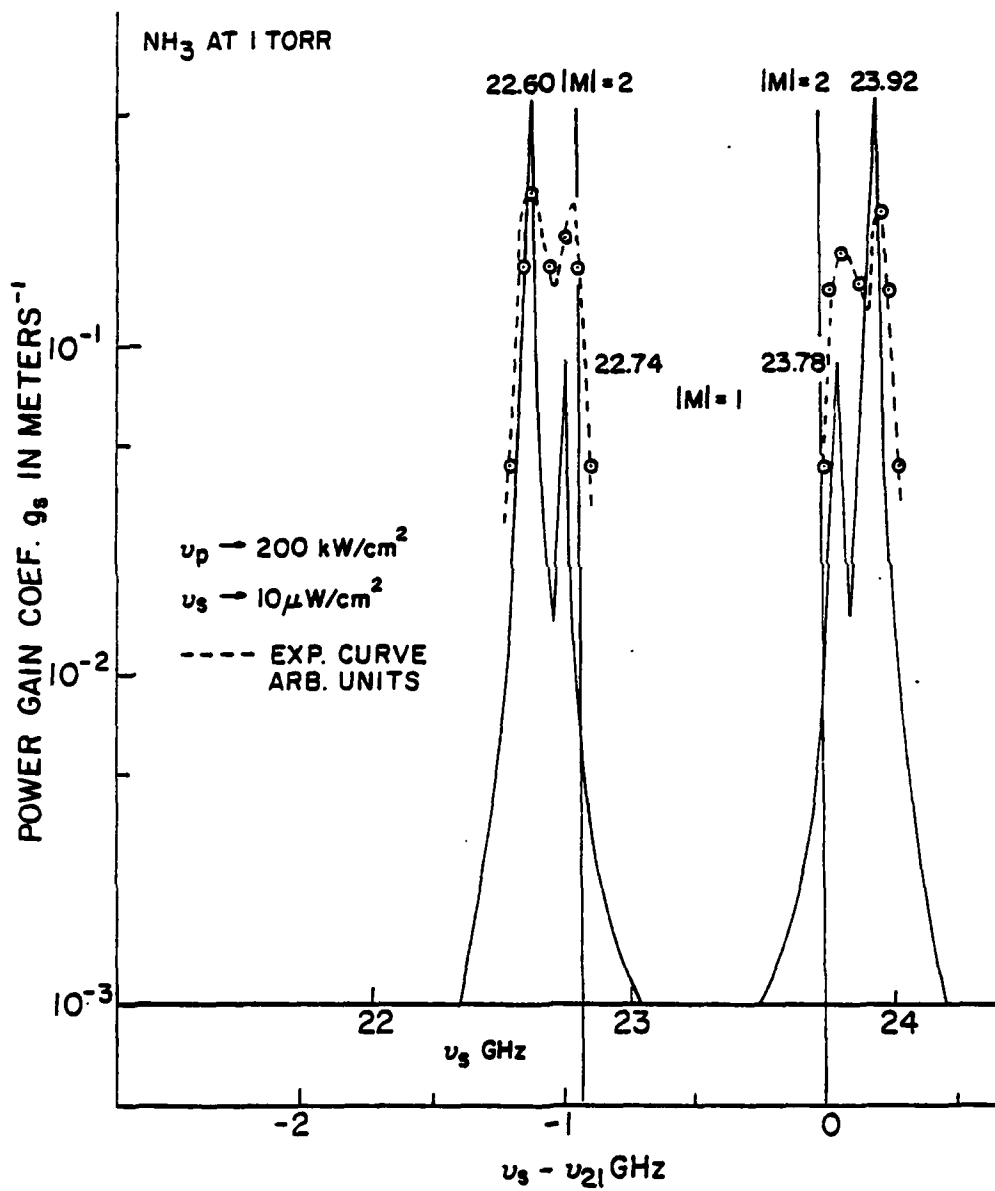
Figure 7.  Calculated gain spectrum (Experiment #2).
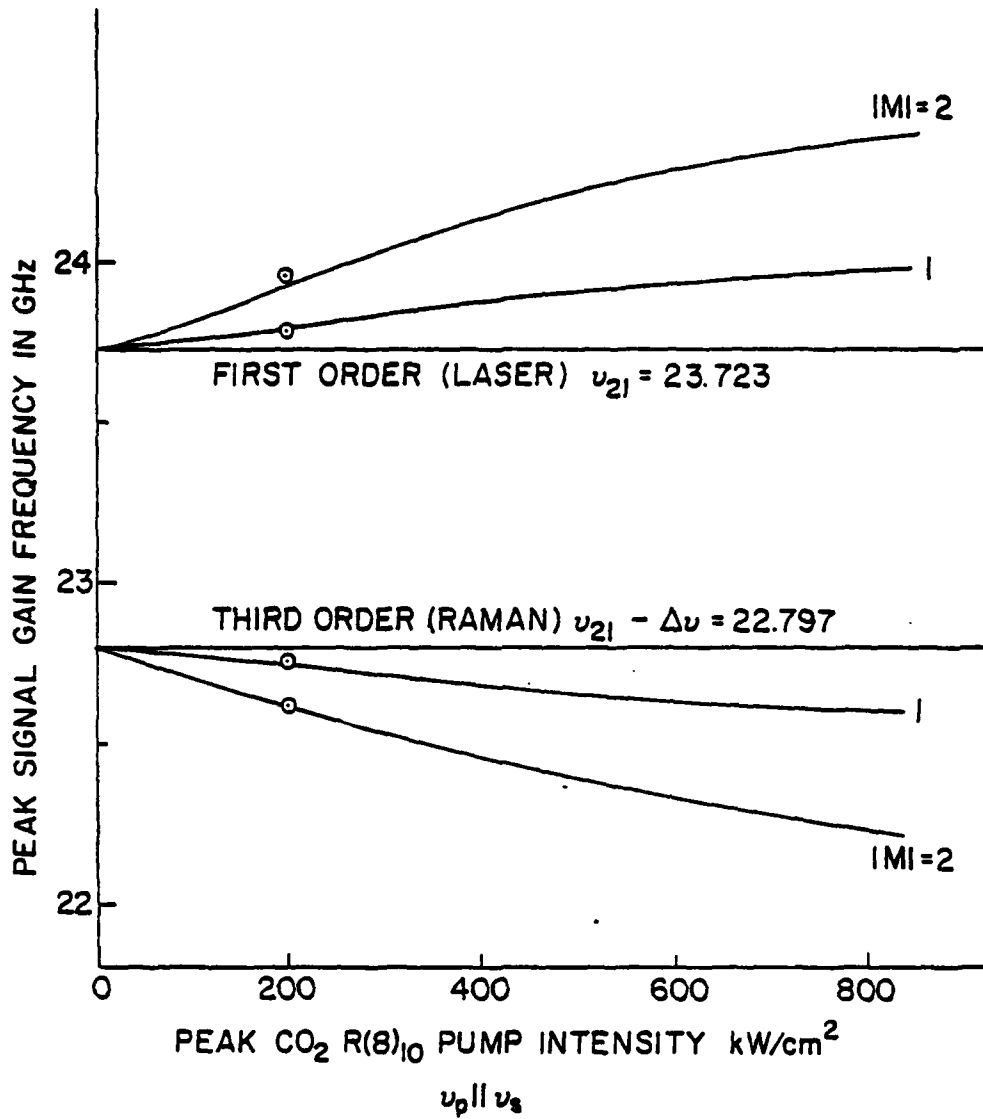
Figure 8.   M-splittings of gain frequency peaks with pump
            intensity for gain experiment gs(2,2).

## Three-Photon, Four Level Absorption Experiment gs(5,4)

In this experiment two counter propagating $CO_2$ pumps $P(34)_{10}$ and $P(18)_{10}$ were used to pump the $ga(5,4) - \nu_2 s(5,4)$ and $\nu_2 s(5,4) - 2\nu_2 a(5,4)$ transitions of $NH_3$ and the 22-23 GHz microwave signal used to probe the absorption of the $gs(5,4) - ga(5,4)$ transition. The counter propagating $CO_2$ pumps should reduce the Doppler broadening of the microwave absorption peaks and yield linewidths near the Lorentzian value.

The calculated absorption spectrum is shown in Fig. 9. In the case of two $CO_2$ pumps, the spectrum will have three absorption peaks (i.e., a triple resonance), associated with the first (Laser), third (Raman), and fifth (hyper-Raman) processes.

Only the first and fifth order absorption peaks are shown in Fig. 9, near the 22.653 and 22.947 GHz values. The Raman peak near 27.609 GHz was not accessible with the BWO source available and was weak because of the large 5.25 GHz frequency mismatch of the $P(34)_{10}$ $CO_2$ pump.

It is seen from the calculated absorption curves, very little M-splitting occurs even up to pump intensities of $P(34)$ 300 $kW/cm^2$ plus $P(18)$ 200 $kW/cm^2$. The experimental absorption data, in arbitrary units, was scaled to be 0.0074 $m^{-1}$ low on the 22.63 GHz peak and 0.0074 $m^{-1}$ high on the 22.94 GHz peak. The FWHM values of the calculated and measured absorption peaks are 24 MHz, the Lorentzian $(\pi T_2)^{-1}$ linewidth. Accuracy of the measured width was the order of $\pm 2$ MHz.
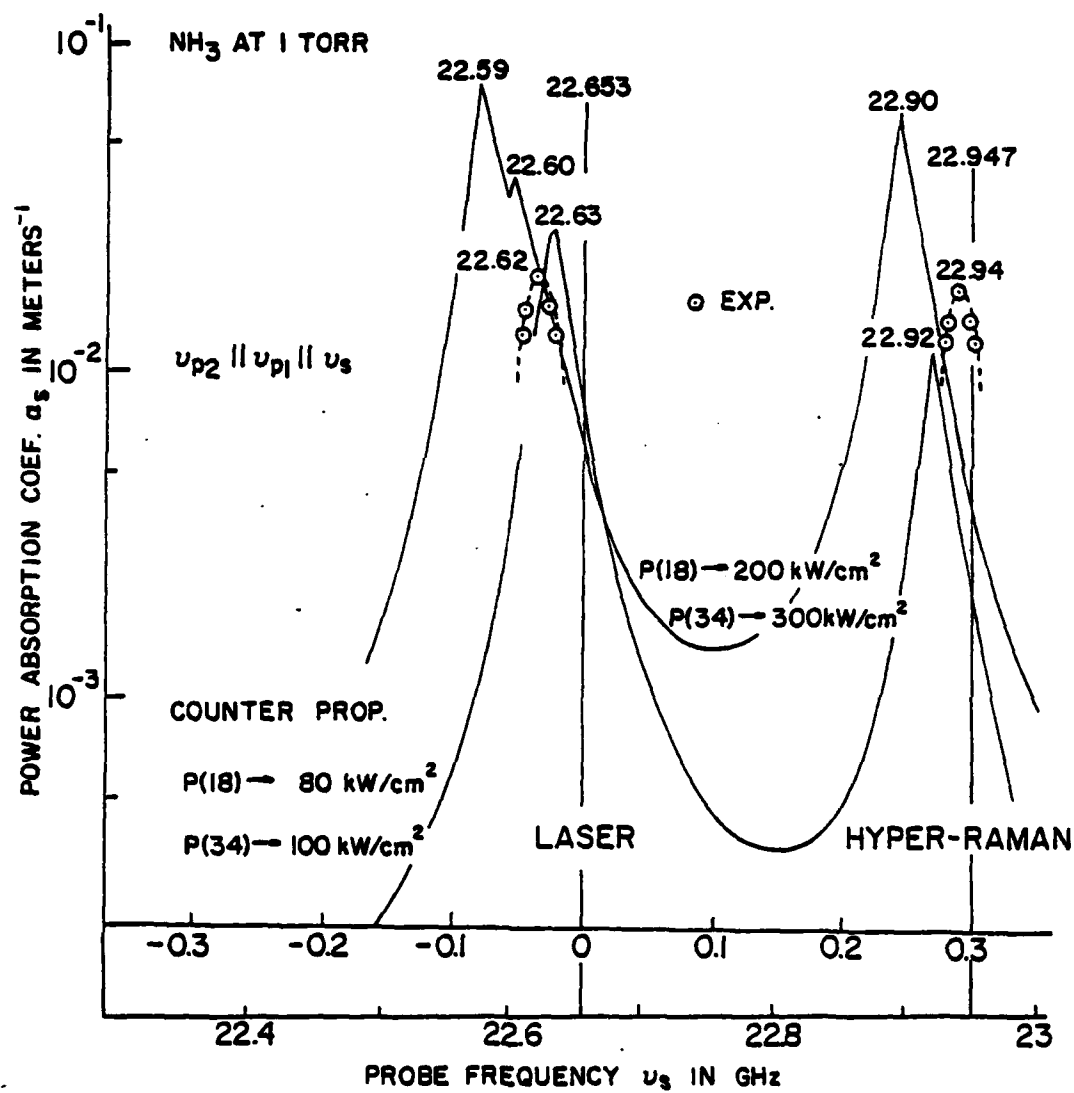
Figure 9. Calculated absorption spectrum (Experiment #3).

## Conclusions

It has been experimentally demonstrated, by the measurement of the gain/absorption spectrum of an optically pumped molecular laser system, that a density matrix calculation, using the usual approximations, accurately describes the system in detail.

The measured gain/absorption peak frequencies in both a double and triple resonance spectrum agree with the calculated values to ±10 MHz. The experimental values of the peak gain/absorption differ are a factor of 2-3 lower than calculated, mainly as a result of the assumptions of homogeneous line broadening and plane wave fields. The FWHM values of the individually M-split gain/absorption peaks reflect the Doppler broadened value of 90 MHz rather than the assumed 24 MHz Lorentzian broadening.

In the case of two counter propagating $CO_2$ pumps, the FWHM values of the gain/absorption peaks are near the 24 MHz Lorentzian linewidth.

A density matrix calculation, presented in a previous paper [10], which includes gain saturation was shown to yield excellent agreement on a two-photon pumped $NH_3$ system with respect to measured output intensity, optimum pressure, and saturated gain.

## Acknowledgement

28

References

1.  J. R. Tucker, "Theory of a FIR Gas Laser", Paper I-3, First
    Int. Conf. on Submillimeter Waves and Their Applications,
    Atlanta, GA, June 1974.

2.  J. O. Henningsen and J. G. Jensen, "The Optically Pumped
    Laser:  Rate Equations and Diagnostic Experiments", IEEE
    J. Quan. Electron., QE-11, 248 (1975).

3.  T. A. DeTemple and E. J. Danielewicz, "CW $CH_3F$ Waveguide
    Laser at 496 μm:  Theory and Experiment", IEEE J. Quan.
    Electron., QE-12, 40 (1976).

4.  R. J. Temkin and D. R. Cohn, "Rate Equations for an Optically
    Pumped FIR Laser", Opt. Comm., 16, 213 (1976).

5.  T. A. DeTemple, "Pulsed Optically Pumped FIR Lasers", Infra-
    red and Millimeter Waves, Vol. I. Sources of Radiation,
    ed. K. J. Button,(Academic Press, NY, 1979) ch. 3.

6.  A. Javan, "Theory of a Three-Level Maser", Phys. Rev. 107,
    1579 (1957).

7.  A. M. Clogston, "Susceptibility of the Three-Level Maser",
    J. Phys. Chem. Solids, 4, 271 (1958).

8.  T. Yajima, "Three-Level Maser Action in Gas I", J. Phys. Soc.
    Japan, 16, 1594 (1961).

9.  R. G. Brewer and E. L. Hahn, "Coherent Two-Photon Processes,
    Transients and Steady State Cases", Phys. Rev., AII, 1641 (1975).

10. D. Kim and P. D. Coleman, "Stimulated Hyper-Raman Scattering
    in a Molecular Gas", IEEE J. Quan. Electron., to be published
    March 1980.

11. R. J. Temkin, "Theory of Optically Pumped Submillimeter
    Lasers", IEEE J. Quan. Electron., QE-13, 450 (1977).

12. R. L. Panock and R. J. Temkin, "Interaction of Two Laser
    Fields with a Three-Level Molecular System", IEEE J. Quan.
    Electron., QE-13, 425 (1977).

13. Z. Drozdowicz, B. Lax, and R. J. Temkin, "Gain Spectrum of
    a Pulsed Laser-Pumped Submillimeter Laser", Appl. Phys.
    Lett., 33, 154 (1978).

14. J. P. Nicholson, "Direct Observation of Raman Shifts in a FIR Superradiant Laser", <u>Opt. Commun</u>., 29, 49 (1979).

15. Z. Drozdowicz, R. J. Temkin and B. Lax, "Laser-Pumped Molecular Lasers-Part II", <u>IEEE J. Quan. Electron</u>., QE-15, 865 (1979).

16. S. M. Freund and T. Oka, "IR-Microwave Two-Photon Spectroscopy", <u>Phys. Rev. A</u>, 13, 2178 (1976).

17. G. D. Willenberg, et al., "Two-Photon Pumped CW Laser", Submitted to Phys. Rev. Lett.

IV.   TUNABLE MASER EMISSION FROM $^{14}NH_3$ OPTICALLY PUMPED BY A
$CO_2$ LASER - E. Malk

## Introduction

Recently Kim and Coleman[1] presented results of calculated-
experimental evaluation of some optically pumped $NH_3$ systems.
Gain and emission at microwave frequencies were reported as a
result of infrared pumping with a TEA-$CO_2$ laser in a traveling-
wave cell.  This paper will report observation of distinctly
different results obtained in a high Q ($\sim$3000) microwave cavity
using a lower power TE-$CO_2$ laser.  Tunable microwave emission,
attributed to a linear process, with excellent frequency stabi-
lity has been observed and studied.

The energy level diagram relevant to this investigation
is shown in Figure 1.  Details regarding spectroscopic notation
and data are the subject of Appendix A1.  The near-resonant
match (i.e., $\Delta\nu$ = 544 MHz[6]) of the $CO_2$ R(6)$_{10}$ ($\nu_p$ = 966.2504
$cm^{-1}$) laser line and the $^{14}NH_3$ G $\rightarrow \nu_2$:sQ(5,4) ($\nu$ = 966.2660
$cm^{-1}$) absorption has been used to produce optically pumped
far infrared (FIR) and infrared emission.  The FIR transitions
labeled 3 and 4 were reported by Fetterman, et al.[2] and
Gullberg, et al.[3]  An additional FIR transition (i.e., G:sR(5,4)
has been reported,[5] but is not shown in Figure 1.  The infrared
transition labeled 4 was observed by Chang and McGee.[4]  The
G:sQ(5,4) transition (labeled 5) occurs in the microwave range
of the frequency spectrum at 22.653 GHz.[7]  The availability of
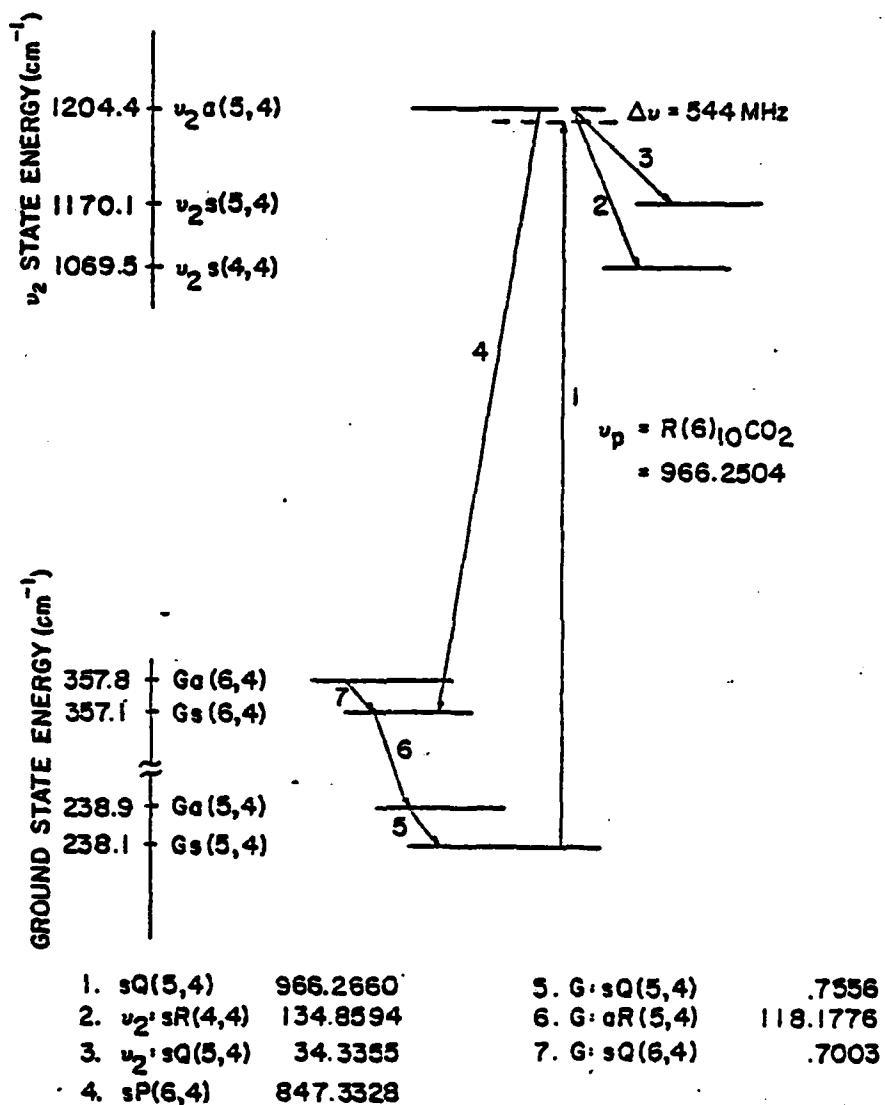
Figure 1. Energy level diagram for $^{14}NH_3$ releveant to the $^{12}C^{16}O_2$ $R(6)_{10}$ laser transition. The numbered transitions are identified and the frequencies $(cm^{-1})$ given.

tunable frequency sources in this range has led to investi-
gation of this transition.

Kim and Coleman[1] recently reported results of the infra-
red-pumped microwave-probed G:sQ(5,4) system.  Microwave fre-
quency gain/absorption spectra were calculated using a two-
photon three-level density matrix theory and compared to the
experimentally obtained transmission spectra.  The characteris-
tic shape of the calculated spectra includes two distinct peaks
near 22.653 GHz and 22.109 GHz.  These peaks are designated
the "laser" (linear order in field) peak and the "Raman" (third
order) peak, respectively.  Fine structure due to the AC Stark
splitting of the M-level degeneracy is predicted for both
peaks.  The theoretical predictions for the laser and Raman
frequency peaks are in excellent agreement with the experiment.
The measured values of the gain magnitudes are within a factor
of 3 when compared to the theoretical values.  These results
prompted further investigation in an experimental cell that
could provide feedback for possible FIR radiation involved in
yet higher order processes.

## Cell Design

The cell used in the Kim experiment is a travelling wave
device that provides no intentional feedback for infrared or
FIR radiation.  This design provides a relatively uniform in-
frared field to pump the $^{14}NH_3$ gas.

The cell designed for this investigation simultaneously provides feedback for the FIR and microwaves. The cell is a right cylindrical microwave transmission cavity operating in the lowest order linearly polarized $TE_{11n}$ mode. The resulting FIR mode is the circularly polarized $TE_{10n}$'. A similar cell has been used by Willenberg, et al.[8] to produce a two-photon pumped CW laser. Further details regarding cell design and calibration are contained in Appendix A2. The infrared radiation is focused through a 1.5 mm coupling hole in a 0.1 inch thick copper mirror. The resulting infrared pump field is spatially non-uniform which causes the effective pumping field to be reduced, and the microwave gain fine structure to become unresolvable.

The compromise in the resonator cell design suggested by Willenberg[8] that the circularly polarized FIR modes are not optimally excited by the linearly polarized pump field and the higher losses for the FIR are of little concern for the case of pumping with a pulsed high-power $CO_2$ laser. The point of resonantly enhancing and confining the microwave to a minimum volume is well taken, and the primary reason for choosing this design.

## Experimental Apparatus

The experimental apparatus consists of four major parts. These include: 1) the infrared pump laser; 2) the optically

pumped FIR laser; 3) the microwave circuit; and 4) the pulse synchronization circuit. Each of these parts will be described in detail, with the experimental cell design features listed where they are important.

### Infrared Pump Laser

The infrared pump laser is a single longitudinal mode TE-$CO_2$ laser capable of energies up to 150 mJ (stronger lines) at a 0.5 Hz repetition rate. The cavity consists of a gold-plated PTR 10m radius of curvature, 100 lines/mm, master diffraction grating blazed at 10.6 $\mu$m and a flat germanium partial reflector (R=75%). The total cavity length is about 3m. The transverse discharge cell pressure was maintained at 300 torr while the longitudinal discharge gain cell pressure was at 15 torr. The premixed laser gas is flowed at a moderate rate and is a mixture of 12% $CO_2$, 14% $N_2$, and 52% He. Pulsed laser energies were measured with a GENTEC joule meter.

### Far Infrared Laser

The FIR laser resonator is the $TE_{11n}$ microwave transmission cavity resonator. The resonator consists of a non-precision 32in long 3/8 in. ID copper tube, a fixed circular (.355 in. OD) copper mirror with a 1.5 mm hole at its center, and a translatable circular (.355 in. OD) copper mirror. The only alignment adjustment is the cavity length. The remaining

alignment is determined by the machined accuracy individual components. Operating pressures of the $^{14}NH_3$ gas range from 0.1 to 20 torr and are easily maintained for many hours in the cell.

The optically pumped FIR radiation is coupled out the 1.5mm hole and deflected through a TPX vacuum window, similar to the arrangement used by Gullberg, et al.[3] The signal is detected with a Si:P detector at 4°K. The detector is also sensitive to the infrared pump radiation, causing additional filters to be required for weak FIR signals.

The stable output of the optically pumped FIR laser and relatively ineffective cavity tuning indicate the FIR losses are low and the machined alignment is adequate for these experiments.

### The Microwave Circuit

The microwave circuit used in the experiment was changed several times, but two similar circuits produce the best results. The basic circuit is shown in Figure 2. The klystron is an OKI 24V10 driven by an FXR Universal Klystron Power Supply. (Beam Voltage = 2000V @ 10ma, Reflector Voltage ≈ -250V, Control Grid ≈ -200V). Swept frequency operation is obtained by applying a 0-200 Volt ramp to modulate the reflector voltage. Quasi-fixed frequency operation is obtained by applying a square wave (0-200V) voltage to the reflector.

36



A1, A2, A3, A4 – VARIABLE
                ATTENUATOR

C1 – DIRECT READING CAVITY
       WAVEMETER

C2– TUNABLE TRANSMISSION
       CAVITY FILTER

C3– TUNABLE INTERACTION CELL

DC– 12 db DIRECTIONAL COUPLER

DS1, DS2 – DOUBLE STUB TUNER

D1, D2, D3 – IN26B DIODE DETECTOR

I – FERRITE ISOLATOR

K– OKI 24VIO KLYSTRON

T– SERIES T JUNCTION
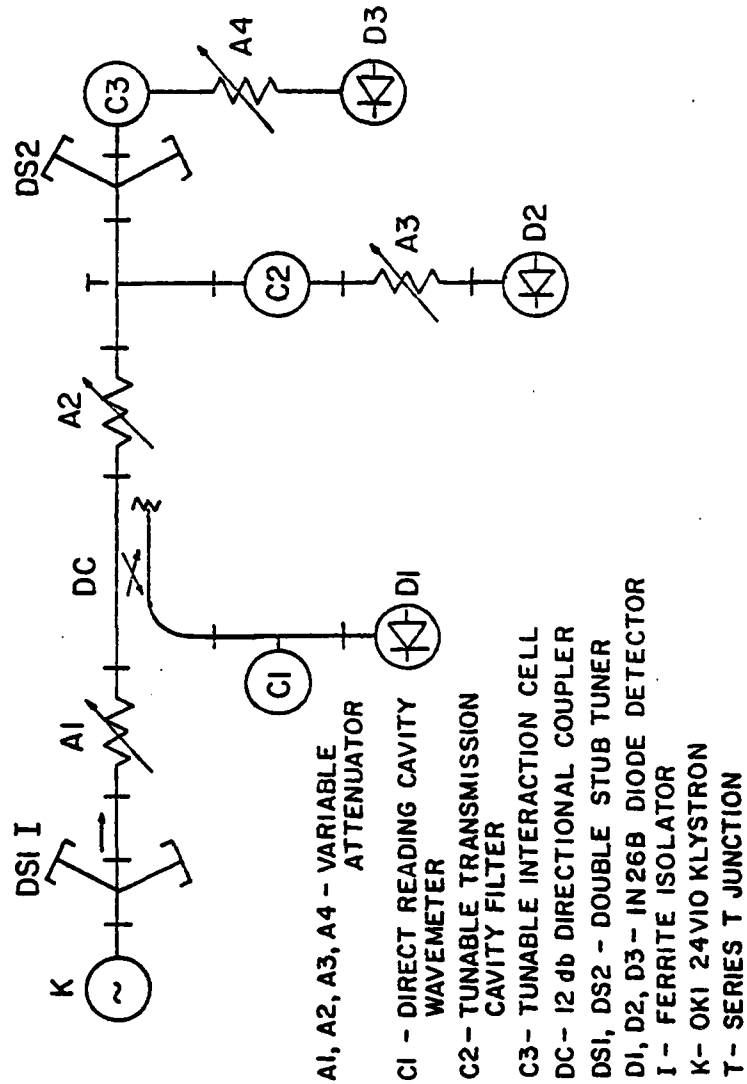
Figure 2.  The microwave circuit.

DS1, I, and A1 serve to pad the Klystron from the rest of the mostly high Q circuit. DC, C1, and D1 serve to monitor the reflected microwave signal from C2 and C3. A2 controls the level of the microwave radiation. T is an E-PLANE (SERIES) T junction used to split the microwave radiation. The purpose of this junction is to facilitate setting of the microwave frequency. This will be considered in detail shortly. C2 is a high Q ($\approx 7000$) critically coupled tunable transmission cavity used as a frequency filter. A3 limits the level of microwave radiation incident on D2, a 1N26B diode. C3 is the designed cell (design details are in Appendix A2), a transmission cavity operating with the lowest order $TE_{11n}$ mode. The measured Q of the cavity is about 3000 and the maximum coupling is less than 10%. The amount of coupling may be varied by tuning DS2. The transmitted microwave level is monitored on D3.

The setting of frequency in this circuit is somewhat ·tedious. The best results are obtained in the following manner. The klystron is operated in a swept frequency mode with the desired frequency located at or near the center of the sweep, as monitored with D1 (the maximum safe signal level from the 1N26B into $1M\Omega$ is 0.5V for $< 1$ msec pulse, for a duty cycle less than 0.1). DS2 is adjusted until a decrease of 5% or more is observed at D1. Careful examination of the change in signal level will demonstrate frequency sensitivity. The

change should be maximized at the desired frequency. D3 should now be monitored with a high gain amplifier. If no signal is present at D3 tune C3 until a signal is observed, taking care not to burn up D3. Additional adjustment of DS2 may be used to maximize the transmitted signal. For most applications this is all that is required.

For more precise frequency settings, C2 is set to a particular frequency. The critical coupling of C2 puts a sharp (high Q and more coupling) dip in the curve monitored at D1. This dip represents maximum transmission through C2 and results in dissipation of the microwave energy in A3 or D2. Following the procedure outlined previously a signal is then monitored at D3. When the cavity C3 is tuned such that the frequency of cavity C2 are the same, the same sharp dip will be observed in the transmitted peak at D3. This technique is important for investigating frequency-time behavior.

The second microwave circuit involves setting up a heterodyne detector. The klystron operating in the quasi-fixed frequency mode is used as the local oscillator. The basic circuit is modified as follows. The directional coupler (DC) is reversed so it splits a fraction of the incident microwave radiation to D1. The tunable transmission cavity filter is completely removed and A2 is placed between T and DS2. D2 now serves as the mixer for the heterodyne detector. This circuit

has been used to study microwave injection effects, frequency
tunability, and frequency stability of the generated microwave
signals.

### Time Synchronization

Pulsed probe experiments require flexible, reliable
triggering if meaningful data is to be obtained. The require-
ments for the experiments performed resulted in several dif-
ferent techniques being developed for triggering. The require-
ment peculiar to these experiments are caused by: 1) low re-
petition rate ($\sim$0.5Hz) firing of the $CO_2$ laser and 2) time
jitter of the reflector modulation power supply.

The low repetition rate firing of the $CO_2$ laser is required
to get reliably stable pulses of infrared pumping radiation.
The time jitter problem of the klystron reflector modulation
could be solved by repairing or replacing the power supply,
but was not practical at the time.

The only experiments performed where synchronization is
required were microwave injection and heterodyne detection ex-
periments. In both of these cases the klystron was operated
in the quasi-fixed frequency mode (i.e., square wave modulation
of the klystron reflector voltage). The triggering technique
is shown in Figure 3.

The modulation output of the FXR universal klystron power
supply is a 0 to 100V square wave with a period of $T_1$. ($T_1$ is

40
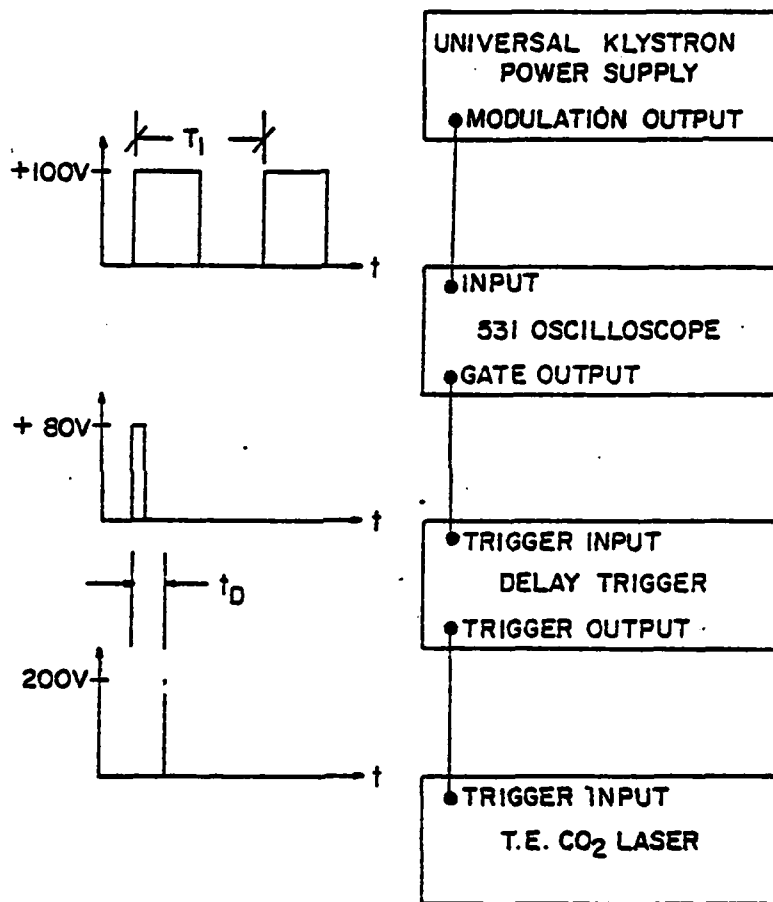


Figure 3. Time synchronization block diagram. The system allows synchronous firing of the TE-$CO_2$ laser with the klystron.

typically 1 msec). The square wave is monitored by a
Tektronix 531 oscilloscope with a vertical sensitivity of 20
V/div. The time base is set at 0.2 sec/div and the scope is
internally triggered by the square wave. The resulting gate
output of the oscilloscope has a period determined by the time
base of the oscilloscope (a 2 second period is typical), and
is used to trigger a four channel delay trigger generator.
The delay trigger ensures the laser trigger pulse occurs during
the fixed frequency part of the klystron reflector modulation.
This technique has produced the simplest synchronization of
the infrared and microwave signals, and is least likely to be
affected by jitter in the reflector modulation power supply.

The experimental details presented thus far are common
to most of the performed experiments. Specific details pecu-
liar to a given experiment will be discussed with the experi-
ment.

## Experimental Results

Optical pumping of $^{14}NH_3$ with a TE-CO$_2$ laser has produced
strong, frequency stable microwave emission. The results to
be presented include characterization of the microwave emis-
sion operating conditions, the emission bandwidth dependence
on pressure, effects of microwave injection, and frequency
stability observations.

### Microwave Emission Characteristics

Microwave emission attributed to the $G:sQ(5,4)$ inversion transition was observed following optical pumping of the $G \rightarrow \nu_2:sQ(5,4)$ transition with a TE-$CO_2$ laser tuned to the $R(6)_{10}$ ($\nu_p$ = 966.2504 $cm^{-1}$) line. The time synchronized photographs shown in Figure 4 show a typical infrared pump laser pulse (E=60mJ), the resulting FIR laser pulse, and the observed microwave emission. The conditions stated on the figure represent the near optimum conditions for the microwave emission. The emission is only observed over a relatively narrow pressure range from 0.3 to 2.2 torr, with stable amplitude behavior from 0.5 to 1.8 torr. Additional data is given in Figure 5. The pulse shapes are observed to change with pressure, becoming shorter with increased pressure. In all cases shown the cavity is set to the length that provides the maximum signal level at 1.13 torr.

To provide further understanding of the microwave emission, the frequency and emission bandwidth required investigation. The technique employed to obtain this information is performance of cavity tuning scans of the observed emission.

### Cavity Scanning Results

A cavity scan is performed in the following manner. A motor drive is mounted to the micrometer tuning plunger of the experimental cell. The microwave emission is monitored

INFRARED
$CO_2$ $R(6)_{10}$
$E \simeq 60\,mJ$
Si:P at 4°K
I Volt/div
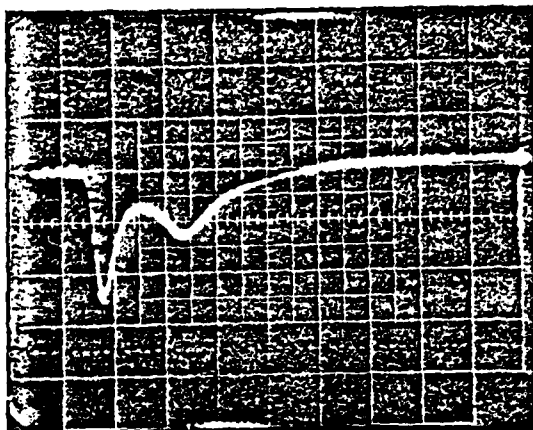
FAR-INFRARED
$^{14}NH_3$ at 1.13 torr
Si:P at 4°K
I Volt/div
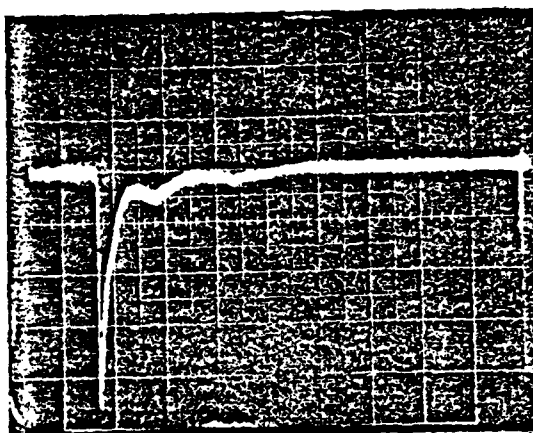
MICROWAVE
$^{14}NH_3$ at 1.13 torr
IN26B into $1000\,\Omega$
50 mV/div

43
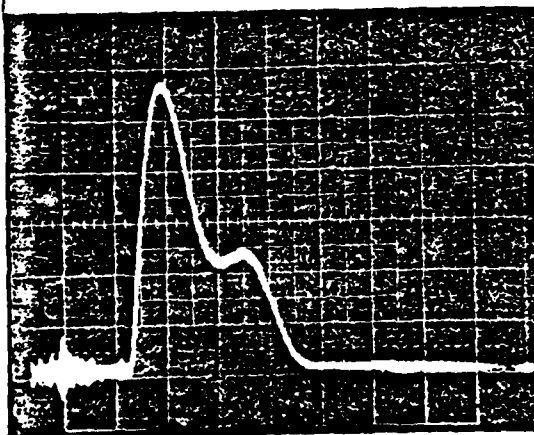
$t = I\,\mu sec/div$

Figure 4.  Time synchronized oscilloscope traces showing the
infrared pump pulse ($CO_2$ $R(6)_{10}$), the optically
pumped far infrared ($\nu_2$:sR(4,4) at 134.86 $cm^{-1}$ and
$\nu_2$:sQ(5,4) at 34.34 $cm^{-1}$) emission, and the resulting
microwave emission attributed to the G:sQ(5,4) at
22.653 GHz.

44

P = .53 torr
y = 20 mV/div

P = .7l torr
y = 20 mV/div
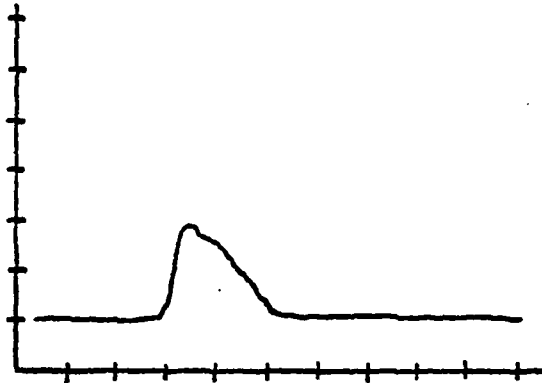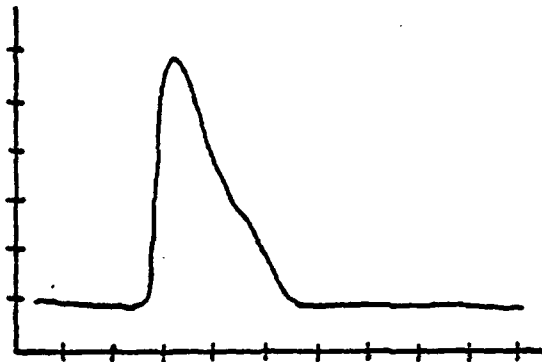
P = .9l torr
y = 50 mV/div
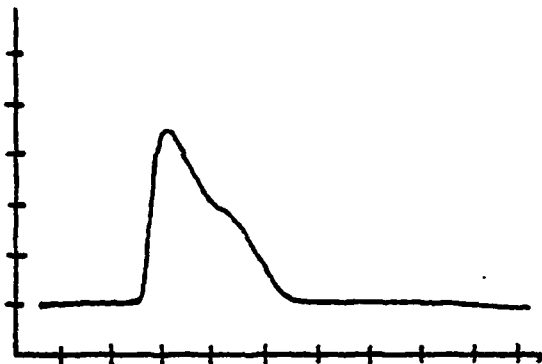
t = 1 $\mu$sec/div

Figure 5.  Oscilloscope traces of the G:sQ(5,4) optically
           pumped emission.

P = 1.11 torr
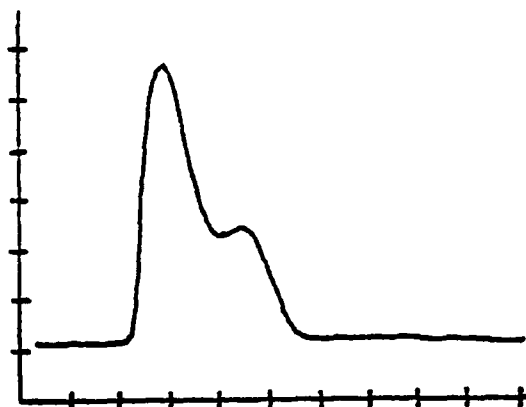
P = 1.31 torr

P = 1.5 torr

t = 1 μsec/div
y = 50 mV/div

**Figure 5.** Oscilloscope traces of the G:sQ(5,4) optically pumped emission.

46



P = 1.71 torr
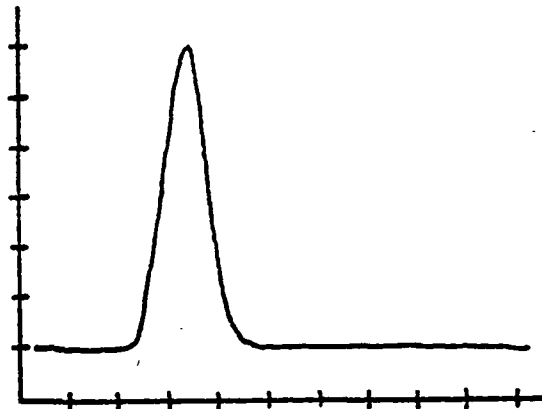
P = 1.90 torr
$CO_2$ MISFIRE
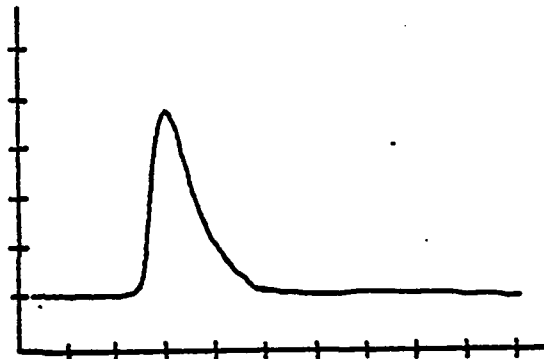
P = 1.90 torr
UNSTABLE
SIGNAL

t = 1 $\mu$sec/div
y = 50 mV/div

Figure 5. Oscilloscope traces of the G:sQ(5,4) optically pumped emission.
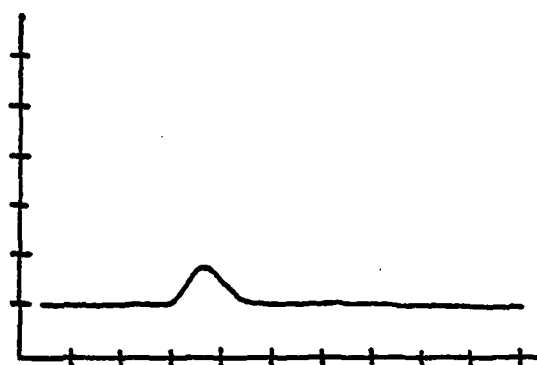
Figure 5.   Oscilloscope traces  of the G:sQ(5,4) optically
             pumped emission.

with a 1N26B diode (D3 in Figure 2) and input to a synchro-
nized PAR Boxcar Integrator. The gate (i.e., integration win-
dow) of the Boxcar is set at 4 μsec to allow for time jitter
of the microwave emission pulse. The integration time of the
Boxcar is set to the minimum value (i.e., 0.01 msec). The
input is AC coupled to the 10kΩ Boxcar input with a shunt 1kΩ
resistor to decrease the rise time of the detector. The sig-
nal output was used as the y input to an x-y recorder. The
x was set to 100 seconds/inch scan rate. The combination of
the motor drive with the x-y recorder produced 0.0452 inches
of cavity scan per inch of graph paper. The initial and
final cavity setting of the scan are placed on the graph for
reference purposes. The upper curves in Figure 6 are the
result of three consecutive cavity scans.

The lower curves give the absolute frequency calibration
data for the upper curves. These curves are considerably more
difficult to record. Detection of microwave absorption in a
microwave cavity is a standard spectroscopic technique (see
Townes and Schawlow,[9] Section 15.11). The result of microwave
absorption is increased loss at the resonant absorption fre-
quency. The increased loss in the cavity reduces the Q of
the transmitted microwave signal which is readily detectable
at low pressures. At a pressure of 0.1 torr the homogeneous
microwave absorption linewidth is about 2.5 MHz, thus a sizeable
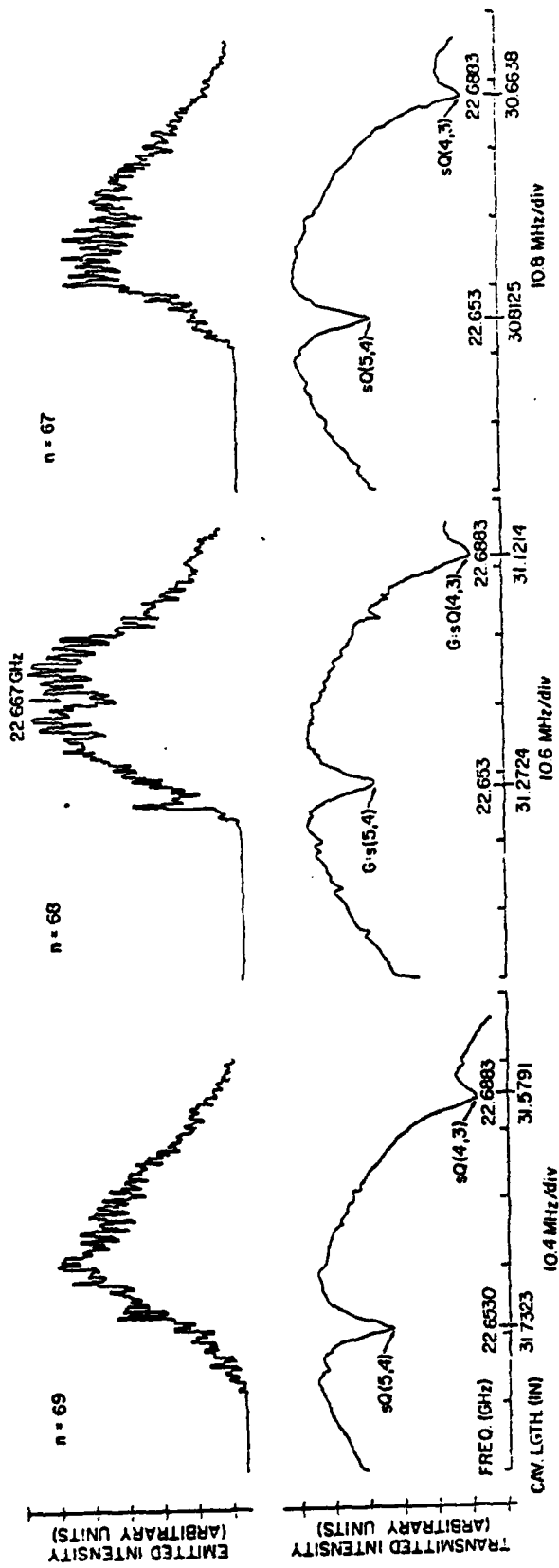
Figure 6. Cavity scans of the G:sQ(5,4) emission (upper curves) and microwave absorption calibration scans (lower curves) for the TE$_{11n}$ (n=67, 68 and 69) modes. The cavity scan length is 0.0452 inches per division, E$_L$ = 60 mJ, $^{14}NH_3$ pressure at 1.1 torr.

49

transmission dip would be observed if the cavity is scanned during microwave frequency sweep containing the resonant frequency. The $^{14}NH_3$ microwave absorption transitions are tabulated in Appendix A1 (see Ref. 7 for a more complete listing).

An absolute frequency calibration graph is recorded using the following method. The cavity wavemeter (C1 in Figure 2) is set to read the desired absorption frequency. For the calibration curves in Figure 6 the desired frequency is 22.653 GHz for the G:sQ(5,4) transition. The evacuated cavity is then set near the resonant frequency using the technique previously described (Section: The Microwave Circuit). Approximately 0.1 torr of $^{14}NH_3$ gas is added to the cell. The cavity tuning micrometer is adjusted to locate the dip in transmission monitored at D3 with a Tektronix 1A7A high gain differential amplifier having a $1M\Omega$ input impedance. The signal output of the 1A7A is then input to channel A of a Tektronix 475 oscilloscope and the $10k\Omega$ input of the boxcar integrator. The gate output of the triggered boxcar is input to Channel B of the 475 oscilloscope. The vertical display is set to "add" channel A and channel B. The gate of the boxcar is chosen to be much shorter in time than the transmission peak of the swept frequency klystron output. The time base of the boxcar is set to allow the gate to be delayed to any point of the frequency sweep. The cavity is adjusted to the desired starting

point and the gate output is adjusted to be at the resulting transmission peak. The cavity scan is then initiated, and manual feedback is used to keep the gate, by varying the delay of the boxcar, at the transmission peak. If the resulting graph exhibits excessive structure (i.e., noise) increase the integration time and/or aperture time. Care must be exercised to ensure there is no significant detection lag time in an accurate frequency calibration graph.

The cavity wavemeter (C1) calibration was verified to be within 5MHz of all the measured absorption frequencies. (For more details, see Appendix A2).

Cavity scans performed at different pressures and fixed input power provide information regarding emission bandwidth, saturation, and optimal operating conditions. Figure 7 shows the resulting cavity scans at various pressures. The emission bandwidth numbers are obtained by measuring the full width at half maximum length on the graph and multiplying it by the length to frequency conversion factor and scan rate factor

$$\Delta f(FWHM) = L \underbrace{x\ 0.0452}_{\substack{\text{SCAN} \\ \text{FACTOR}}} \times \underbrace{\left| \frac{f_2 - f_1}{L_2 - L_1} \right|}_{\substack{\text{LENGTH} \\ \text{FREQUENCY} \\ \text{FACTOR}}} \qquad (1)$$

$\Delta f(FWHM) \rightarrow GHz$

$L \rightarrow$ GRAPH PAPER INCHES
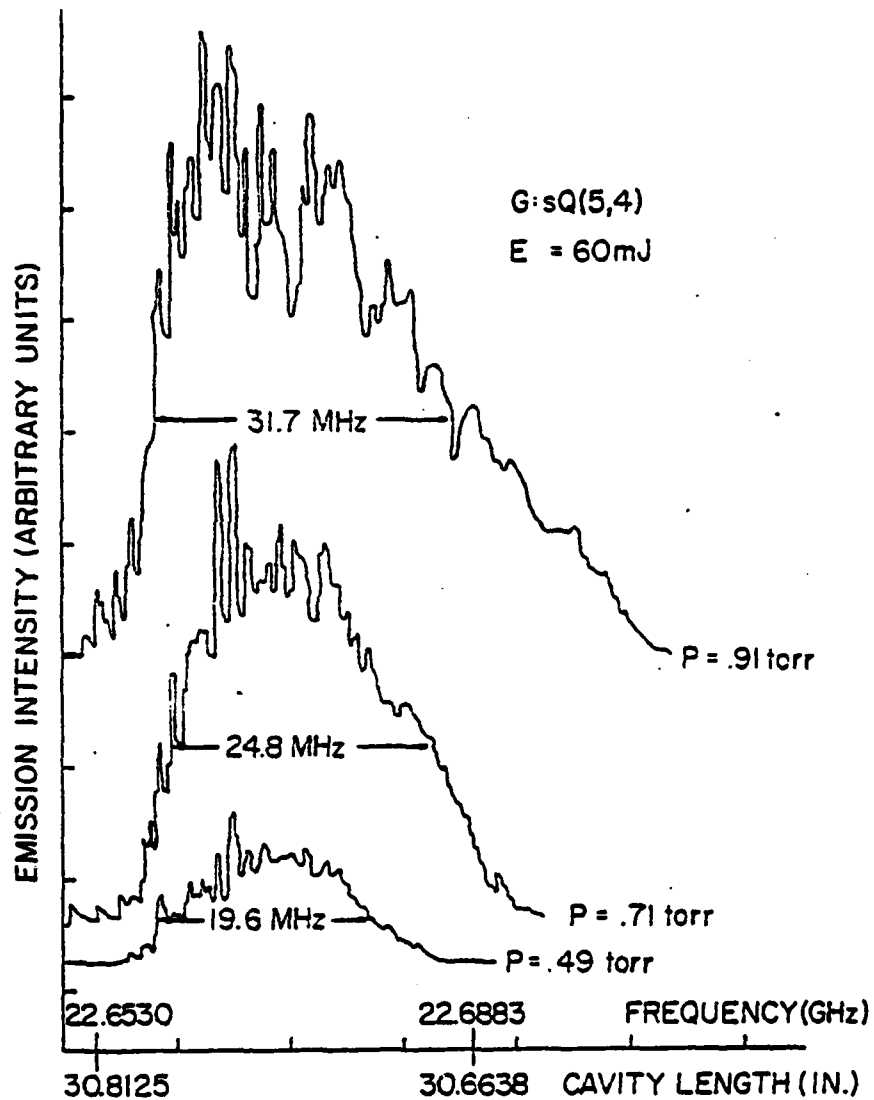
Figure 7.   Cavity scans at different pressures for the G:sQ(5,4)
emission.   (TE$_{11n}$, n=67 mode) cavity length is 0.0452
inches/div., frequency scan is 10.8 MHz/div.

$$0.0452 \rightarrow \text{(CAVITY SCAN INCHES)/(GRAPH PAPER INCHES)}$$

$$f_2, f_1 \rightarrow \text{ABSOLUTE FREQUENCY CALIBRATION POINTS}$$

$$L_2, L_1 = n \frac{\lambda_{g_2}}{2}, \ n \frac{\lambda_{g_2}}{2} \rightarrow \text{ABSOLUTE LENGTH AT THE FREQUENCY CALIBRATION POINTS.}$$

The accuracy of the measured emission bandwidth is limited by the emission structure observed in the cavity scans. Cavity scans at higher $^{14}NH_3$ pressures have been recorded but the structure observed makes it nearly impossible to measure the full-width half-maximum with any certainty.

### Microwave Injection Effects

Microwave injection effects have been investigated with very limited success. The experiments were performed in hopes of producing information regarding magnitude, time, frequency, and saturation behavior of the emission gain. The difficulties in obtaining this information are multiplied by the high Q frequency characteristics of the interaction cell. To obtain reliable experimental data it is believed the cell used in the Kim[1] experiment would be better. Several interesting qualitative observations have been made and will be presented here.

The qualitative observations resulting from microwave injection mentioned above include: 1) change of the delay time for the gain switched microwave emission, 2) increased pressure

range operation of emission, 3) observation of the transmitted
signal frequency beating with observed emission frequency, 4)
increased emission bandwidth, 5) the microwave emission depen-
dence on level of injection indicates the emission is saturated,
and 6) time dependent gain is present in the microwave emission.
The majority of these observations are not particularly sur-
prising. A feature common to all of the observations is the
dependence on injected microwave signal frequency.

Microwave injection effects are only observed when the
injected microwave signal frequency is between 22.645 and
22.725 GHz. This is not symmetric with respect to G:sQ(5,4)
transition at 22.653 GHz, but is consistent with the data ob-
served in the cavity scans. Injection of signals at and around
the Raman frequency peak at 22.109 GHz produced no obvious
effects.

The most interesting observations are the indication of
gain saturation and the time dependent gain of the emission.
The gain saturation is observed by varying the input level of
injection at various pressures. At pressures less than 1 torr
the delay time decreases, the pulse length increases, but the
peak amplitude remains very constant. The level of injection
to produce these effects is not detectable at the transmission
monitor diode (D3 in Figure 2). Increasing the level of in-
jection an amount so as to be detectable at D3 ($\sim$10db in power)

produces the identical result. This was observed near the peak emission cavity tuning. Tuning the cavity and microwave frequency to a point beyond the emission bandwidth half-power points produced similar results with more (but not much) dependence on signal level injection. The most obvious result is increased amplitude stability of the microwave emission. Tuning the cavity and injection frequency 15 MHz beyond the frequency where emission stops produces no effect.

At pressures greater than 1.5 torr, the emission bandwidth is observed to be decreasing. This is attributed to higher losses. Microwave injection can be used to increase the emission bandwidth. Stable amplitude pulses of emission can be observed at frequencies 30 MHz beyond the point where self-oscillation stops. At pressures greater than 3 torr no signals are observed. The particularly interesting feature of higher pressure (i.e., > 1.8 torr) injection experiments is the time behavior of the emitted signals.

The signal is observed to consist of two distinct pulses separated in time. The multi-pulse observation varies from pulse to pulse and cannot be reliably reproduced. The pulse occurring first is slightly delayed but overlaps in time with the infrared pump laser pulse. The later pulse amplitude and delay is relatively constant and is believed to be the usual microwave emission. The frequency dependence of the earlier

pulse on the injected microwave signal was observed to be shifted toward the higher frequency end (i.e., $\sim$ 22.69 GHz) of the emission bandwidth.  The observation of the earlier pulse is consistent with the results of Kim,[1] and will be considered in the discussion of results section.

The injection of single frequency microwave radiation into the optically pumped $^{14}NH_3$ has produced results that could be studied more effectively using a different cell.  An investigation of more importance to this study is tunability and stability of the optically pumped microwave emission.

### Heterodyne Frequency Measurements of Tunability and Stability of the Optically Pumped Microwave Emission

Heterodyne frequency measurements provide a straight-forward method of determining if a signal is tunable.  The equipment required for a heterodyne detector[10] are a mixer, and a local oscillator.  The OKI klystron is used as the local oscillator and a 1N26B diode is used as the mixer (D2 in Figure 2).  The klystron is operated in the fixed frequency mode and the cavity is tuned until a beat note is observed on the 200 MHz bandwidth TEKTRONIX 475 oscilloscope.  Care was taken to avoid injection effects during the heterodyne measurements.  This was achieved by padding the cell with considerable attenuation A2 and adjusting DS2 for minimal coupling.  No injection effects were observed at D3.

Some observed beat frequencies are shown in Figure 8.
The oscilloscope photographs were taken at different cavity
micrometer settings (X). An interesting feature observed during
the first 0.5 μsec is the obviously different period of the
beat frequency. Careful examination of this is inconclusive
at best, the beat is reproducible but not understood. Figure 9
is a slightly different presentation of the data in Figure 8.
The number of beat frequency peaks were counted and divided by
the time interval (neglecting the first 0.5 μsec) to obtain an
approximate beat frequency and plotted as a function of cavity
setting. The resulting curve is linear to within the accuracy
of the measurement in agreement with the expected result. (See
Appendix Al for details on linearity of cavity tuning).

The method used above is a quick and dirty technique to
demonstrate tunability. Stability of the microwave emission
was examined and surprisingly stable reproducible beats were
observed. The stability of the beat note is surprising because.
no attempt has been made to frequency stabilize the experiment.
Recently, Fetterman, et al.[11] performed "real-ti ,ectral
analysis for FIR laser pulses" using a surface acoustic wave
(SAW) reflective array compressor (RAC) device. Bob Miller,
a member of this laboratory, is currently working on a similar
project. The optically pumped microwave emission observed
and the heterodyne detection system already being used suggested

58



X = .711          X = .705

IN26B MIXER OUTPUT

X = .695          X = .685

X = .675          X = .655

t = .5 μsec/div
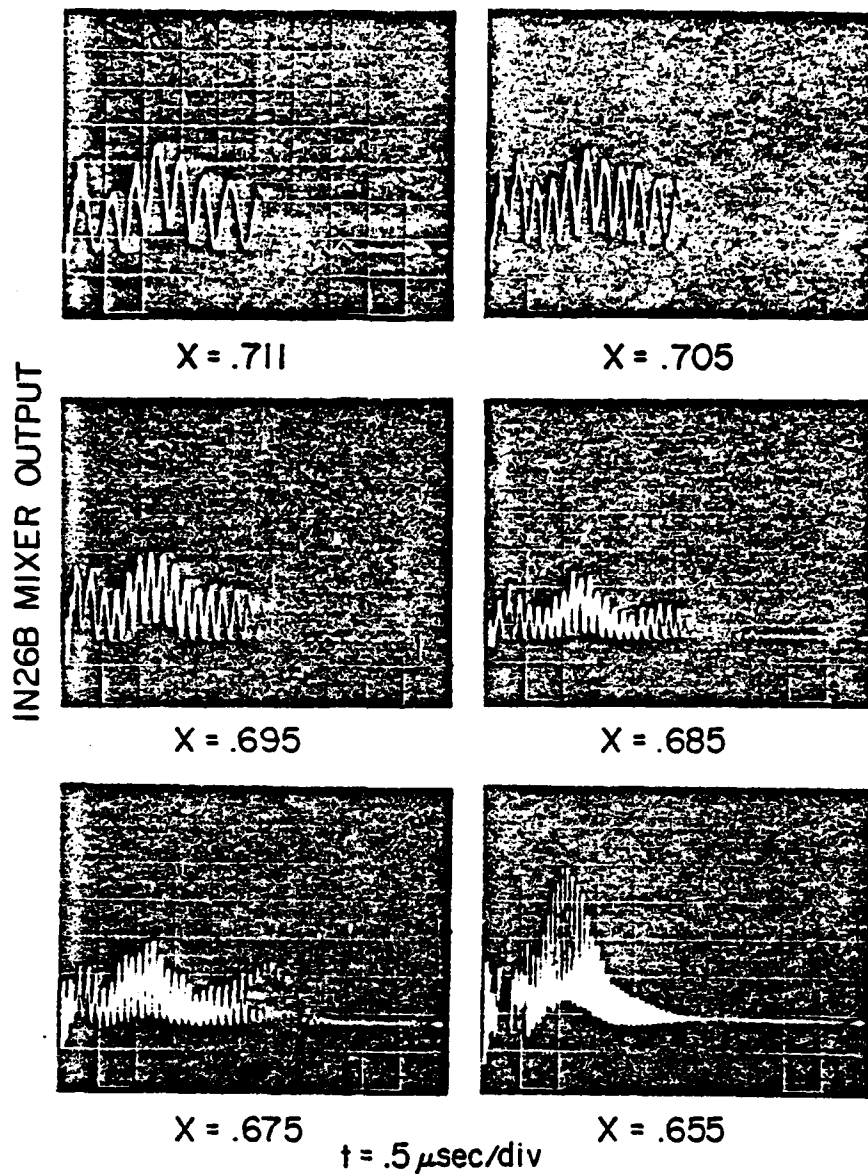
G:sQ(5,4)  $^{14}$NH$_3$ at .54 torr

LOCAL OSCILLATOR FREQUENCY 22.670 GHz

Figure 8.  Oscilloscope trances of observed beat notes at dif-
ferent cavity length settings.  G:sQ(5,4) emission
in TE$_{11n}$ (n=68) mode.

easy implementation of a spectral analysis system. The system used was set up with the help of Bob Miller.

A block diagram of the resulting real-time spectral analysis data acquisition system is shown in Figure 10. The specifications for the Raytheon RAC device are:

$f_o$ = 60 MHz

Bandwidth = 6 MHz ≡ B

Dispersion Time = 20 μsec ≡ T

Number of Resolvable Frequencies 11

Frequency Resolution 0.55 MHz

Minimum Pulse Width 0.667 μsec

Maximum Pulse Width 1.217 μsec

The RAC device acts as a linearly dispersive delay line with the center frequency $(f_o)$ being delayed T/2. The bandwidth divided by the dispersion time (i.e., B/T) gives the dispersion rate (= 0.3 MHz/μsec). Thus if one were to apply a single frequency pulse with the correct frequency $(f_o)$ and pulse width $(t_{min} < t_p < t_{max})$, the Fresnel transform of the pulse will be the output of the RAC device. (For further details, see Refs. 11, 12 and 13). The advantage of using the RAC device to measure the frequency tuning is the linearity of the delay with respect to frequency. Frequency stability measurements become much more quantitative than the observations mentioned previously.
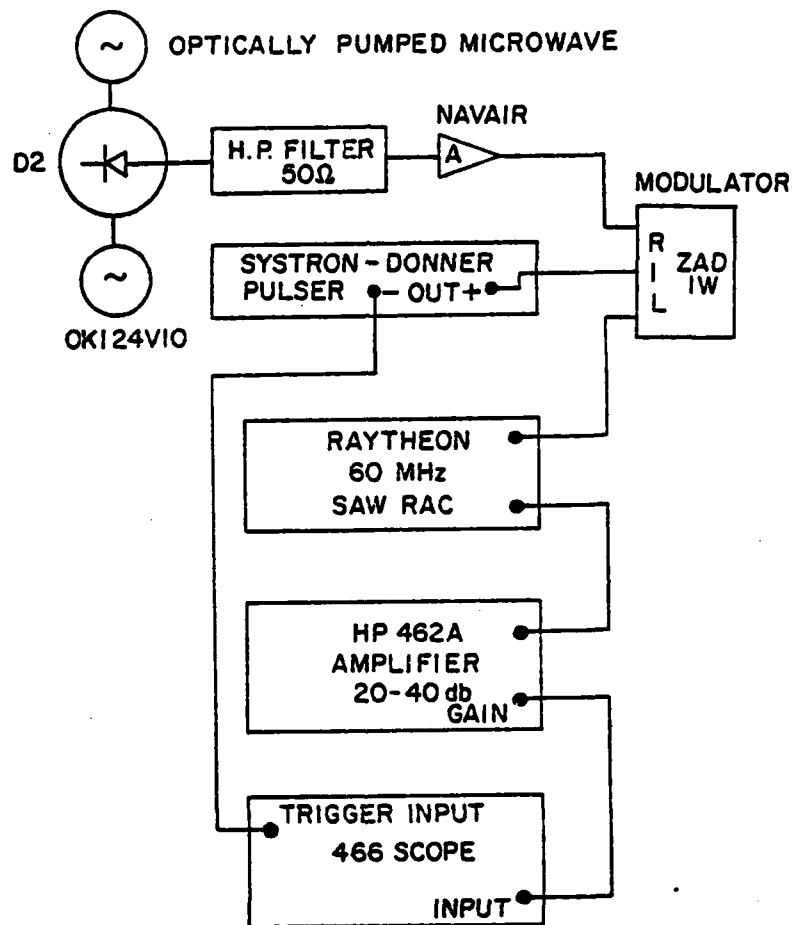
Figure 10.  Real-time spectral analysis of the optically pumped microwave emission block diagram.

Cavity tuning of the optically pumped emission demonstrated a linear dependence of frequency with length in agreement with Figure 9 and Appendix A2. The study of cavity tuning length actually requires a much wider bandwidth RAC device than the 6 MHz bandwidth device used. A 6 MHz bandwidth corresponds to tuning the cavity length approximately 0.025 inches for the 22.66 GHz $TE_{11n}$ (n=67) mode. The measured change in cavity length was 0.028 inches, in good agreement with expected value.

The most impressive results obtained with the 60 MHz RAC device are shown in Figure 11. The microwave emission was gated by a 1 μsec pulse from the triggered SYSTRON-DONNER pulser applied to the moduator in Figure 10. The gate was delayed past the initial 0.5 μsec of the pulse. The photographs shown are the amplified output of the 60 MHz RAC with a local oscillator frequency of 22.605 GHz and a fixed cavity length setting (micrometer reading = 0.305). Each photograph in Figure 11 is a recording of the tenth consecutive pulse. The pulses not recorded exhibit the same stability. The shape of the curves resembles the (sinx)/x frequency distribution expected for square wave pulse input.[13] The results indicate frequency stability of the optically pumped microwave emission, to well within 1.5 MHz over 60 consecutive shots. This is indeed impressive because no attempt to frequency stabilize any part of

62
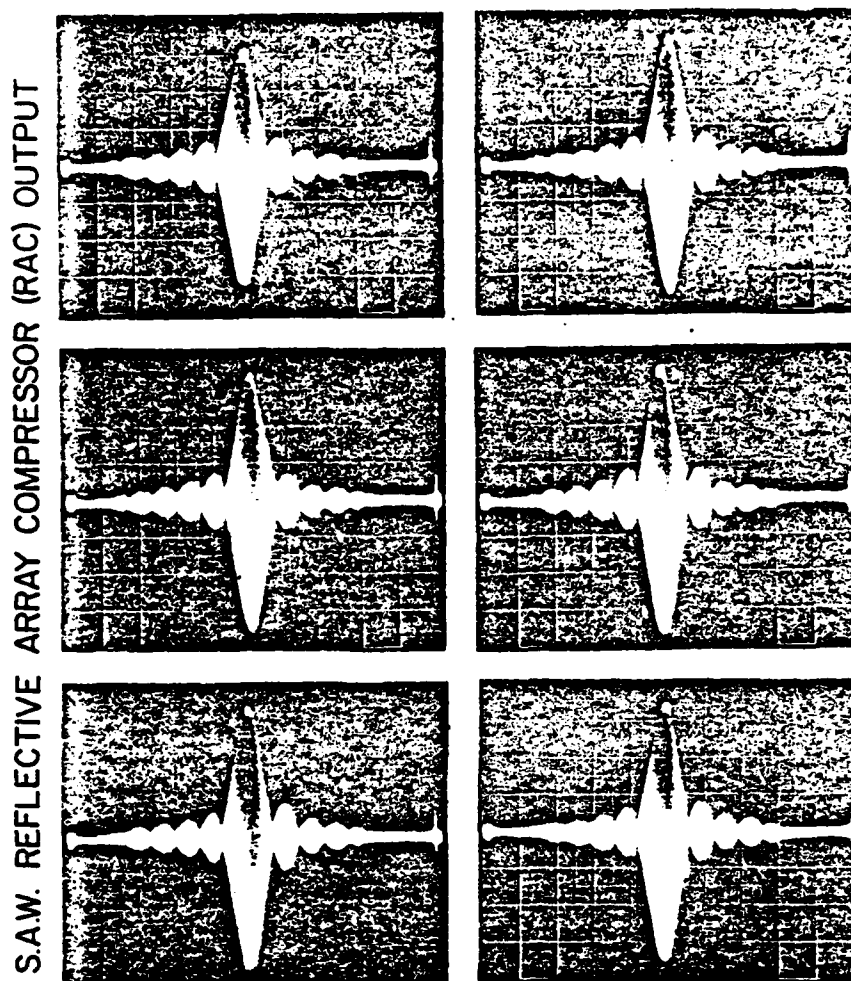


Y = .1 V/div    t = 5 $\mu$sec/div — 1.5 MHz/div

G:sQ(5,4)   $^{14}NH_3$ at .96 torr

LOCAL OSCILLATOR FREQUENCY 22.605 GHz

X = .305

Figure 11.   Oscilloscope traces of real-time spectral analysis
of the optically pumped microwave emission.  Each
photo represents the tenth consecutive pulse.

the system, including the OKI 24V10 klystron was made. Chang-
ing the pump laser power and cell pressure affected the en-
velope of the resulting real-time spectra, but did not change
the observed beat frequency.

It was initially hoped that the index of refraction ef-
fects could be measured with the RAC device, however, the
index changes are so small that no frequency shift larger than
the possible experimental error could be observed over the
emission operating pressure range. A much longer cell length
may be required to obtain a measurable frequency shift.

The surface acoustic wave RAC device has been used to
demonstrate the high level of frequency stability of the opti-
cally pumped microwave emission. The use of a wider bandwidth
(i.e., 100 MHz bandwidth) RAC would provide more detailed in-
formation regarding the emission bandwidth and linearity in
cavity tuning of the pumped emission. The power of real-time
spectral analysis using this technique cannot be overrated.

## Discussion of Results

The results observed in these experiments, present an
alternative method to generate $NH_3$ maser emission. Similar
results have been obtained for the G:sQ(2,2) transition pumped
by the $CO_2$ R(8)$_{10}$ laser line. Cavity scans for this system are
shown in Figure 12. The emission is attributed to the same
type of process.

64
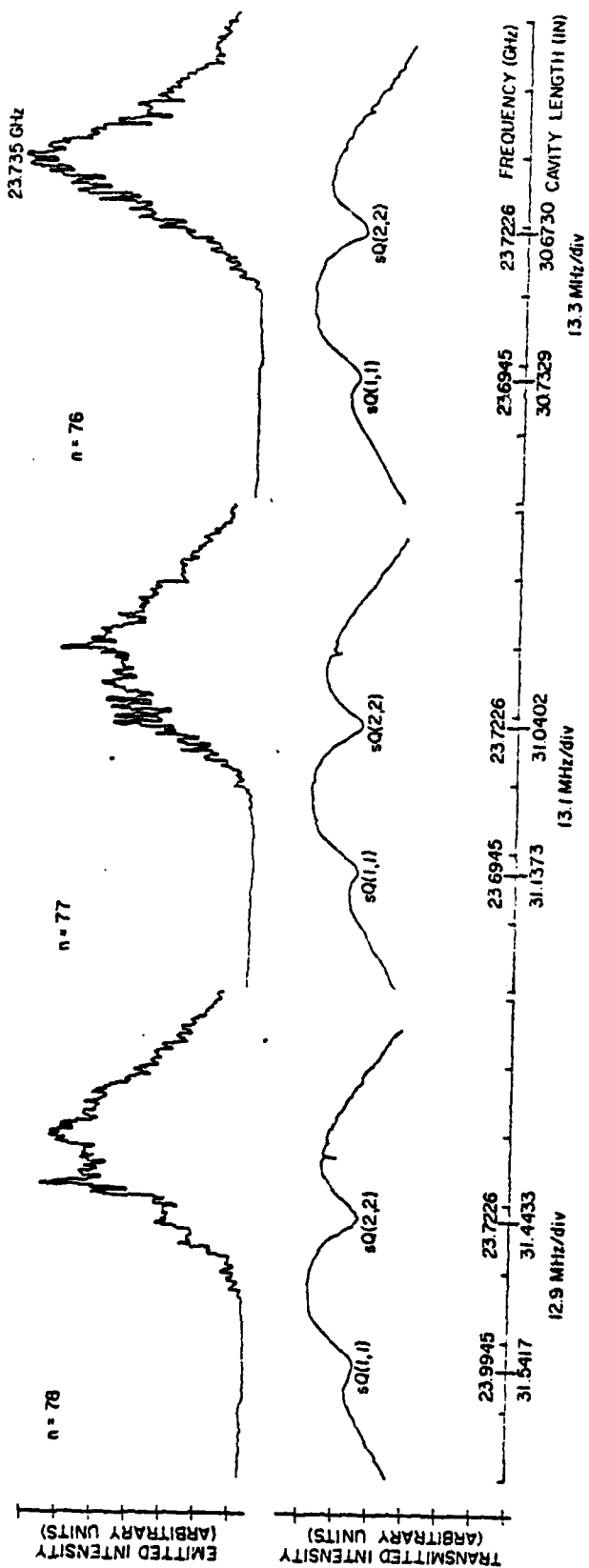


Figure 12. Cavity scans of the $G:sQ(2,2)$ emission (upper curves) and microwave absorption calibration scans (lower curves). The cavity scan length is 0.0452 in/div. The cavity emission modes are $TE_{11n}$ (n=76,77,78). The pump laser is $CO_2$ $R(8)_{10}$, $E_L$ = 80mJ, $^{14}NH_3$ pressure is 1.1 torr.

The microwave emission is attributed to a linear cascade lasing process. The data supporting this includes: 1) the distinctive time delay between the pump laser and the observed emission; 2) the observed emission bandwidth; 3) the frequency stability of the microwave emission; and 4) decoupling of the microwave emission from the FIR emission.

The distinctive delay associated with the initiation of the gain switched microwave emission is a characteristic of cascade emission. The delay has a very weak dependence on cell pressure as can be observed in the time synchronized photos (traced) of Figure 5. The frequency stability of the emission is partially caused by the decoupling of the infrared pump laser pulse. The emission center frequency would exhibit dependence on the infrared pump power. Observations made during several different power runs indicate decreased amplitude stability by lowering the pump power. The location of the emission center frequency does not change.

The microwave emission and FIR emission were simultaneously monitored during several cavity scans. No obvious correlation was observed between the microwave and FIR. The observed decoupling further supports the linearity of the emission.

The bandwidth of the observed microwave emission is saturated and homogeneously broadened. The CW two-photon pumped FIR laser observed by Willenberg[8] exhibits the Doppler

broadened width of the two-photon pump transition. The same behavior would be expected for a single photon optically pumped emission. No evidence of non-linear behavior has been observed for the G:sQ(5,4) emission so the emission is believed to be linear.

The linear emission is different than that observed by Kim and Coleman,[1] but their results provide additional understanding needed to explain some of the observed results.

The microwave emission can be theoretically modeled using a single-photon two-level density matrix formalism. The density matrix theory treats the coherence between the energy levels coupled by the maser field. For a comprehensive explanation of density matrix theory, see Refs. 14, 15 and 16. The detailed derivation of the complex susceptibility is outlined in Section 8.1 of Ref. 16. Two differences in the G:sQ(5,4) system and the single-photon two-level calculation assumptions should be noted. The treatment in reference 16 assumes only two levels are involved in the interaction, the experimental system actually consists of degenerate energy levels. There are eleven degenerate M values (i.e., 2J+1, J=5) for the upper and lower levels. The presence of the G:sQ(4,3) transition may also effect the two level assumption. The remaining assumptions are consistent with the experiment. The imaginary and real parts of the susceptibility are given in Equations (2) and (3).

$$\chi''(\omega) = \frac{\mu^2 T_2 \Delta N_o}{\varepsilon_o \hbar} \frac{1}{1 + (\omega-\omega_o)^2 T_2^2 + 4\Omega^2 T_2 T_1} \tag{2}$$

$$\chi'(\omega) = \frac{\mu^2 T_2 \Delta N_o}{\varepsilon_o \hbar} \frac{(\omega-\omega_o) T_2}{1 + (\omega-\omega_o)^2 T_2^2 + 4\Omega^2 T_2 T_1} \tag{3}$$

$\Delta N_o$ - Population difference at zero field

$T_2 = T_1 = 1.326 \times 10^{-8}$ sec-torr

$\Omega = \mu E_o / 2\hbar \equiv$ Precession (Rabi) frequency

The absorption/gain can be calculated from the imaginary part of the susceptibility and the index of refraction may be calculated from the real part. The importance of equations (2) and (3) is the resulting Lorentzian line shape of the absorption/gain. This width is 23 MHz/torr for $^{14}NH_3$ ground state inversion transitions. A consequence of saturation is broadening of the Lorentzian line shape given by Equation (4)

$$\Delta\nu_{SAT} = \Delta\nu \sqrt{1 + \frac{\mu^2 E_o^2 T_2 T_1}{\hbar^2}} \tag{4}$$

The problem with using this model is that the frequency shift of the microwave emission observed in the cavity scans is not explained.

The emission frequency shift observed in the cavity scans is believed to be the result of the time dependent gain observed during the microwave injection experiments. The

results of Kim indicate strong gain occurring during the presence of the infrared pump pulse. Figure 13 (reproduced from Kim's paper) gives the AC Stark shifted laser and Raman frequencies as a function of the laser power density. The laser frequency peak is always shifted to a higher frequency for the G:sQ(5,4) system. If the emission level occurring during the laser pulse was lower than the noise level (i.e., non-detectable), injection locking of the observed emission by the non-detectable emission could occur. The large delay and gain switched pulse shape of the microwave emission would tend to disprove this explanation.

The cavity scans produce emission bandwidth greater than the homogeneous linewidths. Equation (4) can be used to determine the Rabi frequency and hence relative field strengths of the microwave emission. The calculation results are:

| PRESS(torr) | $\Delta\nu_H$ (MHz) | $\Delta\nu_{SAT}$ (MHz) | $\frac{\mu E}{\hbar}$ (MHz) | $\frac{\mu E}{\hbar}\Delta\nu_H$ |
|---|---|---|---|---|
| .49 | 11.27 | 19.6 | 31.77 | 2.819 |
| .71 | 16.33 | 24.8 | 38.56 | 2.36 |
| .91 | 20.93 | 31.7 | 49.23 | 2.35 |

Using the measured emission linewidth at 0.91 torr and neglecting the M degeneracy, a circulating power density of 0.54 watts/cm$^2$ is calculated. The ratio of the Rabi to the homogeneous linewidth is the measure of saturation. The results
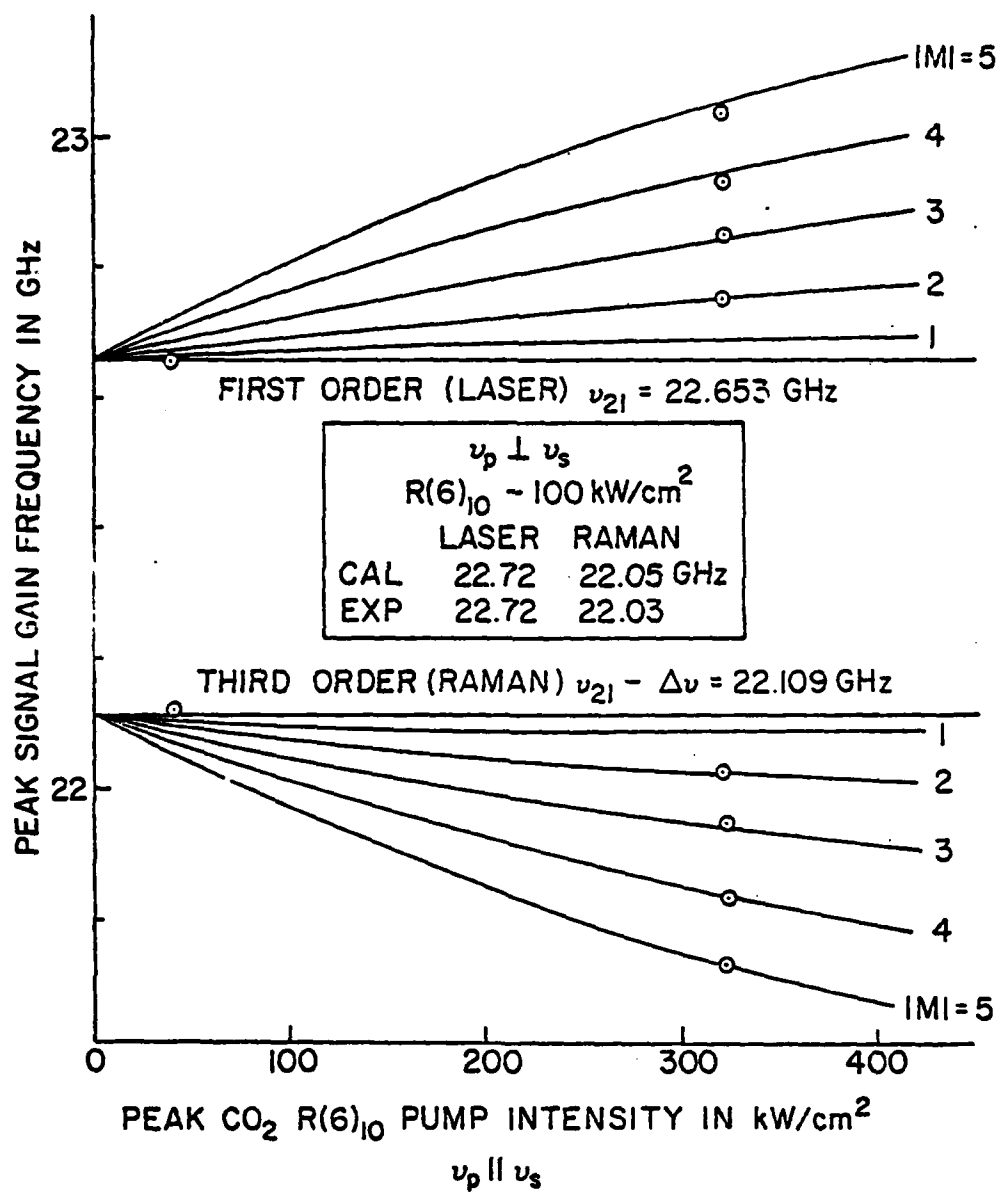
Figure 13. M-splittings of gain frequency peaks with pump intensity for gain experiment G:sQ(5,4).[1]

of microwave injection experiments concerned with saturation agree with the cavity tuning results in that the degree of saturation decreases with increasing pressure. The saturation, tunability, and frequency stability suggest the observed emission may be a valuable tool as a source to study other processes in $^{14}NH_3$.

## Conclusions

Microwave emission attributed to a linear cascade effect has been observed from $^{14}NH_3$ optically pumped by a TE-$CO_2$ laser. The emission is tunable over the saturated homogeneous linewidth (i.e., > 24 MHz/torr) and exhibits a high degree of frequency stability. The output power density determined from the saturated emission bandwidth is 0.54 watts/cm$^2$ at 0.91 torr. The observed emissions are assigned to G:sQ(5,4) and G:sQ(2,2) ground state inversion transitions.

There are many other candidate systems for which this type of microwave emission should be observed. The criterion for a candidate system is: 1) a laser-$^{14}NH_3$ absorption match with a frequency mismatch less than 1.5 GHz, 2) the lower level of the $NH_3$ absorption must be the symmetric energy level of the inversion doublet, 3) the inversion doublet exists (i.e., $K \neq 0$). The obvious candidates are the laser-absorption matches that produce optically pumped FIR emission. Appendix A1 includes

a "match list" to be examined for possible candidates. Only $^{14}NH_3$ has been considered in this investigation, further study should produce similar results for other molecules with inversion symmetry.

72

V.  INTERACTION BETWEEN MULTIPLE GENERATED LASER SIGNALS IN
    OPTICALLY PUMPED FAR IR SYSTEMS - W. Lee

## Introduction

Single-photon pumping of gaseous molecules to generate
IR or FIR radiation has been analyzed usually by the density
matrix calculation of a two-wave three-level system.[1]  The
processes being studied consisted of one-photon (lasing) and
two-photon (Raman) interactions.  For multi-line emission, how-
ever, the simple model becomes inadequate.  As shown in Fig-
ure 1, the pump P generates emissions $E_1$ and $E_2$ either directly
or by a cascade process.  When $E_1$ and $E_2$ are weak, there is
negligible interaction between them and the system can be con-
sidered as two independent, two-wave, three-level systems.  As
the signals $E_1$ and $E_2$ increase, the emissions will affect each
other through two-photon and three-photon processes.  To
study the coupling between the signals, a density matrix cal-
culation has been applied to a three-wave four-level system in
$NH_3$.

## Emission Coupling in Optical Triple Resonance

In triple resonance systems, studies have been reported
on the hyper-Raman[2,3] and Raman[4] processes.  The nonlinear
effects on the emission was investigated with fixed detuning
of the other two waves.  When there are two emissions, the de-
tuning of one of them will be affected by the detuning of the
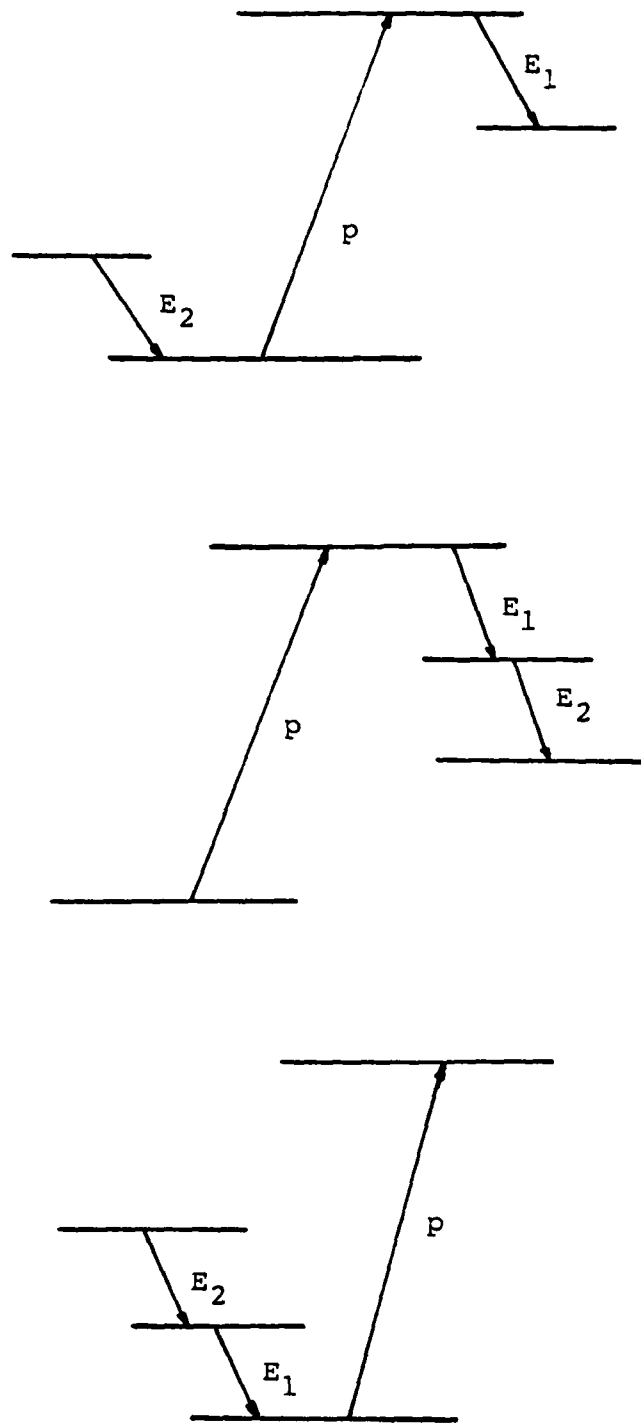
Figure 1.  Triple resonance by single-photon pumping.

other one and vice versa. Because there is no direct way to determine the detuning of any one of the emissions when they are both strong, the problem becomes very tedious to solve. That is, the detuning of $\Delta_1$ of Emission $E_1$ as a function of detuning $\Delta_2$ of emission $E_2$, i.e., $\Delta_1 = \Delta_1(\Delta_2)$ has to be found, and similarly for $\Delta_2 = \Delta_2(\Delta_1)$. A self-consistent calculation of $\Delta_1(\Delta_2)$ and $\Delta_2(\Delta_1)$ will be given the coupling frequencies of the two emissions.

## FIR-Microwave Emission Coupling System in $^{14}NH_3$

Because the spectroscopy of $NH_3$ is well-known[5] and a tunable microwave source in the 18-26 GHz region is readily available, $NH_3$ is a good candidate for emission coupong studies.

The triple resonance system considered here is shown in Figure 2. The $R(14)_{10}$ line from a $CO_2$ TEA laser pumps the Ga(1,1) state to generate the FIR (256.7μ) emission,[6] which then induced the cascade emission of the 23.1 GHz microwave signal.[7] A tunable backward oscillator provides the microwave signal to probe the energy shifts of states G(1,1) and Gs(2,1) so that the detuning $\Delta_1$ and $\Delta_2$ can be determined.

## M-Splitting and Polarization

For the pumping transition Ga(1,1) $\to$ $\nu_2$s(2,1), the change of the angulat momentum ($|\Delta J| = 1$) implies that the preferable direction of the quantization axis $J_z$ is perpendicular to the polarization direction of the pump. Since the pump is linear
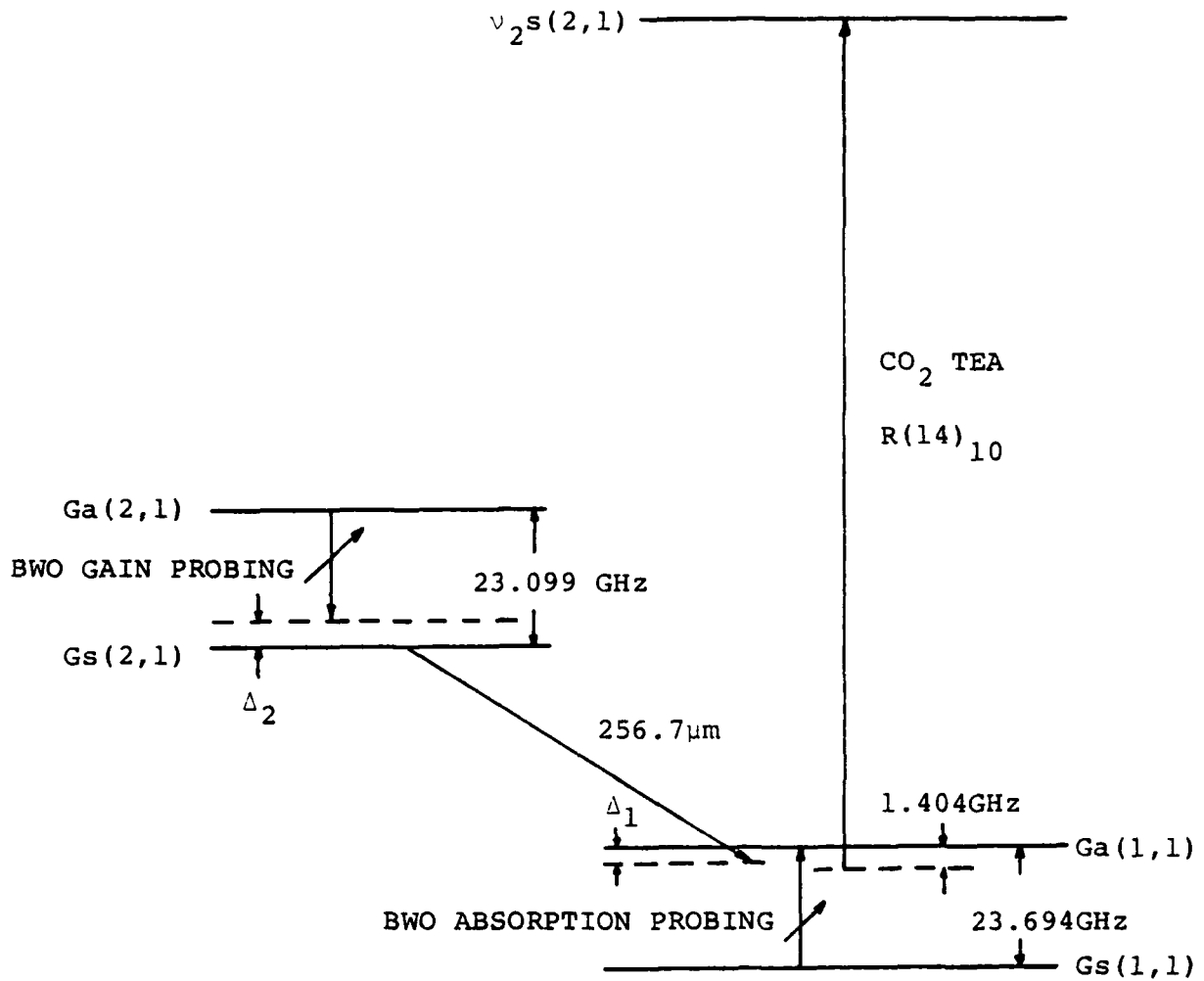
Figure 2.   Infrared, far infrared and microwave triple resonance
system for emission coupling study.

76

polarized along $\hat{x}$ or $\hat{y}$ direction, in terms of the raising and
lowering operator $J_x \pm iJ_y$, the selection rule for the M-sublevel
will be $\Delta M = \pm 1$. Similarly, the same rule applies to the FIR
transition Gs(2,1) → Ga(1,1). Due to the cell design (Section
III),the microwave will be polarized along the same direction
as the other two waves.

Using the selection rule $\Delta M = \pm 1$ for all three transitions,
it is seen that twenty transitions will be involved as listed
in Table 1. The transition matrix element between two M-sublevel
can be calculated by the Wigner-Eckart theorem.[8]

## Result of Calculations

The calculations were based on the density matrix equations
for a three-wave four-level system as described in Section III.

1) Threshold and Saturation Intensities of the Pump

Small signal gain for the FIR was plotted as a function
of its detuning from line center. The intensities of the micro-
wave and the FIR signals were set a 1 $\mu W/cm^2$, while the inten-
sity of the pump was changed from 1 $kW/cm^2$ to 400 $kW/cm^2$, as
shown in Figures 3 through 8. The negative gain peak around
zero detuning is the linear contribution. The threshold inten-
sity of the pump for generating the FIR was shown to be about
10 $kW.cm^2$ as a Raman peak appeared about 1.4 GHz detuned from
the line center in Figure 4. The Raman gain kept on increasing
with the pump intensity until the pump reached about 200 $kW/cm^2$,

Table 1. Twenty combinations of three M-sublevel transitions.

| Ga(2,1) | Gs(2,1) | Ga(1,1) | $\nu_2 s(1,1)$ |
|---------|---------|---------|---------|
| $M_1 \longleftrightarrow M_2 \longleftrightarrow M_3 \longleftrightarrow M_4$ | | | |
| 2 | 1 | 0 | 1 |
| 2 | 1 | 0 | -1 |
| 1 | 2 | 1 | 2 |
| 1 | 2 | 1 | 0 |
| 1 | 0 | 1 | 2 |
| 1 | 0 | 1 | 0 |
| 1 | 0 | -1 | 0 |
| 1 | 0 | -1 | -2 |
| 0 | 1 | 0 | 1 |
| 0 | 1 | 0 | -1 |
| $M_i \longrightarrow -M_i$ | | | |

78

IR = 1.0 kW/cm$^2$ - R(14)$_{10\mu}$

FIR = 1.0 $\mu$W/cm$^2$

$\mu$W = 1.0 $\mu$W/cm$^2$

$\Lambda$(IR) = 1.404 GHz

$\Lambda$($\mu$W) = 0

Pressure = 2.0 torr

IR

$\Lambda$($\mu$W)

FIR

$\mu$W

1.404GHz

FIR SIGNAL DETUNING (GHz)

1.8   1.2   0.6   0   -.6

0   -2.075   -4.15   -6.226   -8.301

FIR SIGNAL GAIN IN 1/M
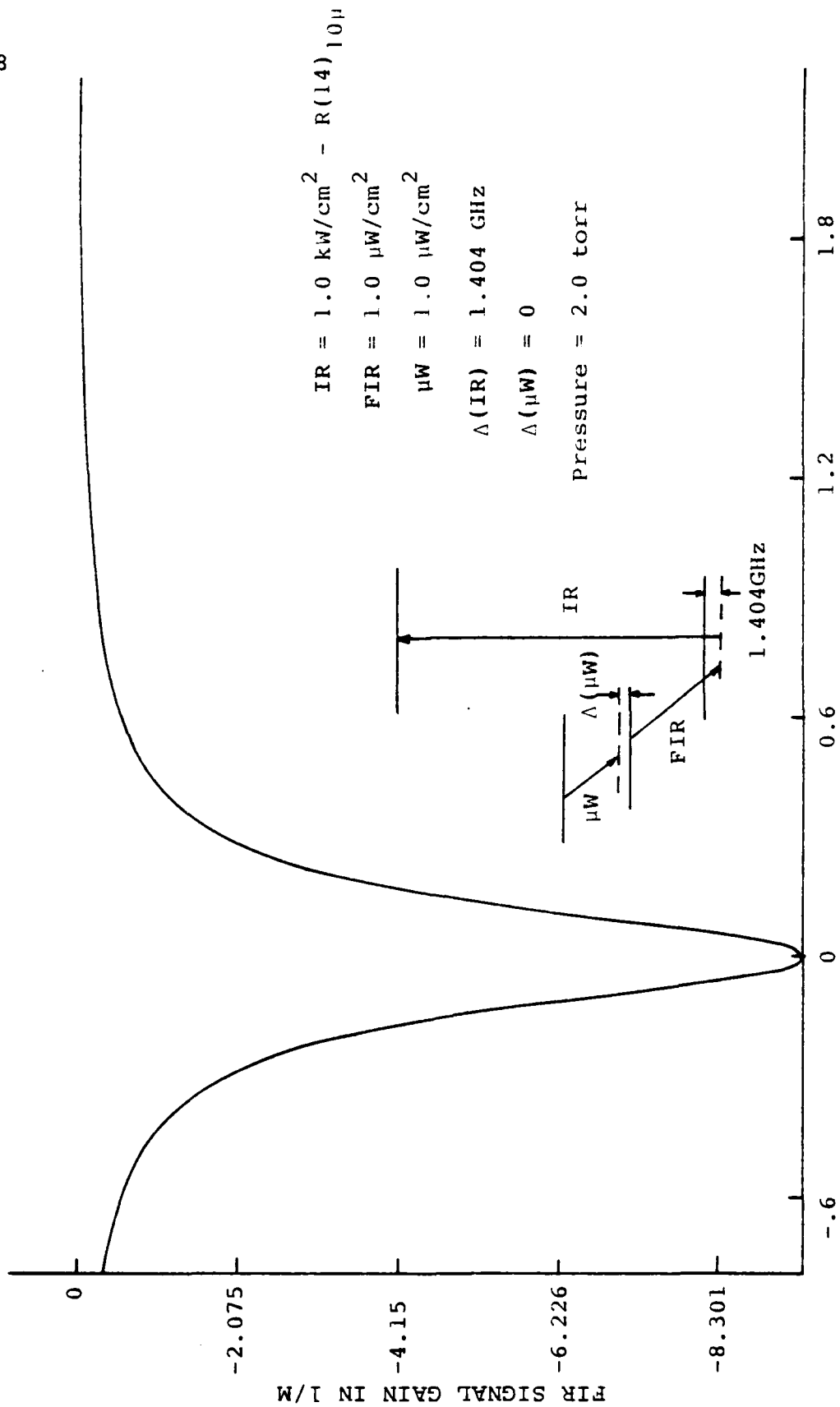
Figure 3. Gain curve for FIR pumped by R(14)$_{10}$ of 1 kW/cm$^2$ intensity.
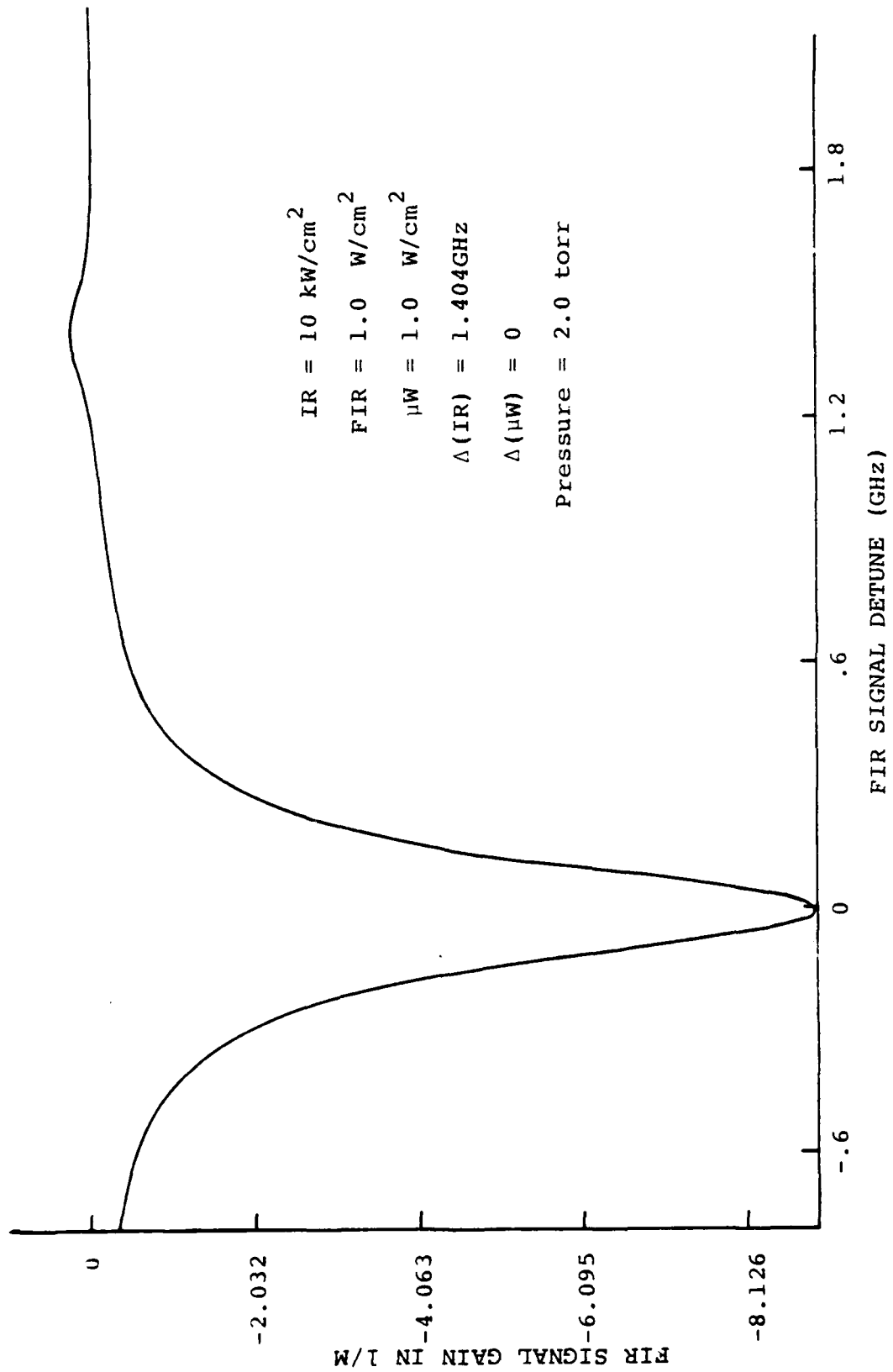
Figure 4.  Gain curve for FIR pumped by R(14)$_{10}$ of 10 kW/cm$^2$ intensity.

The figure shows a plot with:
- X-axis: FIR SIGNAL DETUNE (GHz), with markings at −.6, 0, .6, 1.2, 1.8
- Y-axis: FIR SIGNAL GAIN IN 1/M, with markings at 0, −2.032, −4.063, −6.095, −8.126

Parameters shown on the plot:

IR = 10 kW/cm$^2$

FIR = 1.0  W/cm$^2$

μW = 1.0  W/cm$^2$

Δ(IR) = 1.404GHz

Δ(μW) = 0

Pressure = 2.0 torr
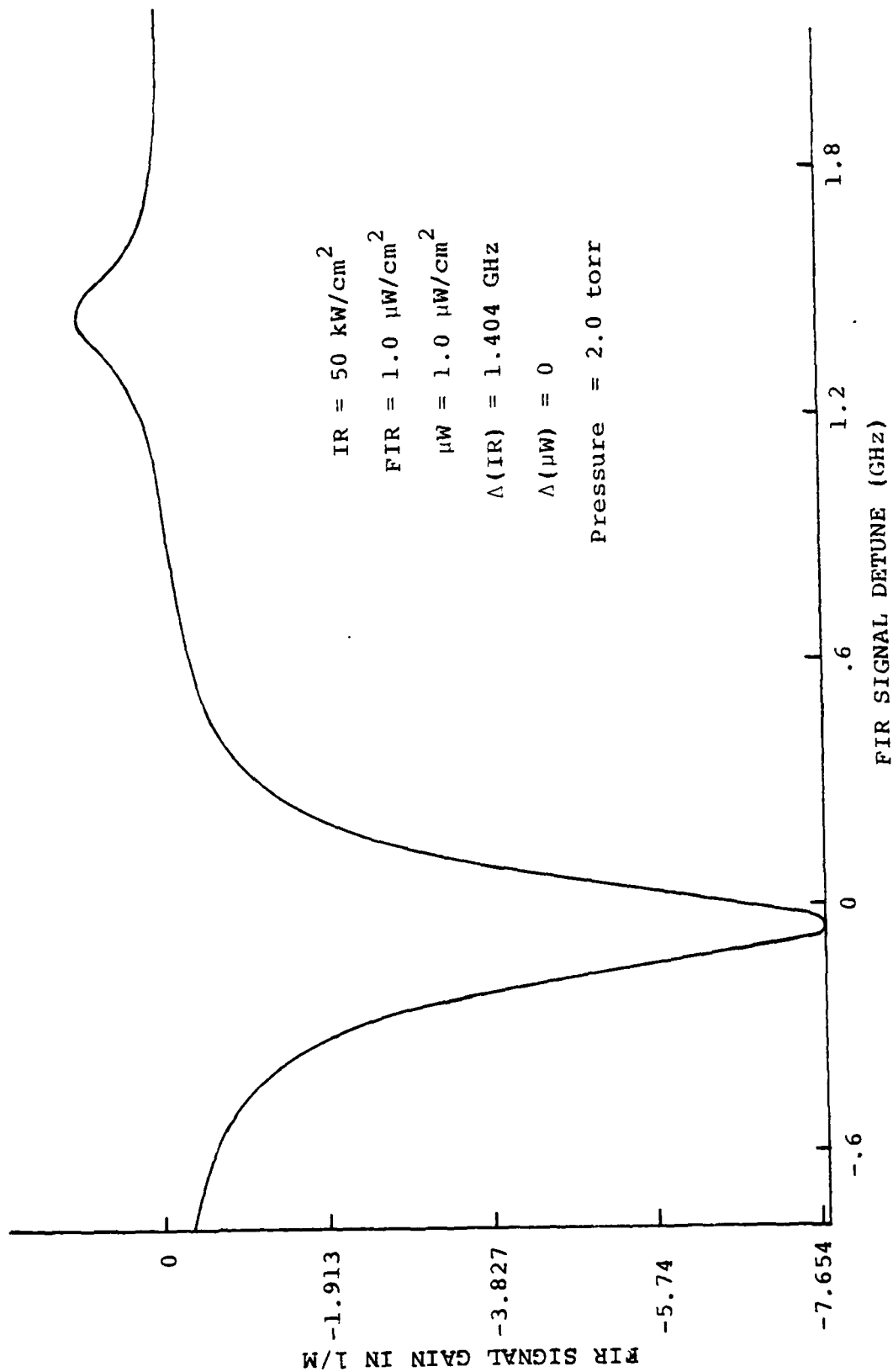
Figure 5. Gain curve for FIR pumped by $R(14)_{10}$ of 50 kW/cm$^2$ intensity.

81

**FIR SIGNAL DETUNE (GHz)**

IR = 100 kW/cm$^2$

FIR = 1.0 μW/cm$^2$

μW = 1.0 μW/cm$^2$

Δ(IR) = 1.404 GHz

Δ(μW) = 0

Pressure = 2.0 torr

**FIR SIGNAL GAIN IN 1/M**
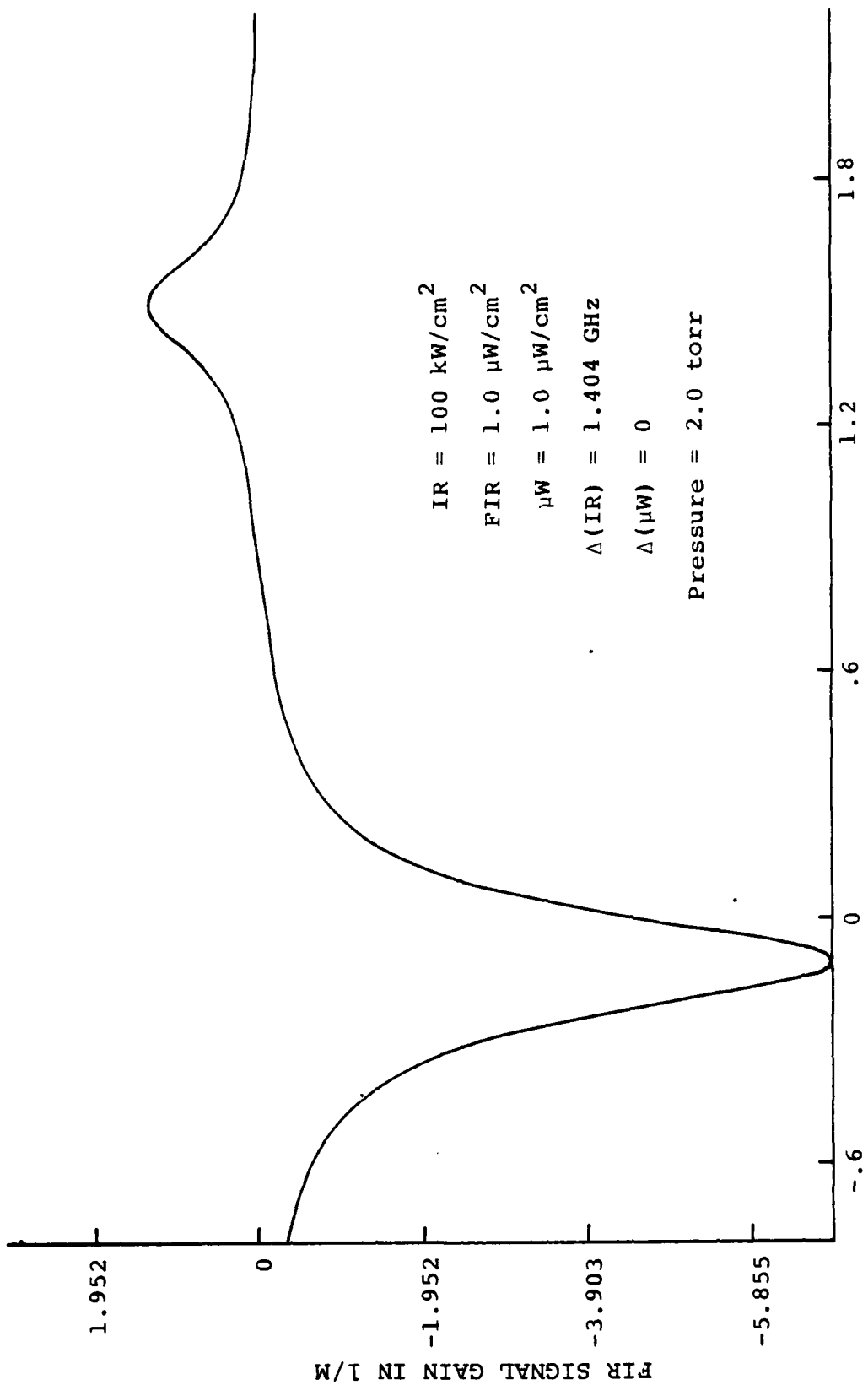
Figure 6. Gain curve for FIR pumped by R(14)$_{10}$ of 100 kW/cm$^2$ intensity.

82
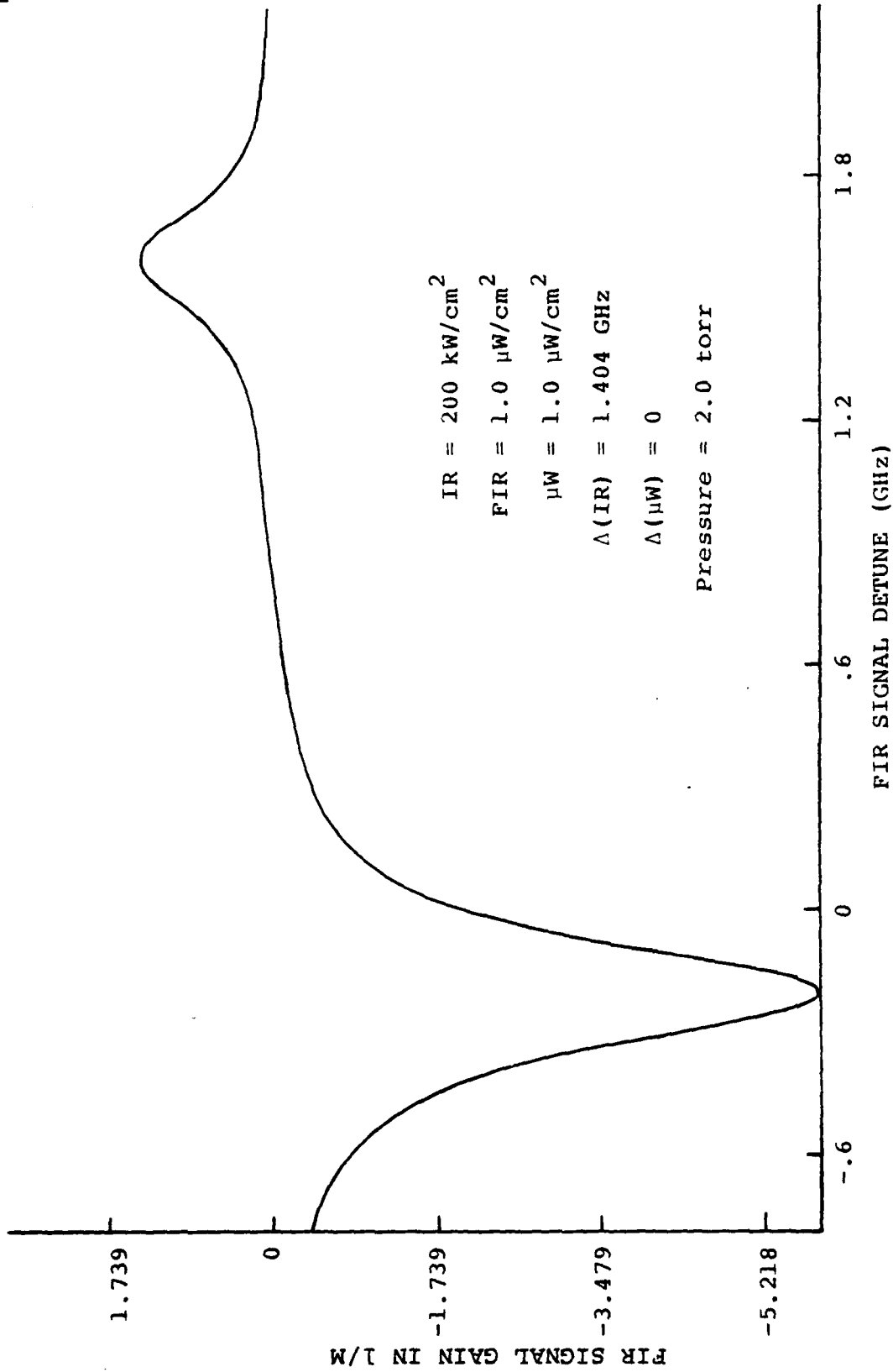


Figure 7. Gain curve for FIR pumped by $R(14)_{10}$ of 200 kW/cm$^2$ intensity.

The figure shows a gain curve with axes labeled "FIR SIGNAL DETUNE (GHz)" (horizontal) and "FIR SIGNAL GAIN IN 1/M" (vertical). Horizontal axis values: -.6, 0, .6, 1.2, 1.8. Vertical axis values: 1.739, 0, -1.739, -3.479, -5.218.

Parameters listed:

IR    = 200 kW/cm$^2$
FIR   = 1.0 μW/cm$^2$
μW    = 1.0 μW/cm$^2$
$\Lambda$(IR)  = 1.404 GHz
$\Delta$(μW)  = 0
Pressure = 2.0 torr
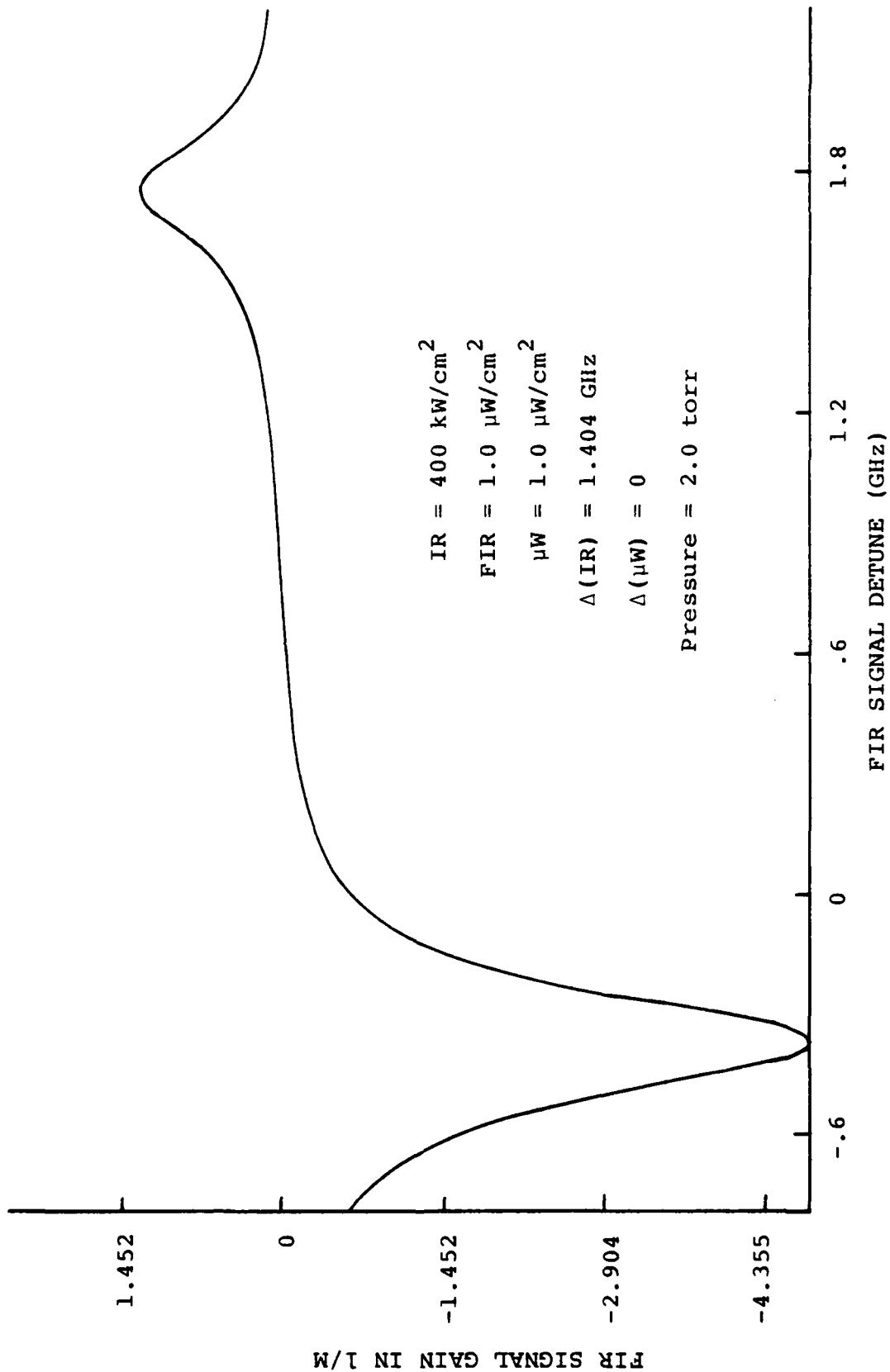
Figure 8. Gain curve for FIR pumped by $R(14)_{10}$ of 400 kW/cm$^2$ intensity.

84

which would be the saturation intensity.

2) Saturation Intensity of the FIR

Fixing the pump intensity at 200 kW/cm$^2$, changing FIR
intensity from 1 μW/cm$^2$ to 100 kW/cm$^2$ (Figure 7, Figures 9-12),
showed appreciable drop of the gain of FIR from intensity 1 kW/
cm$^2$ to 10 kW/cm$^2$. With pump depletion, optical cell losses and
limit of quantum efficiency, the FIR generation would be dif-
ficult to reach more than 10 kW/cm$^2$.

3) Microwave Spectra

Gain curves for microwave signals were plotted for three
different microwave intensities (Figures 13-15). The absorp-
tion peak at 0.9 GHz detuning is the linear contribution while
the one on the other side is the Raman contribution. The posi-
tive gain peak at -0.07 GHz is the hyper-Raman contribution.

4) FIR and Microwave Frequency Coupling

The microwave detuning was plotted as a function of
the FIR detuning shown in Figure 16 as $\Delta_{\mu W}(\Delta_{FIR})$. The same
was done for $\Delta_{FIR}(\Delta_{\mu W})$. The frequency offsets were found to
be 1.60 GHz for FIR, and -0.006 GHz for the microwave signal.

## Conclusion

The emission coupling of a triple resonance system has been
analyzed. A method of calculation, based on density matrix
equation, has been developed to reveal Raman and hyper-Raman
contribution to each of th emissions. The calculation also
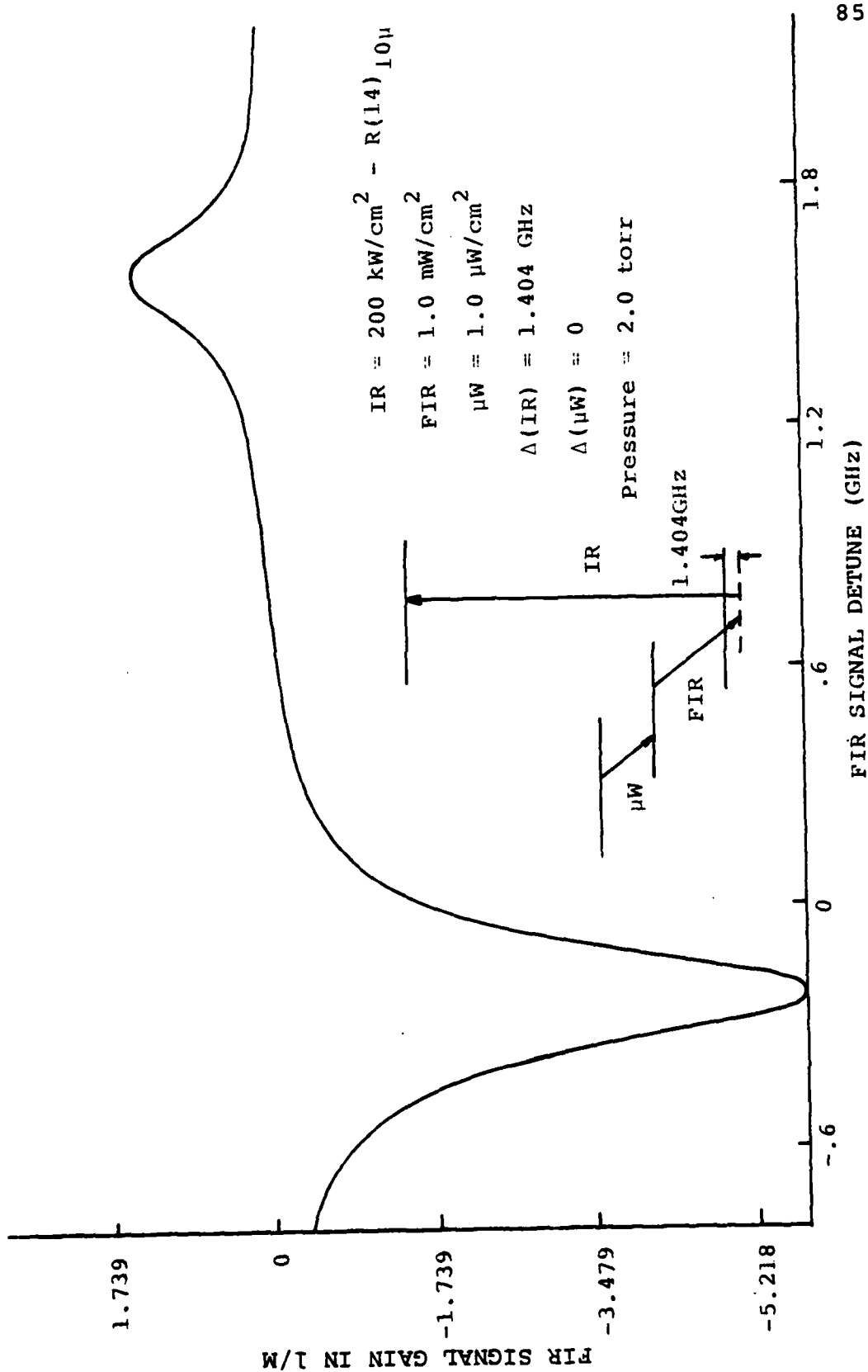
Figure 9. Gain curve for FIR of 1.9 mW/cm² intensity.

86
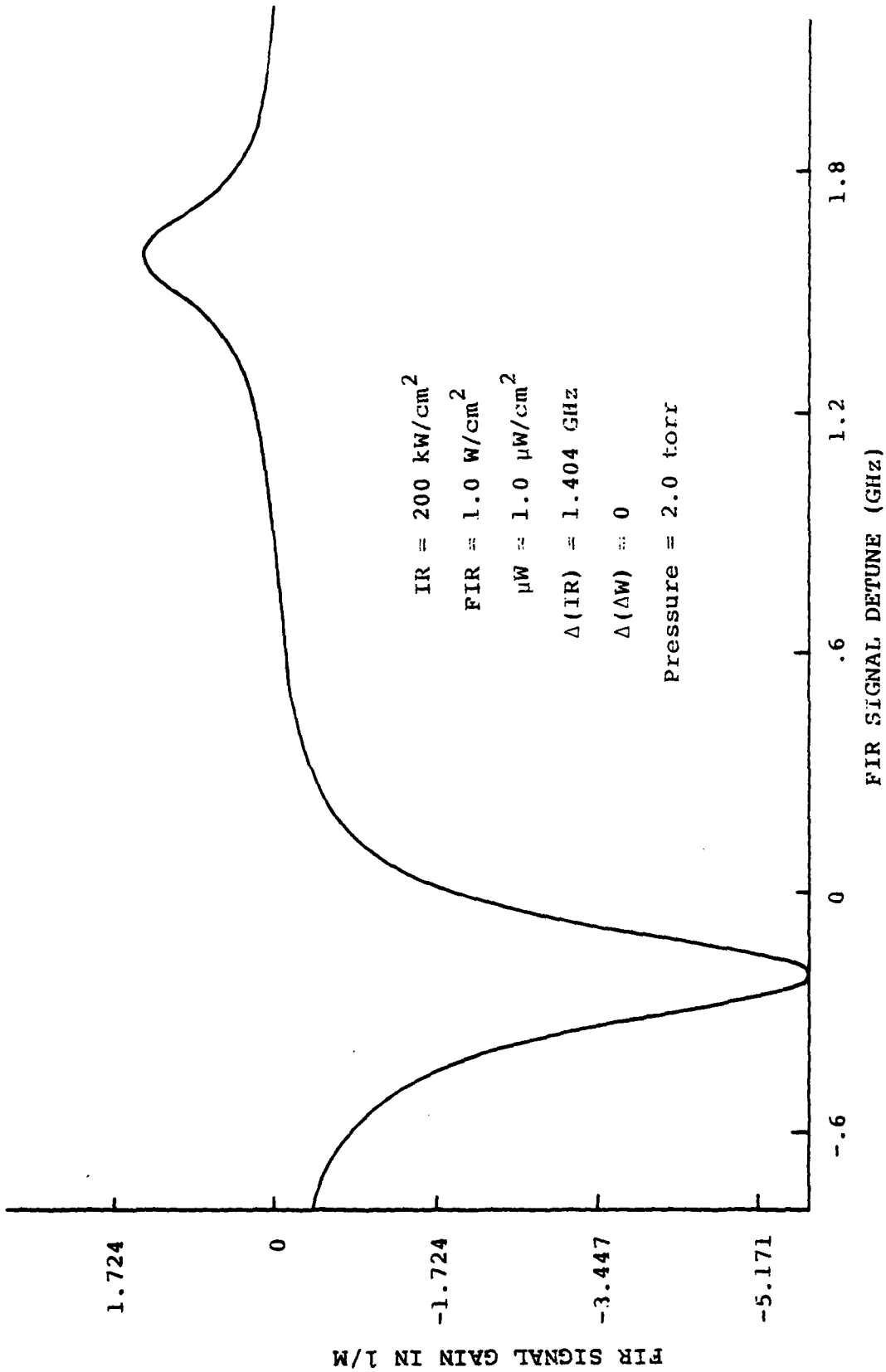


Figure 10.  Gain curve for FIR of 1.0 W/cm² intensity.
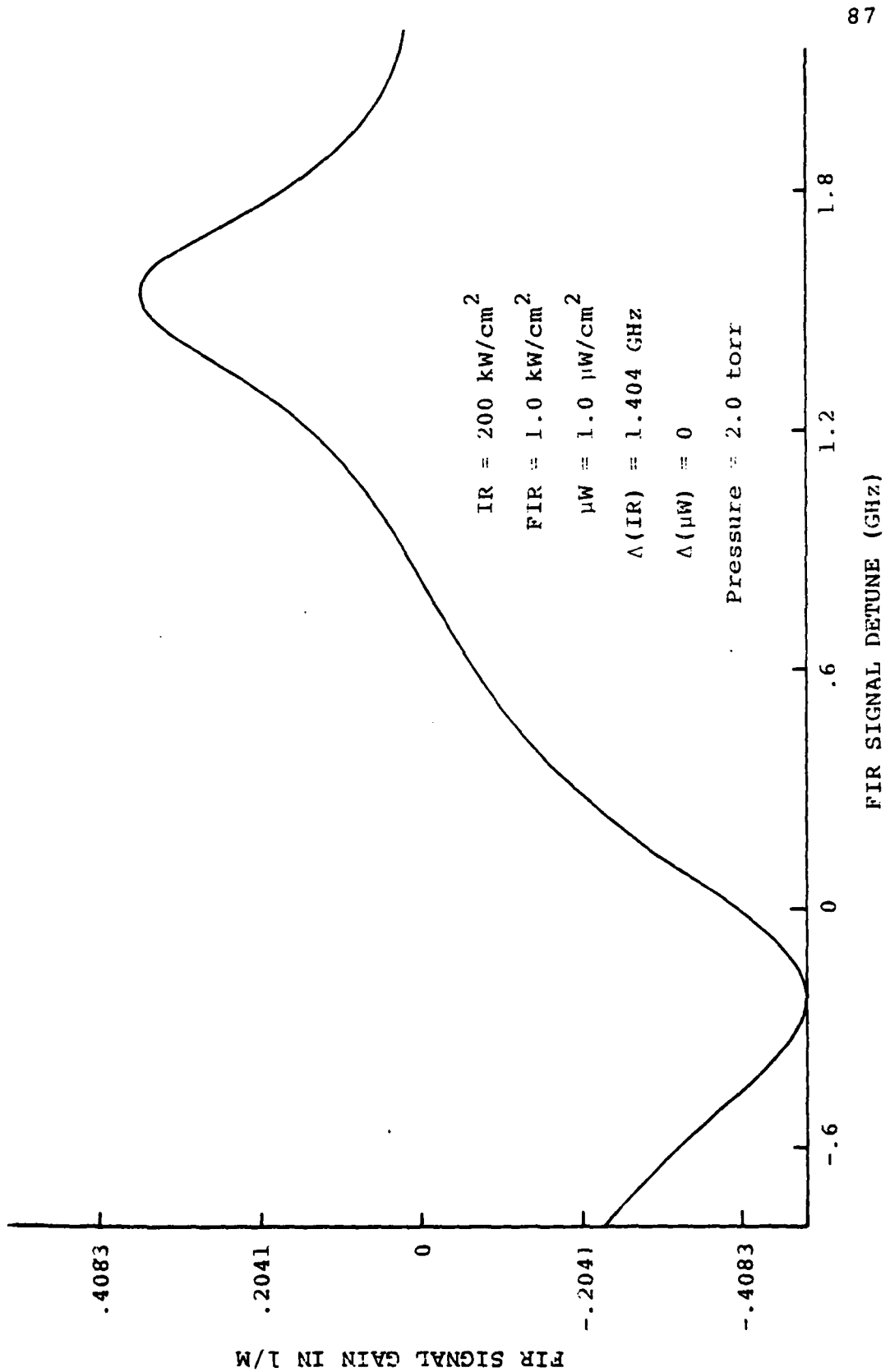
Figure 11. Gain curve for FIR of 1 kW/cm² intensity.

IR = 200 kW/cm²

FIR = 1.0 kW/cm²

μW = 1.0 μW/cm²

Λ(IR) = 1.404 GHz

Λ(μW) = 0

Pressure = 2.0 torr

88
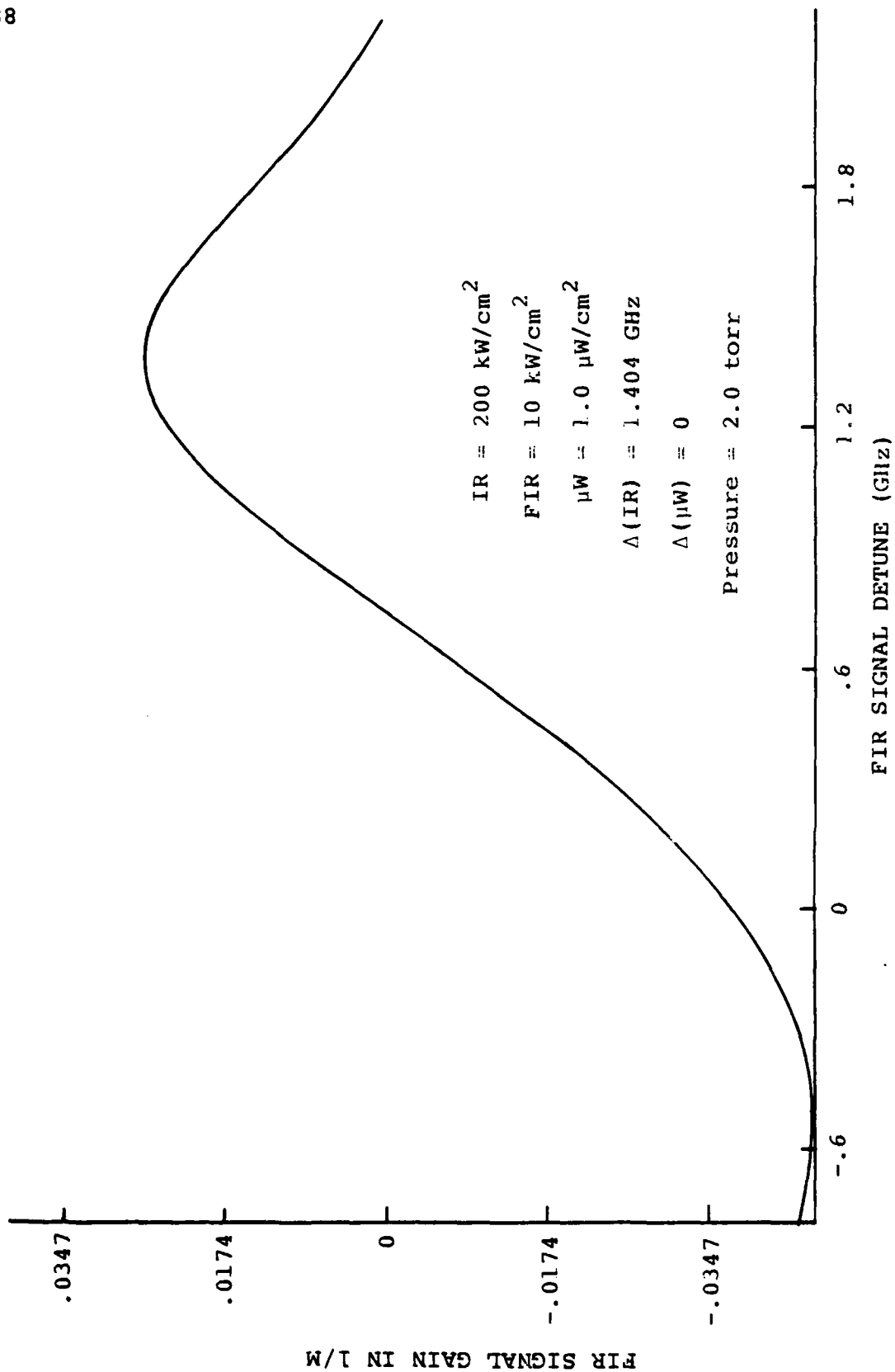


Figure 12. Gain curve for FIR of 10 kW/cm² intensity.

IR = 200 kW/cm$^2$

FIR = 1 kW/cm$^2$

μW = 1.0 μW/cm$^2$

Δ(IR) = 1.404 GHz

Δ(FIR) = 1.545 GHz

Pressure = 2.0 torr

IR

.141GHz

1.404GHz

FIR

μW

MICROWAVE SIGNAL DETUNE (GHz)

MICROWAVE SIGNAL GAIN IN 1/M

.0114

.0076

.0038

0

-.0038

2.4

1.2

0

1.2

2.4

89
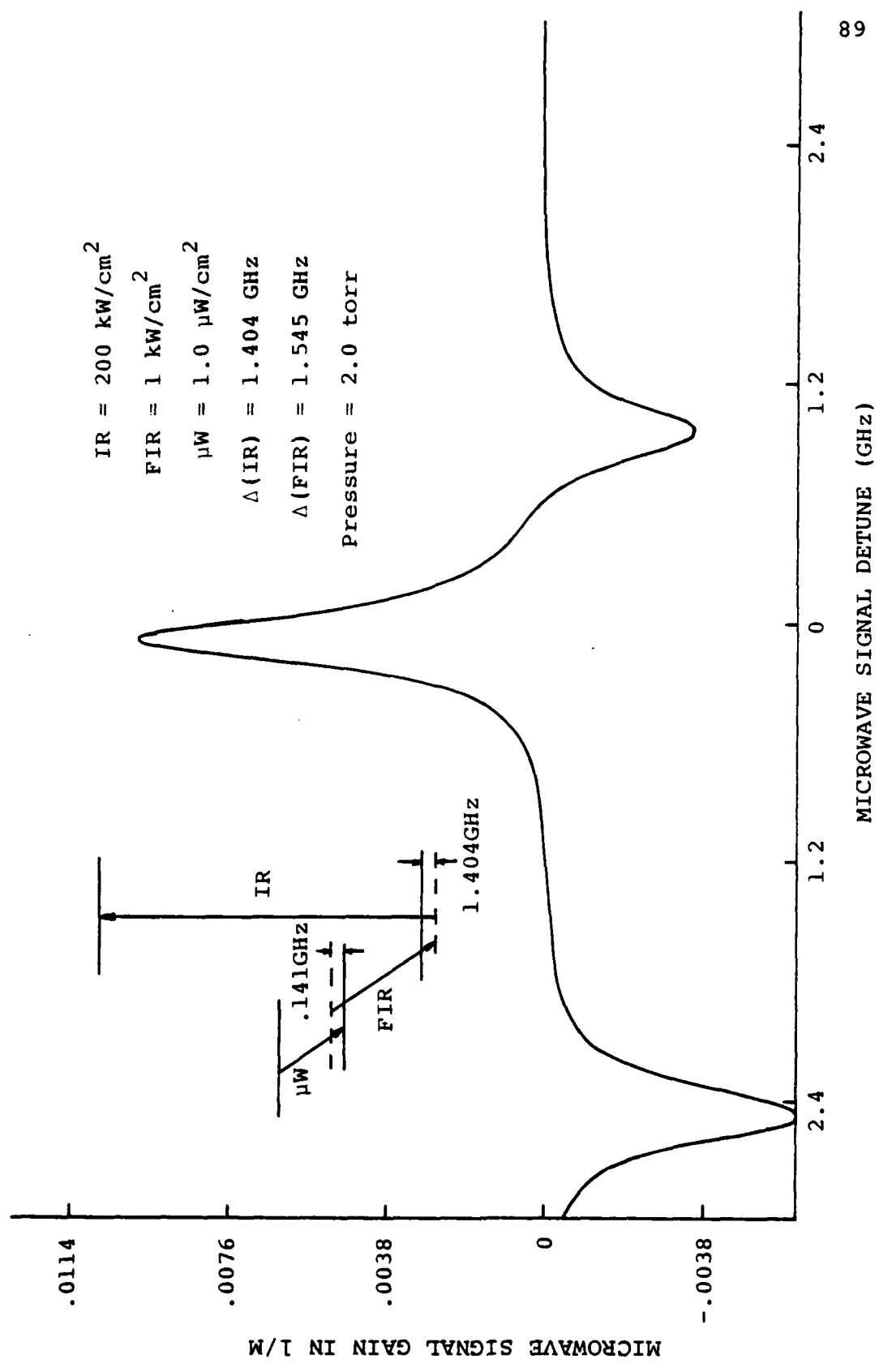
Figure 13. Gain curve for microwave of 1.0 μW/cm$^2$ intensity.

90
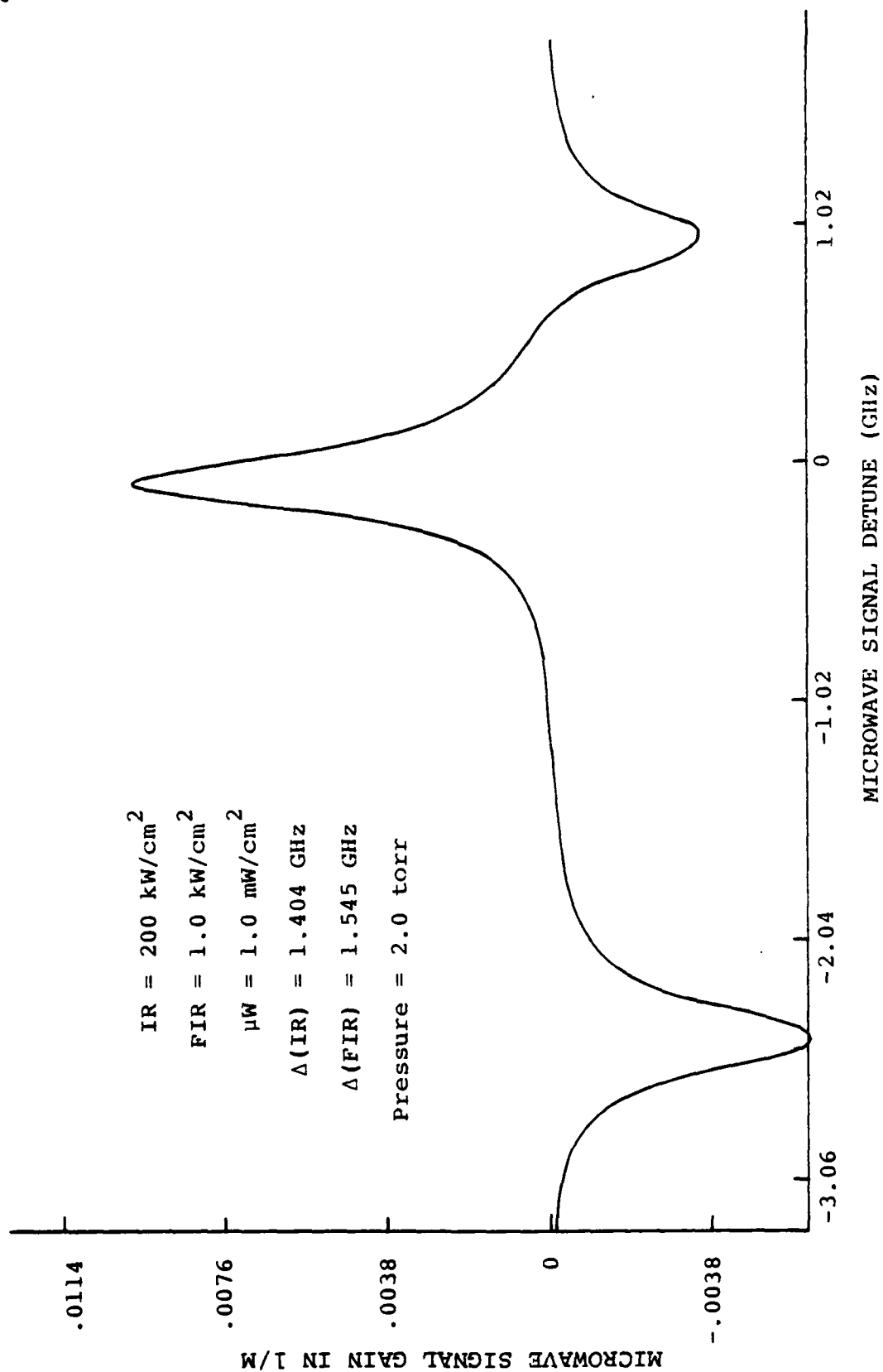


Figure 14. Gain curve for microwave of 1.0 mW/cm² intensity.

IR = 200 kW/cm²

FIR = 1.0 kW/cm²

μW = 1.0 mW/cm²

Δ(IR) = 1.404 GHz

Δ(FIR) = 1.545 GHz
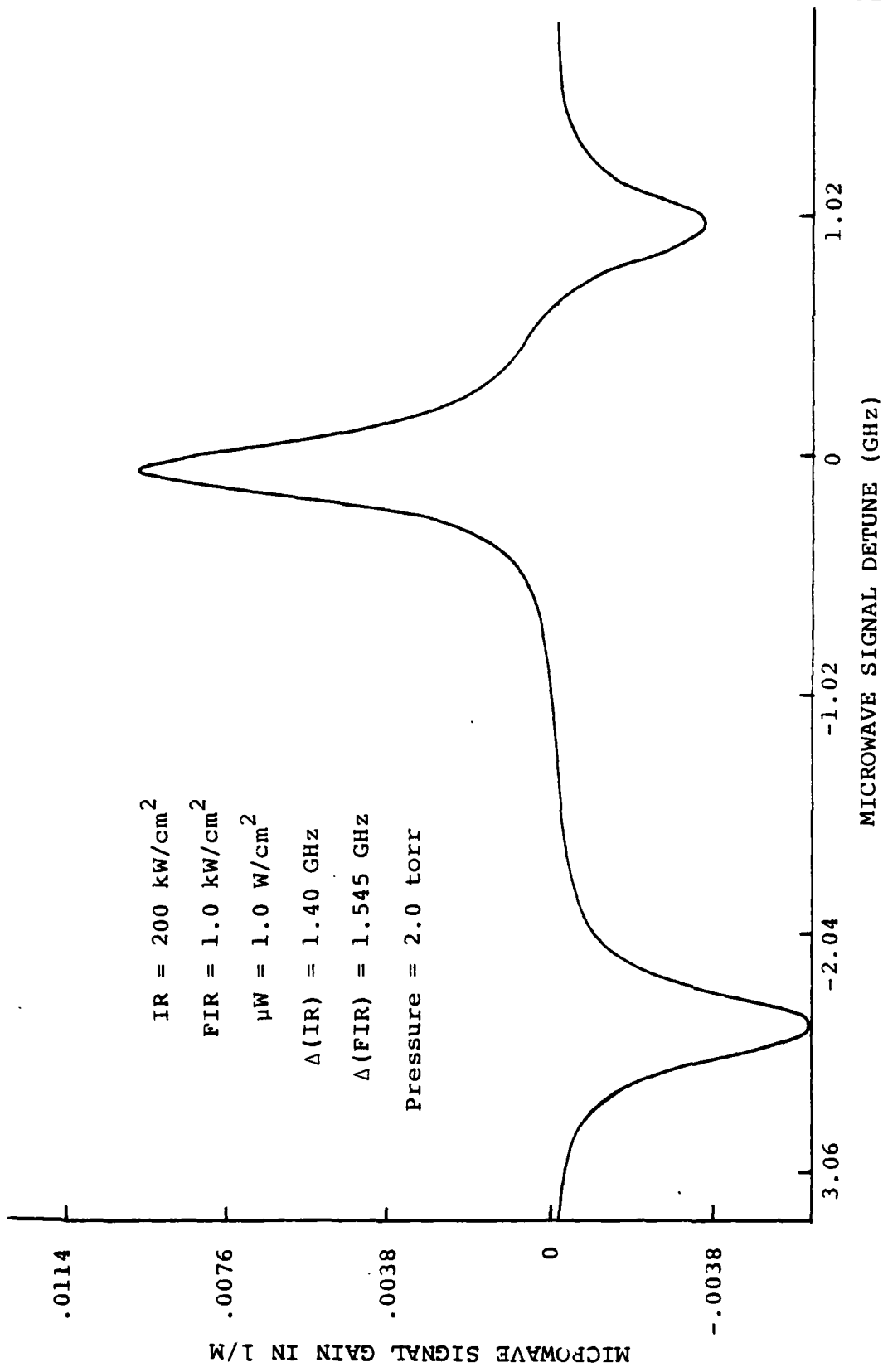
Pressure = 2.0 torr

Figure 15. Gain curve for microwave of 1 W/cm$^2$ intensity.

IR        = 200 kW/cm$^2$
FIR       = 1.0 kW/cm$^2$
μW        = 1.0 W/cm$^2$
Δ(IR)     = 1.40 GHz
Δ(FIR)    = 1.545 GHz
Pressure  = 2.0 torr

MICROWAVE SIGNAL DETUNE (GHz)

MICROWAVE SIGNAL GAIN IN 1/M

92
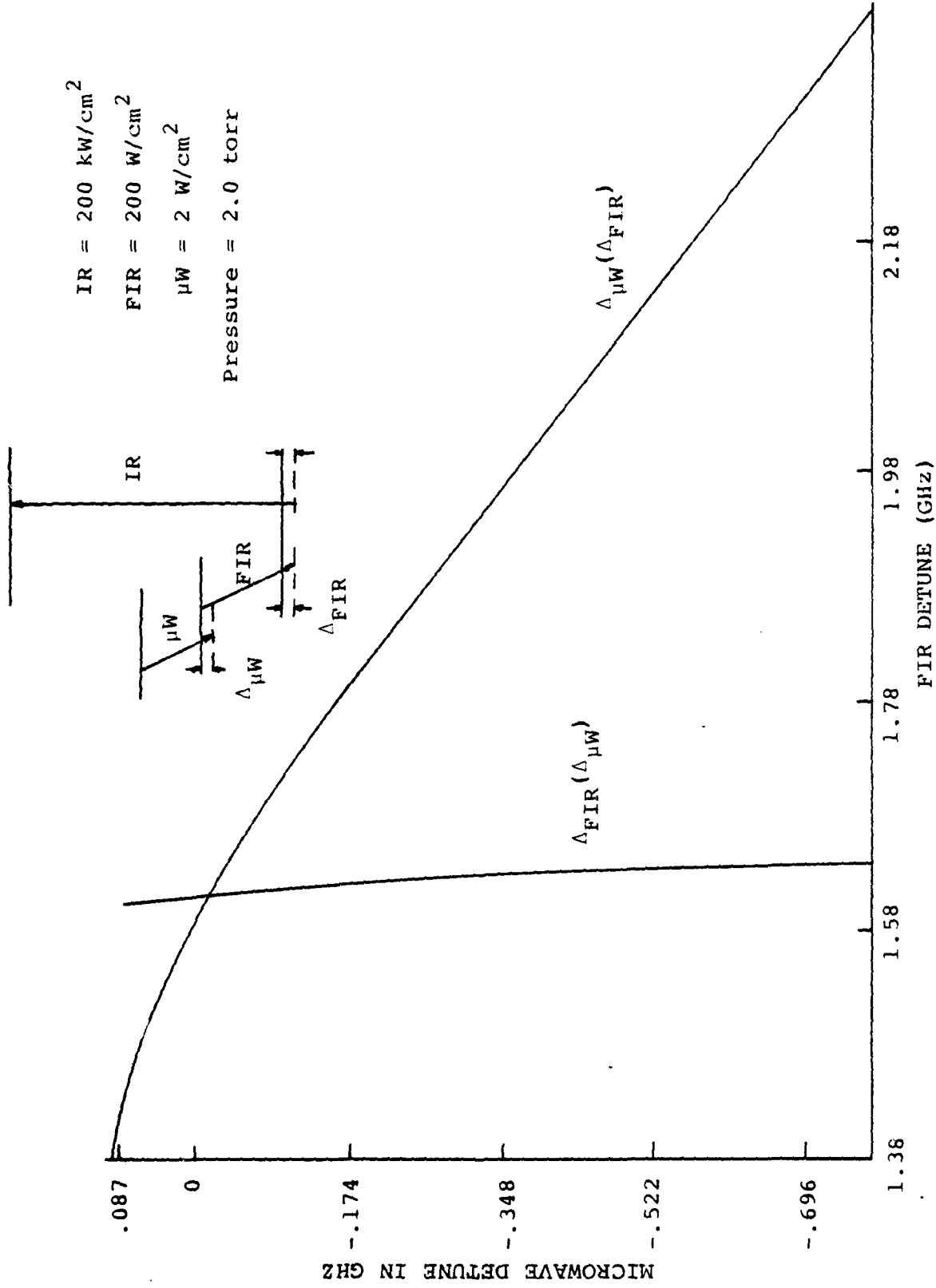


Figure 16. Microwave detune dependence of FIR detune and vice versa.

includes the polarization dependent M-sublevel transition.
Relevant values, such as threshold intensity, signal detuning
of each nonlinear process and offset frequency has been ob-
tained which will be most helpful in an experiment.

## References

1.  R. L. Panock and R. J. Temkin, "Interaction of Two Laser
    Fields with a Three-Level Molecular System", IEEE J. Quan.
    Elec., QE-13, 425 (1977).

2.  P. D. Coleman, "Hyper-Raman Scattering and Related Phenomena",
    Proc. Int. Conference, Lasers '78, p. 73.

3.  S. J. Petuchowski, J. D. Oberstar, and T. A. DeTemple, "Opti-
    cal Triple Resonance", Phys. Rev. A, 20-2, 529 (1979).

4.  S. J. Petuchowski, A. T. Rosenberger and T. A. DeTemple,
    "Stimulated Raman Emission in Infrared Excited Gases", IEEE
    J. Quan. Elec., QE-13, 476 (1977).

5.  J. Curtis, "Vibrational-rotational Bands of $NH_3$ in the 670
    to 860 $cm^{-1}$ Region", Ph.D. Dissertation, The Ohio State
    University, Columbus, OH, 1974.

6.  K. Gullberg, et al., "Submillimeter Emission from Optically
    Pumped $^{14}NH_3$", Physica Scripta, 8, 177 (1973).

7.  K. J. Kim, "Stimulated Raman and hyper-Raman Scattering in
    the FIR Region", Ph.D. Thesis, University of Illinois,
    Urbana, IL, 1980.

8.  C. H. Townes and A. O. Schawlow, Microwave Spectroscopy,
    Dover Publications, Inc. (1975).

## VI. REAL TIME, SINGLE-PULSE SPECTRUM ANALYSIS OF FAR IR LASER SIGNALS USING SAW CHIRP TRANSFORMS - Robert Miller

### Introduction

An important property of any coherent radiation source is its spectral characteristics. While it is believed that optically pumped molecular gas lasers yield high quality spectral signals, few measurements and papers have appeared on this subject. There is good reason for this: such measurements are difficult to do, especially for pulsed FIR lasers. Yet the potential use of such lasers on applications such as laser radar systems, where both range and velocity information is desired from the return signal, makes spectral characterization of these lasers of practical interest. Quantitative knowledge of such things as pulse-to-pulse frequency stability, amount of frequency chirping during a pulse, variability of spectral content of the output with changes in various system parameters, would be of great usefulness to system designers.

The researcher also stands to gain from such measurements. Detailed knowledge of the spectral content of laser signals can give valuable insights into the lasing mechanisms involved. For example, if the frequency of an optically-pumped laser is linearly related to pump frequency, a Raman process is suggested.[1,2]

## Approaches to Spectrum Analysis

The low repetition rate and narrow pulse widths of pulsed FIR lasers make spectral measurements difficult. Moreover, most spectrum analysis techniques are only capable of determining an average spectrum of many pulses.

Purely optical methods either suffer from poor spectral resolution, or, in the case of Fabry-Perot resonator techniques, spectral mode-matching and mechanical stability problems which make measurements tricky and tedious. In order to obtain a spectral display, one of the mirrors of the Fabry-Perot resonator is usually moved (scanned). As will be shown below, the type of display which would be obtained from passing a low duty-factor pulse through such a scanning filter is not a true frequency domain display, but one which contains a combination of frequency and time information.[3] It is not possible to obtain the spectrum of a single pulse using a Fabry-Perot resonator; many pulses are needed.

Optical heterodyne methods followed by electron spectrum analysis of the resulting infrared signal offer some advantages with regard to resolution and convenience. However, the intermediate-frequency signal is also of low repetition rate and narrow pulse width, which can cause severe problems with some electronic spectrum analysis techniques.

Figure 1 shows a greatly simplified block diagram of a conventional electronic spectrum analyzer. It consists of a
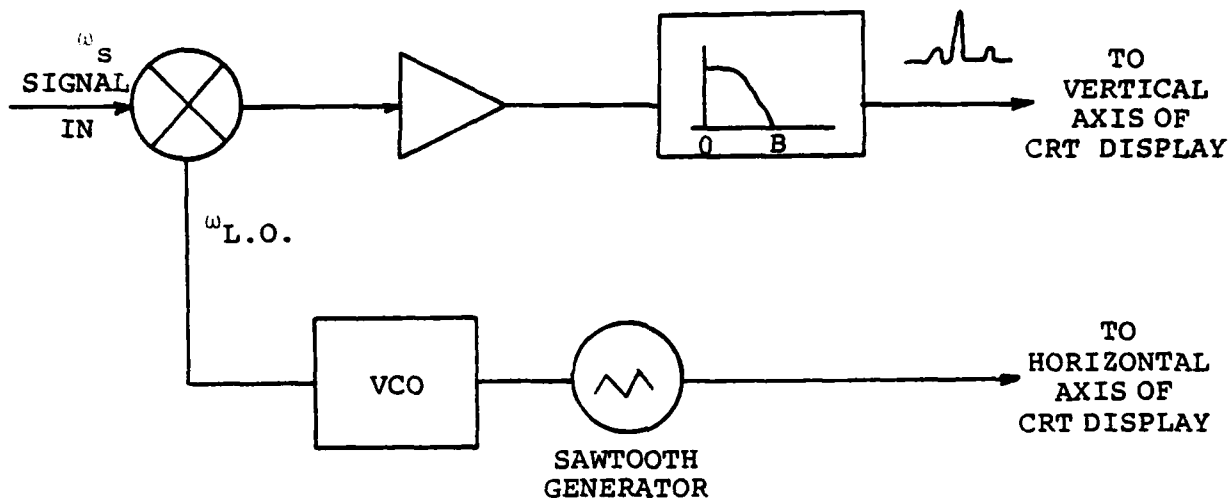
Figure 1.   Highly simplified block diagram of conventional
electronic spectrum analyzer.

swept local oscillator at frequency $\omega_{L.O.}(t)$, a mixer, and a
baseband filter of bandwidth B.   For CW signals, the L.O. and
mixer translate these signal components in the range $\omega_{LO}$ -
$B \leq \omega_s \leq \omega_{LO} + B$ down to baseband, where they are passed by
the baseband filter and sent to the vertical axis of a CRT dis-
play.   The same sawtooth which casuses the L.O. to sweep is
also used to drive the horizontal axis of the CRT.   For CW
signals, this results in a true display of the signal's spec-
tral content, if baseband filter B is narrow enough.

For pulsed signals, though, the situation will be quite
different if the filter bandwidth B is greater than 1/T, the
pulse repeition frequency.   (This will probably be the case

for low duty-factor pulses obtained from pulsed FIR sources).
In this case, the vertical output will be non-zero only when
the input signal is non-zero. It will consist of narrow
pulses separated in time by T. The amplitude of each pulse
will be the amplitude of the envelope of the pulse spectrum
$G(\omega)$, evaluated at the particular frequency of $\omega_{L.O.}$ when the
pulse occurred.

Thus the output of a conventional spectrum analyzer would
be misleading since it would look like a line spectrum, but the
line spacing would actually be the repetition time T of the
pulses. (For very low repetition rates, this would hardly be
a useful display unless some storage were used). The envelope
of the spectrum would clearly be the average envelope of the
pulse spectrum. The same type of display would be obtained
with a scanning Fabry-Perot resonator; the only difference there
is that the filter is scanned past the signal.

A very powerful method of analyzing signals, which is now
becoming more practical, is based on digital techniques. The
infrared signal pulse from an optical heterodyne experiment
is A/D converted in its entirety, and sent to a computer, which
can then apply a whole arsenal of signal averaging techniques,
can Fourier transform all or any part of the signal, and per-
form whatever calculations may be needed. The only problem
with applying this technique to FIR signals is that of the
high data rates required, which require very fast A/D converters

able to perform a conversion in a few nanoseconds.  A/D con-
verters of this speed do exist, but they tend to be limited
in the number of bits of resolution.  This resolution problem
can be cleverly circumvented by signal averaging techniques:
a number of low resolution samples, each with some random
noise added to it, are digitized and accumulated by the com-
puter.  As the number of samples summed together increases,
the random noise not only cancels out, but the statistics of
the process of digitizing samples plus noise effectively fills
in the coarse resolution of the digitizing process.  Once again,
though, the technique is unable to obtain a high resolution
spectrum of a <u>single</u> pulse -- only averages can be obtained.

There is one method of spectrum analysis which can per-
form a high-resolution Fourier transformation of a single pulse,
and in real time:  chirp transform techniques, based on Surface
Acoustic Wave (SAW) technology.  A surface wave device known
as a Reflective Array Compressor (RAC)[4] was developed for just
this sort of problem in the radar community.  Recently,
Fetterman, et al.[1] at Lincoln Labs were the first to report
application of this technique to the measurement of IR laser
signals.

A RAC (shown in Figure 2) is a linearly dispersive delay
element; two superimposed pulses of different frequencies put
into the device will appear separated at the output by a time
difference proportional to their frequency differences.  In
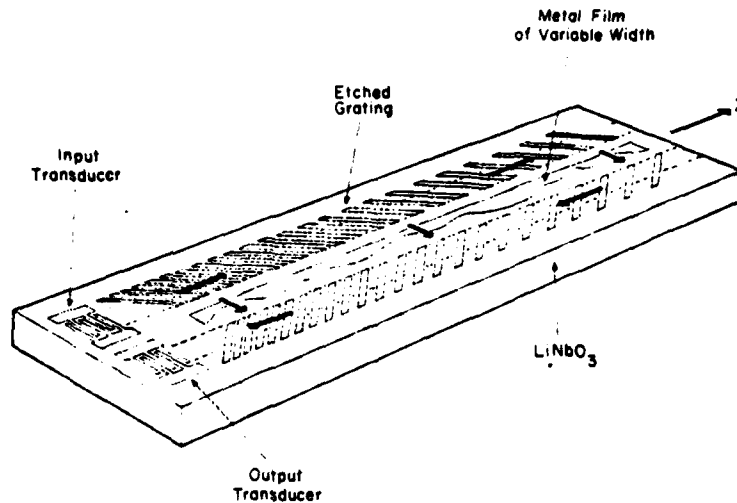
Figure 2.  Reflective array compressor vs. reflections of sur-
face acoustic waves from etchec grating of linearly
varying pitch to provide long dispersive delays and
wide bandwidth.   (From Ref.8).

the next section, we shall show that under certain conditions

the output will be a nearly exact Fourier transform of an in-

put pulse, allowing real-time spectrum analysis of FIR sources

to be performed with the experimental set-up shown in Figure 3.

SAW devices, having a range of characteristics, were kindly

supplied by Raytheon, Hughes and Lincoln Labs to us in the

latter part of the contract year for study and evaluation.

These are described in the section on "Short Description of

Donated SAW Devices."

HARMONIC
MIXER

NMW
SIGNAL

```
              ┌────────┐   ┌──────┐   ┌────────┐
   ⊗ ───────► │ IF AMP │─► │ SAW  │─► │ DIODE  │
   │          └────────┘   └──────┘   └────────┘
   │                                      │
   ▲                                      ▼
┌──────┐  f_o                      ┌────────────┐
│  LO  │                           │   SCOPE    │
└──────┘                           └────────────┘
   │
┌──────────┐
│STABILIZER│
└──────────┘
```
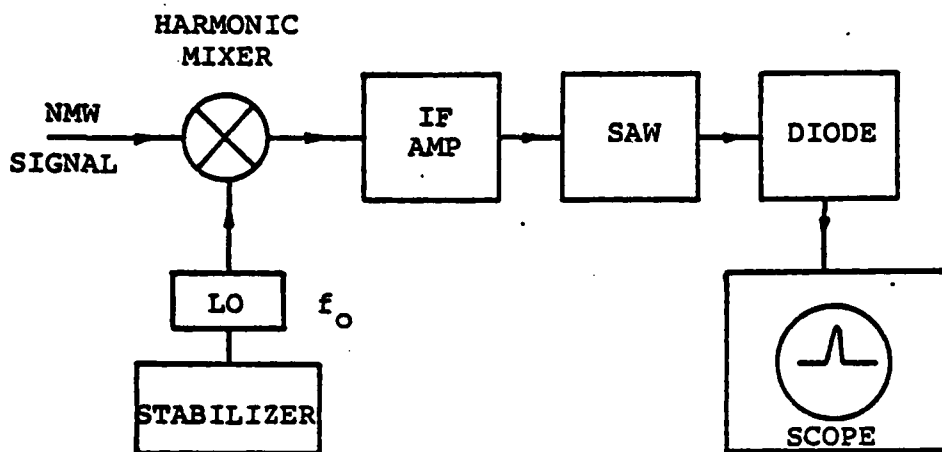
Figure 3.   Experimental arrangement for pulsed Fourier trans-
form analysis of NMW sources.

The problems involved in applying the SAW technique to far
IR laser signals are:  1) the development of an optical hetero-
dyne system (i.e., a suitable mixer and a stable local oscil-
lator) to produce an infrared signal of the right frequency for
the RAC, and 2) making the pulse width of this infrared signal
compatible with the particular SAW device being used.  The
section, "Experimental Measurements" will describe a number of
experiments in spectrum analysis.

Application of these methods to the spectral measurement
of the 22.65 GHz maser signal generated in $NH_3$ is also reported
elsewhere in this report, Section IV by E. G. Malk.

## Fourier Analysis with SAW Device

If a signal $s(t)$ is put into a SAW dispersive delay line which has an impulse response $h(t)$, the output response $r(t)$ is given by the convolution integral:

$$r(t) = \int_{-\infty}^{t} s(t)h(t-\tau)d\tau \tag{1}$$

For a physically realizable RAC device, the impulse response is idealized by a linear chirp:

$$h(t) = \begin{cases} \cos[\omega_s(t-t_d) + \mu(t-t_d)^2], & t_d \leq t \leq t_d + T \\ 0 \text{ otherwise} \end{cases} \tag{2}$$

where:   $\omega_s$ = starting frequency

$t_d$ = initial delay

$T$ = dispersion time

$\mu$ = chirp slope

The instantaneous frquency of this linear chirp is

$$\omega(t) = \frac{d\phi}{dt} = \omega_s + 2\mu(t-t_d)$$

or                                                                                   (3)

$$f(t) = f_s + \frac{\mu}{\pi}(t-t_d)$$

We can simplify the  ensuing discussion, however, by ignoring the initial delay $t_d$, the starting frequency $\omega_s$, and expressing $h(t)$ as a complex impulse response:

102

$$h(t) = e^{j\mu t^2} + cc$$

Equation (1) then becomes

$$r(t) = \int_{-\infty}^{t} s(t)e^{j\mu(t-\tau)^2}d\tau + cc \qquad (4)$$

Equation (4) is in the form of a Fresnel transform,[5] not a Fourier transform. However, we shall show that for small enough input pulse widths, the Fresnel transform is a good approximation to a Fourier transform.

Since

$$(t-\tau)^2 = t^2 - 2t\tau + \tau^2$$

Equation (4) can be written

$$r(t) = e^{j\mu t^2} \int_{0}^{t} d(t)^{j\mu\tau^2} e^{-j(2\mu t)\tau} d\tau \qquad (5)$$

where the lower limit of the integral has been changed to reflect the assumption that signal s(t) starts at t=0.

The integral in Equation (5) is almost a Fourier integral, with kernal function

$$e^{-j(2\mu t)\tau}$$

implying the transformation of variables

$$\omega' \leftrightarrow 2\mu t \qquad (6)$$

relating the time scale of the output pulse to frequency.

However, the integrand of Equation (5) is multiplied by a chirp. If the input pulse duration $t_p$ is small enough though, this chirp is not highly different from a CW burst of the same duration. We may say that this is true if the phase of this chirp differs from that of a CW pulse by not more than $\pi/2$ in the inteval $t_p$ or:

$$\mu t_p^2 < \pi/2 \quad . \qquad (7)$$

For a RAC having total dispersion time T and bandwidth $\Delta F$, Equation (3) shows that

$$\mu \equiv \pi \frac{\Delta F}{T} \qquad (8)$$

Combining Equations (7) and (8) tells us that the output of the RAC will be sufficiently close to a Fourier transform if the input pulse length $t_p$ is shorter than

$$t_p \gtrsim \frac{2}{3} \sqrt{\frac{T}{\Delta F}} \quad . \qquad (9)$$

Experimental verification is shown in the next section below.

Equation (6) thus shows that, for short enough input pulses, the magnitude of the RAC will be proportional to a Fourier transform. The exponential term in front of the integral is a unit amplitude chirp just like the impulse response h(t) of the RAC. If we are only interested in the magnitude

of the spectrum of our pulse signal, we need do nothing more
than pass it through the RAC, and look at the envelope of what
comes out.

If our pulsed signal has a duration $t_p$ which is larger
than the limit given in Equation (9) above, or if we desire a
more exact Fourier transformation, we may pre-multiply s(t) be-
fore the RAC by a chirp of opposite slope, and post-multiply
the output of the RAC by a similar chirp of opposite slope as
that of the RAC (See Figure 4). In general, if

$\mu_1$ = pre-multiply chirp slope

$\mu_2$ = RAC chirp slope

$\mu_3$ = post-multiply slope
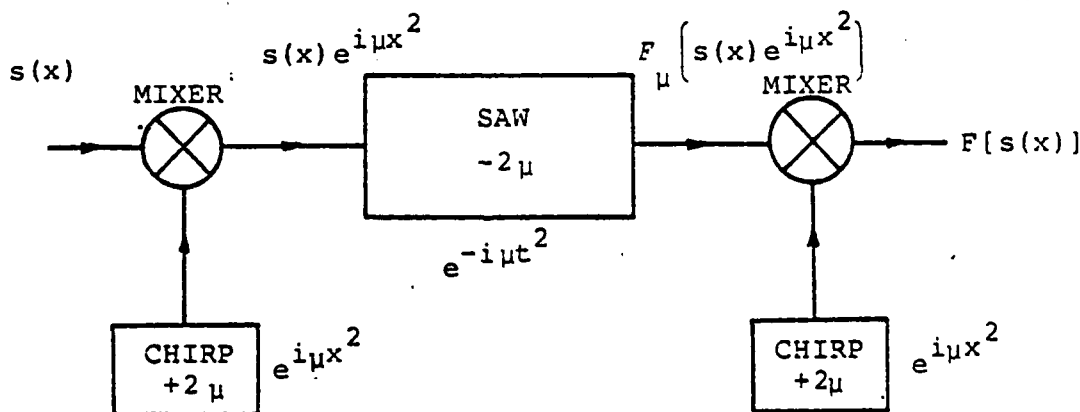


Figure 4. Chirp Fourier transformation using SAW RAC. Input
signal is pre-multiplied by chirp of opposite slope
as RAC, passed through RAC.

then

$$r(t) = e^{j(\mu_2-\mu_3)t^2} \int_0^t s(t) e^{j(\mu_2-\mu_1)\tau^2} e^{-j(2\mu t)\tau} d\tau$$

(10)

$$= [r(t)] \quad \text{if } \mu_1 = \mu_2 = \mu_3.$$

This multiply-convolve-multiply mode of operation[6,7] will be referred to hereinafter as the chirp Fourier transform mode, as opposed to the Fresnel transform mode which merely involves passing a signal through the RAC.

Equation (10) clearly shows the result of mismatch between pre-multiply chirp slope $\mu_1$ and device chirp slope $\mu_2$. If the two do not exactly cancel, the integral in Equation (10) is still of the Fresnel transform type, but with reduced chirp slope $(\mu_2-\mu_1)$. If the input pulse duration is small enough the arguments leading to Equation (7) apply, but the remanent chirp slope $(\mu_2-\mu_1)$ leads to a larger allowable pulse width $t_p$. This will be discussed further in the section below.

It should be pointed out that, although narrow input pulses are needed to assure an accurate Fourier transformation, the finite bandwidth of the SAW device places a lower limit on pulse width as well. This lower limit is harder to define, since the output of the device will just look like a truncated spectrum. Clearly the lower pulse width limit is determined by how much of the spectrum we need to see in a single shot. (If the input pulses are reproducible, on the other hand, then a

wide spectrum can be reconstructed from small pieces of it, obtained by changing the local oscillator each time).

The usual criterion given in the literature for a non-deformed spectrum output[7] is that the time-bandwidth product of the RAC be at least four times that of the input signal. This leads to a lower limit on the pulse width of

$$t_p \geq \frac{4}{\Delta f} \tag{11}$$

which, by the reasons given above, may be relaxed if one is content with viewing only a portion of the spectrum at a time.

In summary, in the Fresnel mode of operation, a signal pulse is simply passed through a SAW dispersive delay line or RAC. The output pulse will be an accurate representation of the Fourier transform of the input signal if the duration $t_p$ of the input signal falls within the limits

$$\frac{4}{\Delta f} \leq t_p \leq \frac{2}{3} \sqrt{\frac{T}{\Delta f}} \tag{13}$$

For longer signal durations, it is necessary to either pre-multiply the signal by a chirp of opposite slope as that of the RAC (chirp Fourier transform mode of operation), or to gate out a small portion of the input pulse and look at its spectrum as a function of position in the signal pulse. The latter procedure has interesting possibilities as will be shown in the next section.

## Short Description of Donated SAW Devices

We are very grateful to the Raytheon Corporation, Hughes
Industries, and MIT Lincoln Laboratories for their donation
or loan of surface wave devices for this work. These are
state-of-the-art devices in some cases, employing ion-etched
grooves of precisely controlled depth (depth variation along
the grating array is one of the design parameters) as well as
width. At least in the case of the Lincoln Labs device,
additional phase correction is determined for and fabricated
on each individual device, to make the phase response closer
to exactly parabolic.[8] (Some of the other devices may employ
this technique as well, but we are sure that the MIT device
does).

Table 1 summarizes the important parameters of these devices,
such as bandwidth, dispersion time, and frequency resolution.
Figures 5 through 8 show frequency response curves.

Table 1. Summary of operating characteristics of SAW RAC devices donated or lent to The University of Illinois Electro-Physics Lab.

| MANUFACTURER | CENTER FREQUENCY (MHz) | BANDWIDTH F (MHz) | DISPERSION TIME T (µsec) | T-B PRODUCT | NUMBER OF RESOLVABLE FREQUENCIES | FREQUENCY RESOLUTION (MHz) | MINIMUM PULSE WIDTH (µsec) | MAXIMUM PULSE WIDTH (µsec) |
|---|---|---|---|---|---|---|---|---|
| RAYTHEON | 60 | 6 | 20 | 120 | 11 | 0.55 | 0.667 | 1.217 |
| RAYTHEON | 120 | 24 | 3 | 65 | 8 | 2.98 | 0.167 | 0.224 |
| HUGHES | 500 | 150 | 3 | 450 | 21 | 7.07 | 0.027 | 0.094 |
| MIT | 420 | 100 | 16 | 1600 | 40 | 2.50 | 0.040 | 0.267 |
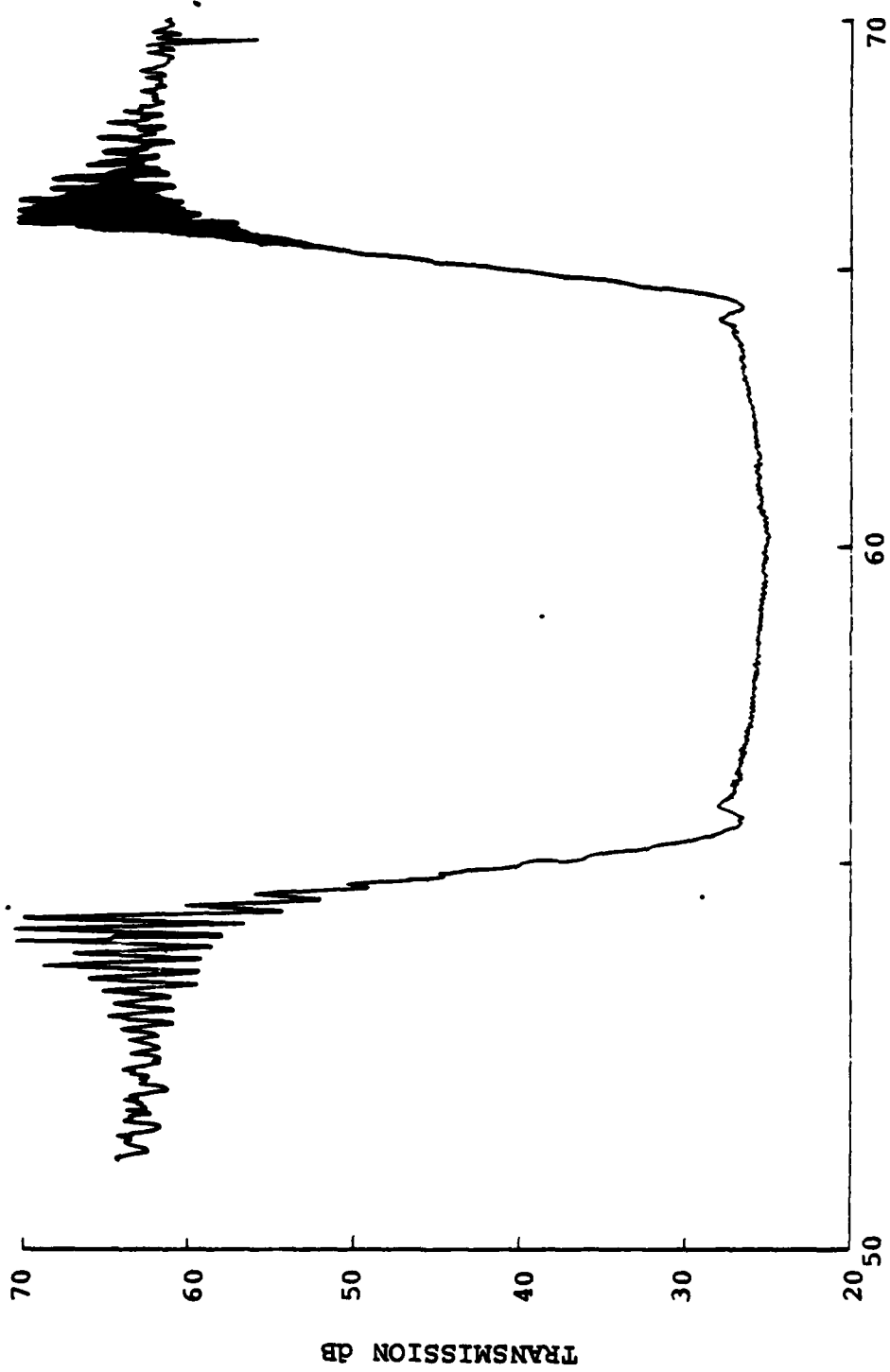
Figure 5.  Frequency response of Raytheon 60 MHz RAC.

110
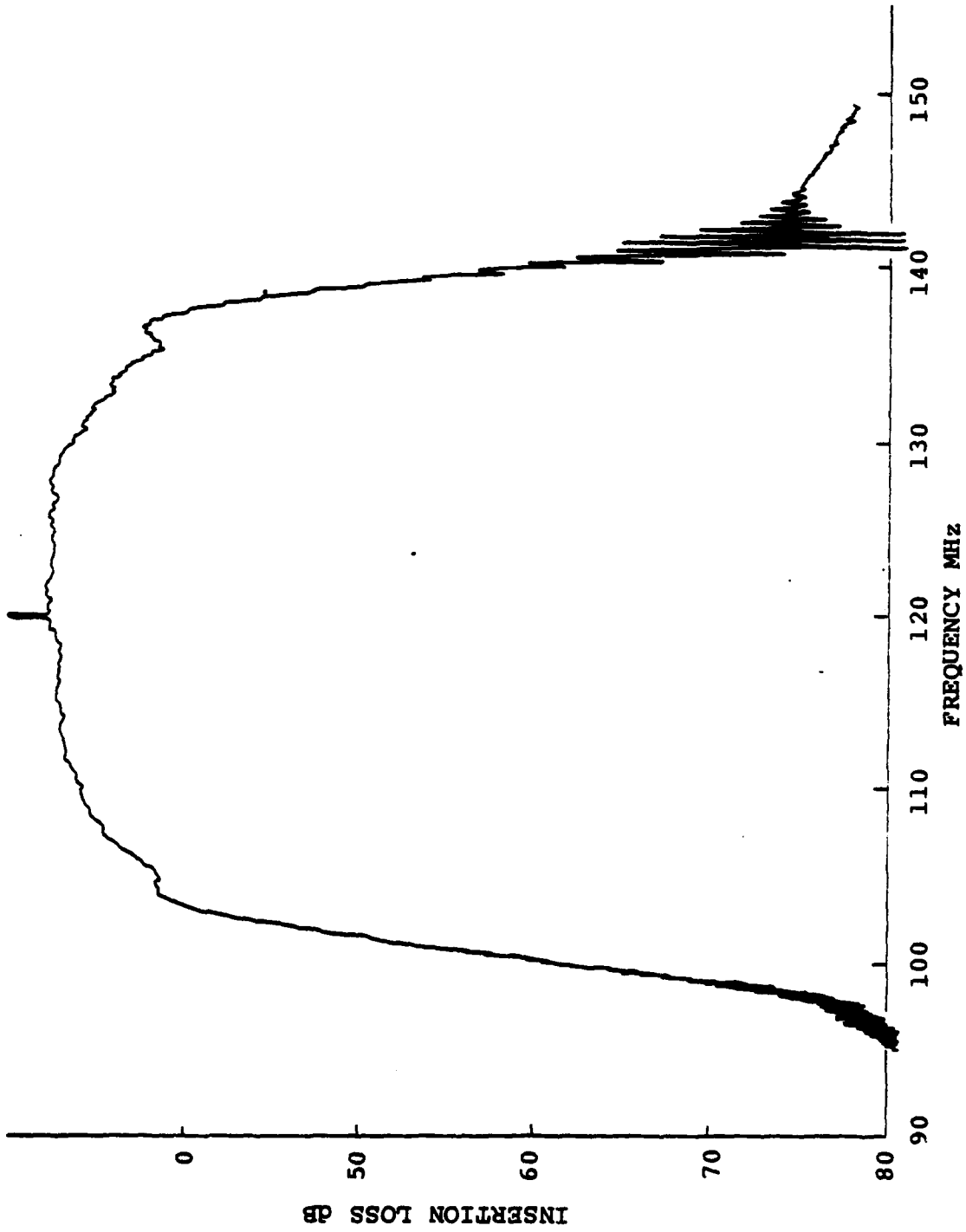


Figure 6. Frequency sources of Raytheon 120 MHz RAC.
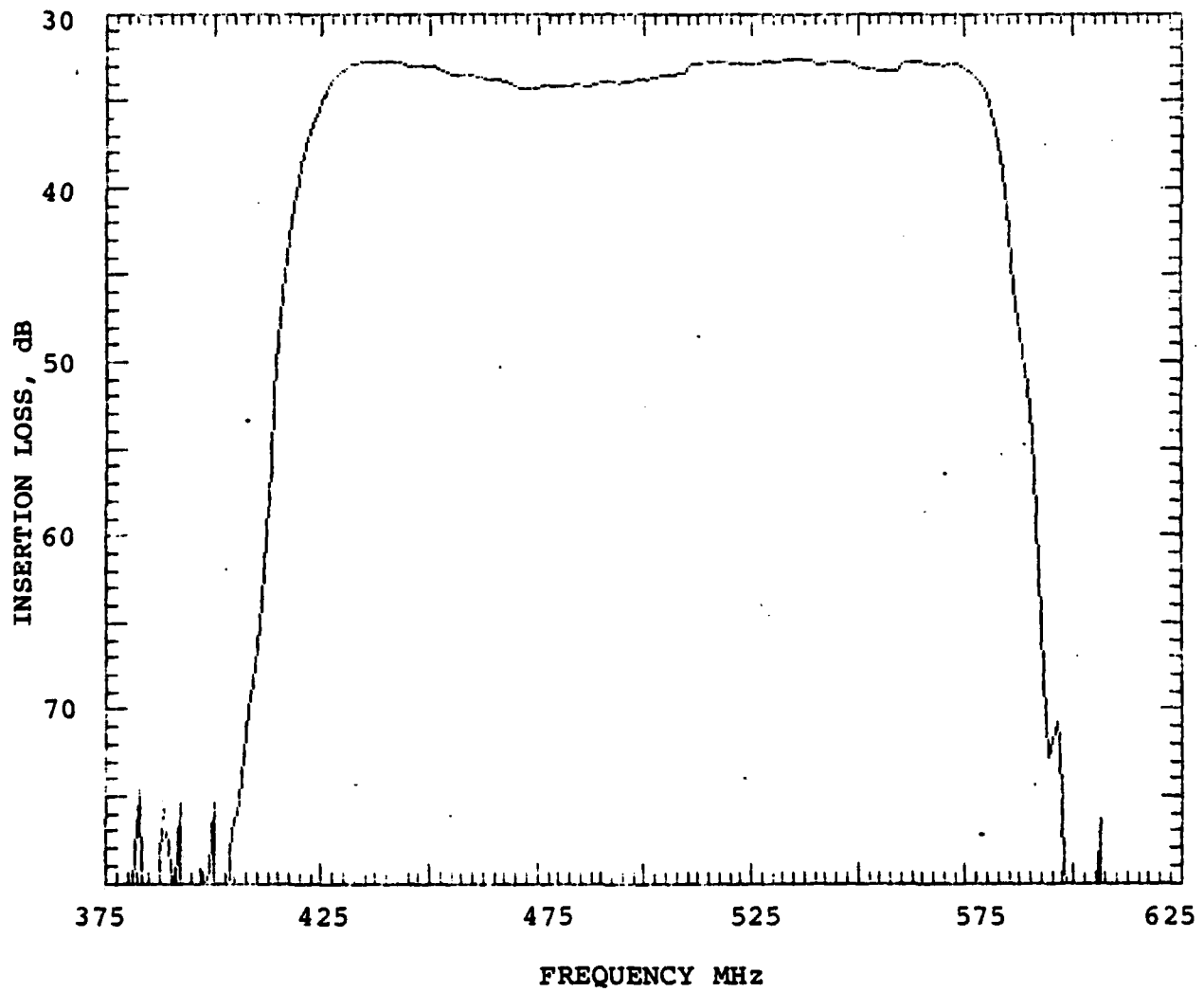
Figure 7.   Frequency response of Hughes RAC.

112
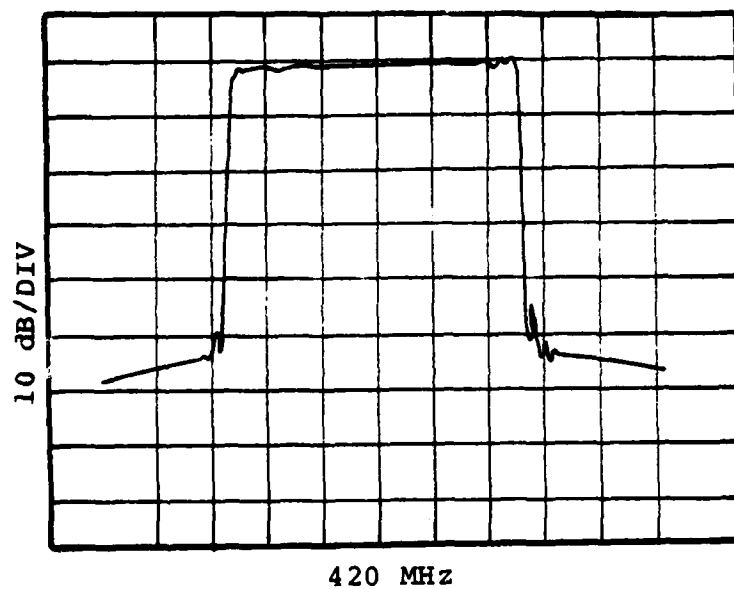


Figure 8.  Frequency response of MIT RAC.

Experimental Measurements

### Demonstration at IF

We have shown in a previous section that in order to obtain a true Fourier transformation of a signal, it is necesary to first pre-multiply it by a chirp of opposite slope as the RAC, pass this product through the RAC, and then post-multiply the output by another chirp of opposite slope as the RAC (Figure 4). We further showed that if the input pulse width fell within certain limits, that passing the signal through the RAC alone produced a good approximation to a Fourier transform, without the need for pre- and post-multiplying chirps.

It is useful to ask questions about the limitations of this technique. How critical are the pulse width limits? If a pre-multiply chirp must be used, what happens if its chirp slope does not exactly match that of the RAC? What happens if its frequency vs. time characteristic is slightly nonlinear?

We have preformed some experiments aimed at answering these questions at 60 MHz using the Raytheon 6 MHz bandwidth, 20 microsecond dispersion RAC.

Figure 9a) and b) show experimental set-ups used. In Figure 9a). a CW signal is gated with two cascaded double-balanced mixers (for good on-off radio) and the resulting narrow pulse is amplified and passed through the RAC. This simulated a Fresnel transform, which should approximate a Fourier transform

114
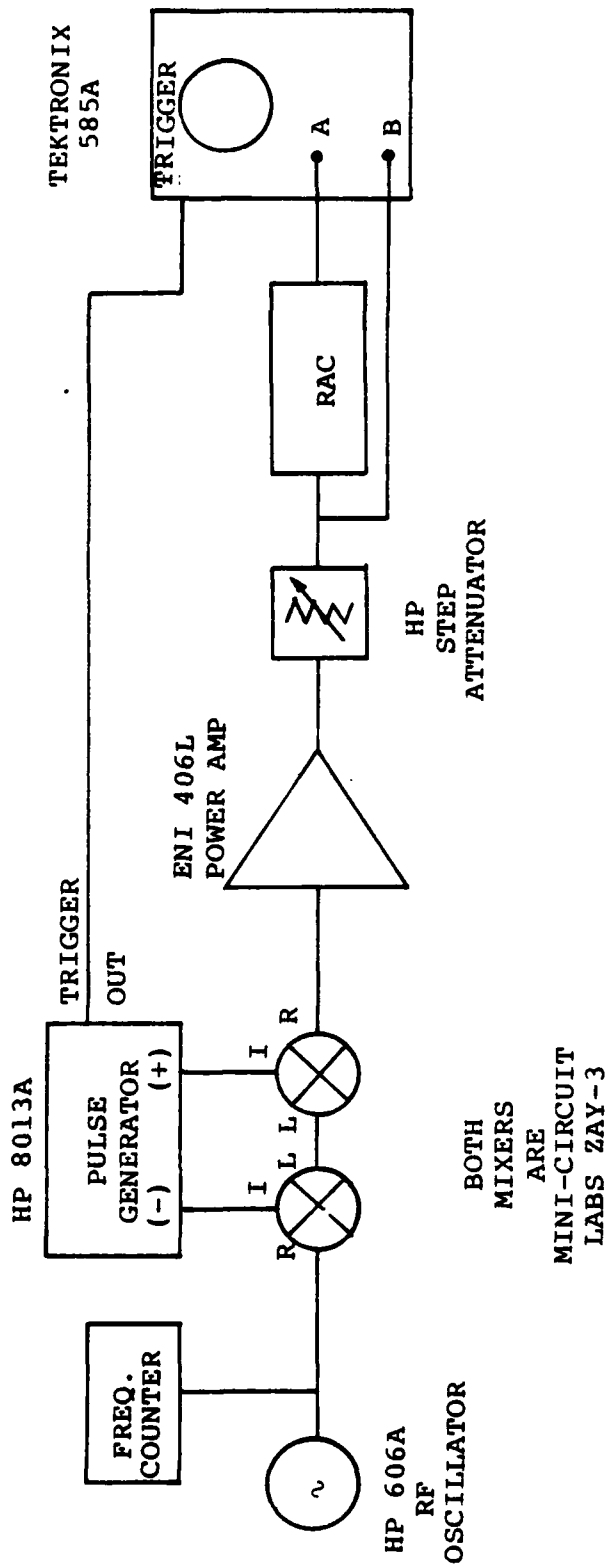


Figure 9a. Experimental setup to measure Fresnel transform with SAW RAC.

115
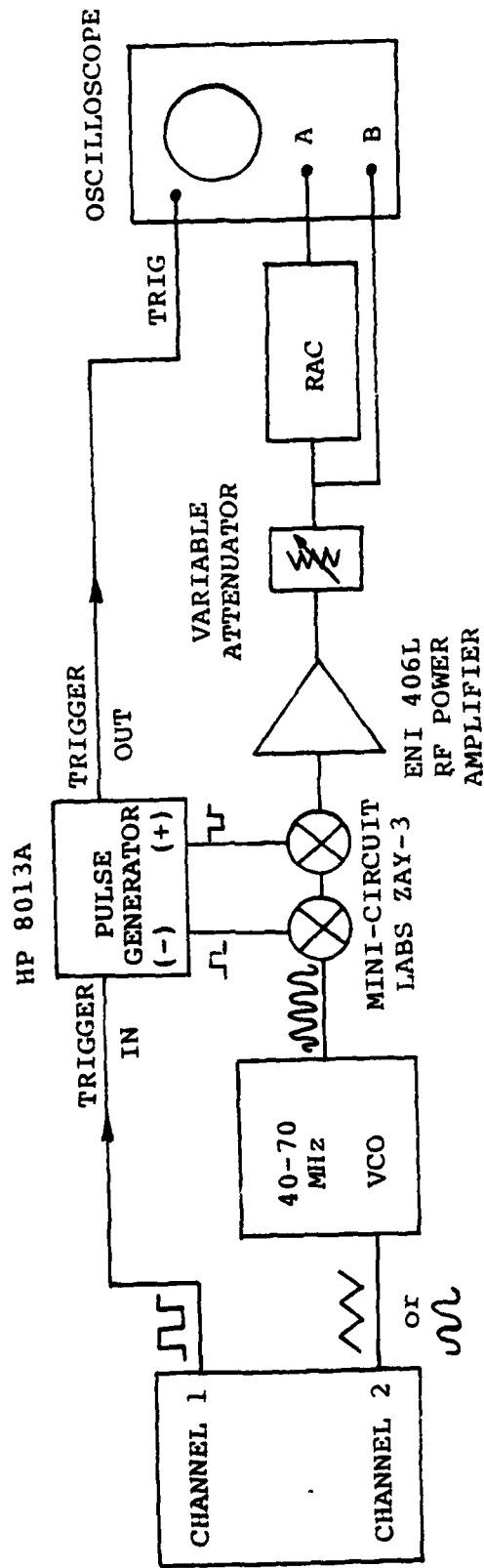


Figure 9b. Experimental setup to measure Chirp Fourier transform with SAW RAC.

if the pulse width lies within 0.67 μsec $\leq \tau_{pulse} \leq$ 1.22 μsec
for this particular RAC.

Figure 9b) shows a simulation of a true Chirp Fourier transform. A sawtooth wave driving a voltage controlled oscillator provides the necessary pre-multiply chirp; no post-multiply chirp is needed, since we are only interested in the envelope of the signal. The signal to be pre-multiplied by the chirp is the rectangular pulse generated by the pulse generator. The envelope of the output of the RAC is expected to be the Fourier transform of the rectangular pulse, which is a sin(x)/x.

To be more quantitative, the input pulse of amplitude A and width $\tau_i$ has a Fourier transform

$$V(f) = A\tau_i \frac{\sin(\pi f \tau_i)}{(\pi f \tau_i)} \tag{13}$$

which has a main lobe width $\Delta f = \frac{2}{\tau_i}$ MHz between first zeroes. The chirp slope μ of the device is

$$\mu = \pi \frac{\Delta F}{\Delta T} = \pi \cdot \frac{6 MHz}{20 \mu sec} \tag{14}$$

The relationship between output pulse width and frequency is

$$\Delta \omega = 2\mu\tau_{out}$$

or $\tag{15}$

$$\Delta f = \frac{\mu}{\pi} \tau_{out}$$

From Equation (13) above, the output pulse width should vary inversely with input pulse width, while the output amplitude should be directly proportional to input pulse width.

Figure 10a) and b) shows a side-by-side comparison of these two modes of operation, the Fresnel mode, Figure 10a), (left side) and the chirp Fourier transform (Figure 10b), (right side) as the width of the input pulse is varied. Within the pulse width limits mentioned above, the two results are as identical as experimental determination will allow. Numerical data taken from these photographs, in the recommended pulse width range, shows the output to indeed be a true Fourier transform for either mode of operation. The output pulse width varies inversely with input pulse width, and the peak amplitude varies directly with input pulse width as expected from the Fourier transform relationship described above.

As the pulse width limits are exceeded, however the Fresnel mode output pulse begins to deviate from a simple sin $x/x$ shape, becoming a more complicated shape reminiscent of optical diffraction patterns. (In fact, the progression of pulse shapes is exactly like the progression of amplitude profiles one would obtain in an optical diffraction experiment, at various distances from a rectangular slit). Beyond the pulse width limits established above, widening the input pulse increases the output pulse width, and the approximation to a Fourier transform
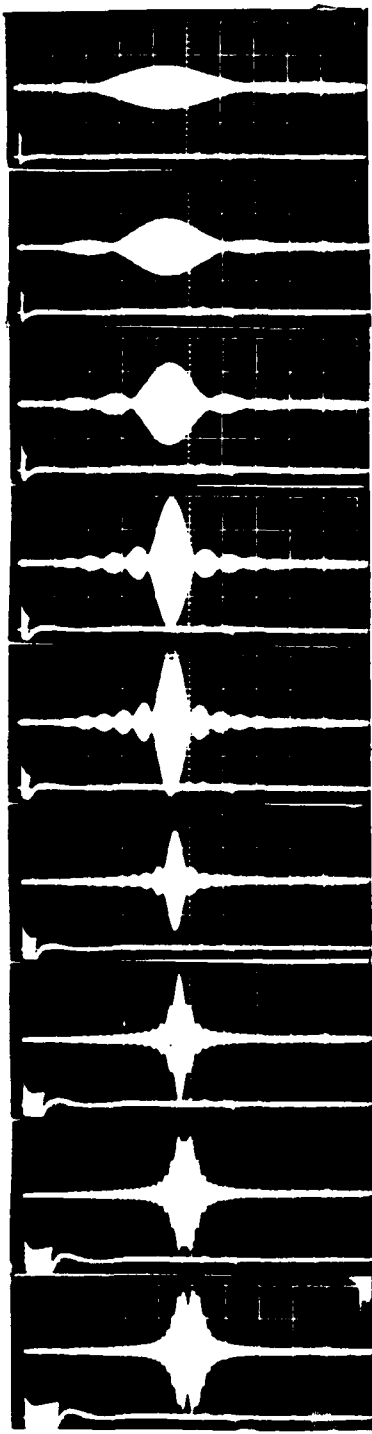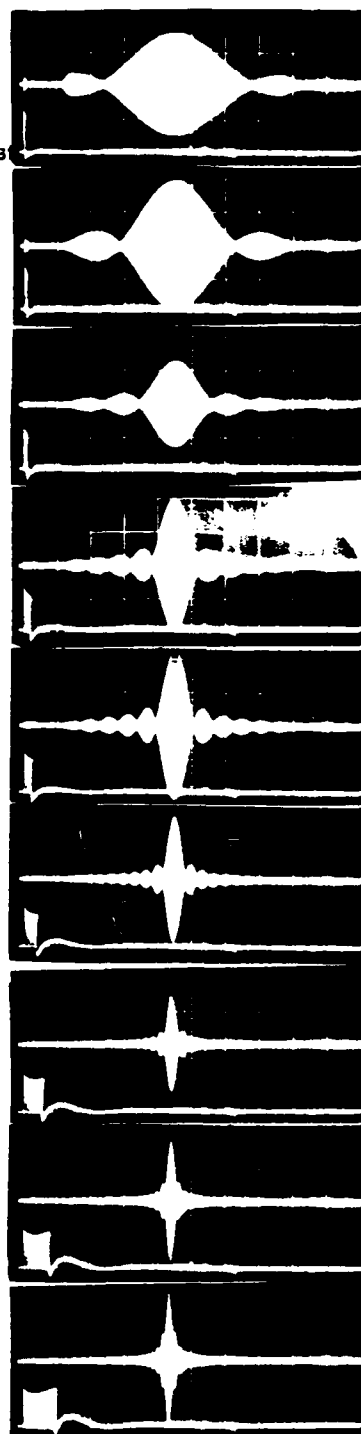
Figure 10.  Comparison of Fresnel vs. Chirp Fourier transform
performance for various pulse widths.

relationship breaks down. Still, the output pulse shape looks fairly close to a sin x/x out to about twice the upper pulse width limit, so these pulse width limits given earlier are not critical.

The photographs clearly show that for short pulse widths, there is no advantage to doing the extra pre-multiplication by a chirp, since the Fresnel transform is not discernably different from the Fourier transform. For larger pulse widths, however, that is no longer true, and one is forced to either pre-multiply or simply gate the signal on for a short time, and look at only a piece of the signal at a time. (There are advantages to this latter approach, which will be described in the next section).

If it is necessary to pre-multiply, then the allowable mismatch $\Delta\mu$ between pre-multiply chirp slope and device chirp solpe [$(\mu_2-\mu_1)$ in Equation (10)] can be found by an argument similar to the one used to find the upper pulse width limit. We insist that

$$\Delta\mu t_p^2 \leq \pi/2$$

where $t_p$ = input signal duration. If we express $t_p$ as a fraction of the dispersion time T:

$$t_p = \alpha T$$

then the allowable chirp slope tolerance may be expressed as

$$\frac{\Delta\mu}{\mu} \leq \frac{1}{\alpha^2(T\Delta f)}$$

i.e., inversely proportional to the device time-bandwidth product, and to the square of the pulse duration. Figure 11 supports this. The three traces a) - c) are a result of varying the chirp slope by ±43% about the nominal value used in the center trace b). The pulse shapes are essentially identical, because the input pulse width were only 1 μsec ($\alpha$=0.05, so our allowed tolerance is $\Delta\mu/\mu \leq$ 167%). Traces d) to f) show the opposite extreme: the effective input pulse width is now equal to the entire dispersion time of the device ($\alpha$=1, so the allowable $\Delta\mu/\mu \leq$ 0.4%); a chirp slope variation of ±5.5% distorts the spectrum beyond all recognition.

Finally, the effects of a non-linear chirp slope in the pre-multiplying chirp are shown in Figure 12. The same experimental set-up as Figure 9b) was used, but the VCO was driven with a sine wave instead of a triangle wave. By adjusting the amplitude and frequency of the sine wave, as well as the triggering of the pulse generator, it was possible to generate a chirp whose average slope was equal and opposite to that of the RAC, but whose frequency vs. time chracteristics had varying degrees of nonlinearity. In Figure 12a) - c), the amplitude and frequency of the sine wave driving the VCO was adjusted so that

PHOTOS a) - c) HAVE 1 μsec
PULSE (α = 0.05) INTO
RAYTHEON 60 MHz RAC



UPPER TRACES:  RAC OUTPUT
   1.5 MHz DIVISION

LOWER TRACES:  RAC OUTPUT
      5 μsec DIVISION

a) PRE-MULTIPLY CHIRP SLOPE
   MISMATCHED - 43%

b) PRE-MULTIPLY CHIRP SLOPE
   MATCHED TO RAC

c) PRE-MULTIPLY CHIRP SLOPE
   MISMATCHED + 43%
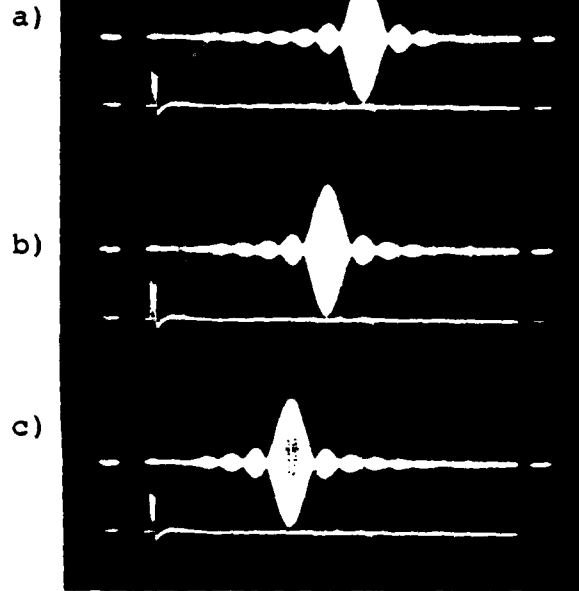
PHOTOS d) - e)
20 μsec PULSE INTO RAC
(α = 1.0)



d) PRE-MULTIPLY CHIRP SLOPE
   MISMATCHED - 5.5%

e) PRE-MULTIPLY CHIRP SLOPE
   MATCHED TO RAC DEVICE

f) PRE-MULTIPLY CHIRP SLOPE
   MISMATCHED + 5.5%
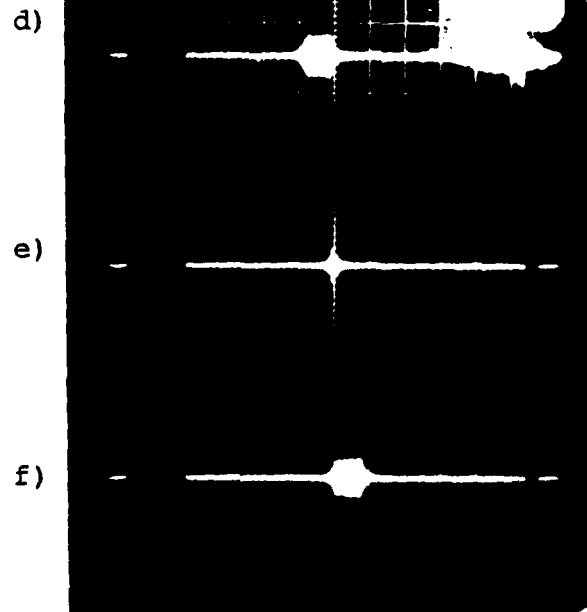
Figure 11.   Effects of chirp slope mismatch between pre-multiply
             chirp and RAC device.

122

a) X-Y TRACE; HORIZONTAL AXIS
IS SINE WAVE SHICH SWEEPS VCO
(AMPLITUDE 10 DIVISIONS)
VERTICAL AXIS IS RAC OUTPUT.
CHIRP SLOPE MATCH OCCURS ON
LINEAR PORTION OF ARM CURVE,
1.8 DIVISIONS FROM ZERO
CROSSING.

b) CLOSEUP OF CORRELATION PEAK
ON NORMAL TIME SWEEP (0.2 μsec/
DIV). SHOWS SYMMETRICAL SHAPE.

c) FURTHER CLOSEUP OF CORRELATION
PEAK: 0.1 μsec/DIV.
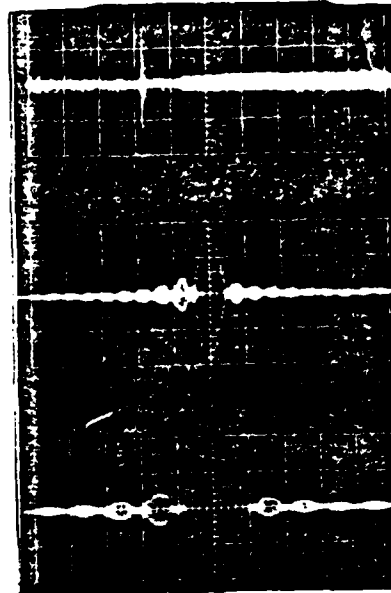
d) X-Y TRACE AS IN a) ABOVE:
CHIRP SLOPE MATCH MADE TO
OCCUR CLOSE TO PEAK OF SINE
CURVE, INTRODUCING MORE NON-
LINEARITY IN PRE-MULTIPLY CHIRP.

e) CLOSEUP OF CORRELATION PEAK
ON NORMAL TIME SWEEP (0.5 μsec/
CM). DISTORTION OF CORRELATION
PEAK DUE TO NONLINEAR PRE-
MULTIPLY CHIRP IS EVIDENT.

f) COMPARISON OF SINE WAVE VCO
INPUT (UPPER TRACE) TO RAC
OUTPUT (LOWER TRACE) SHOWS
POSITION OF CHIRP SLOPE MATCH
ALONG SINE CURVE.
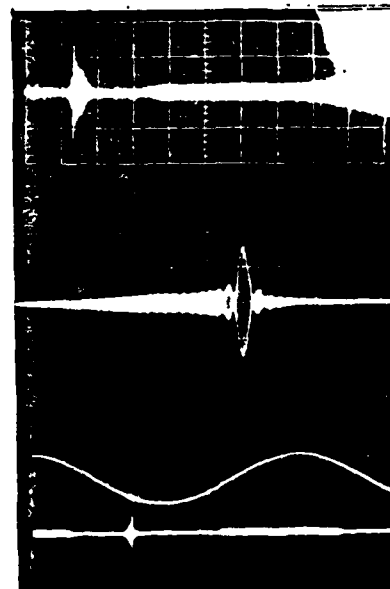


Figure 12.  Effected chirp slope nonlinearity in pre-multiply
chirp.  VCO in Fig. 9b) driven by sine wave, whose
amplitude and frequency are adjusted to match aver-
age slope of chirp to that of RAC at different
positions on sine curve.

sine wave had the proper slope close to its zero crossing,
where the sine wave is most linear.  The pulse generator was
made to trigger when the sine wave was in that vicinity; the
signal which passed through the mixers was thus a brief chirp
whose frequency slope was fairly linear.  The output of the
RAC, shown in Figure 12a) - c), is very much like a sin (x)/x.
In Figure 12d) - f), the sine wave driving the VCO was adjusted
to have the proper average slope closer to its negative peak,
where the sine curve is more nonlinear.  When the resulting
chirp is passed through the RAC, the output pulse is highly
asymmetrical and distorted.

### Experiments at 35 GHz

Our original intention was to develop an optical hetero-
dyne system to test a 1220 μm $^{13}CH_3F$ laser (245 GHz).  For the
local oscillator, the seventh harmonic of a 35 GHz stabilized
klystron was to be used.  Time did not permit us to complete
the 245 GHz system, but were able to simulate the features of
such a system by pulsing a 35 GHz klystron on and off, mixing
its output pulse with the output of a frequency-stabilized
klystron local oscillator, and spectrum-analyzing the resultant
IF pulses.

The local oscillator was stabilized by a frequency-lock
loop arrangement incorporating a Pounds discriminator[9] and an
electronics package graciously loaned to us by Micro-Now, Inc.
of Chicago.  The arrangement is shown in Figure 13.

124
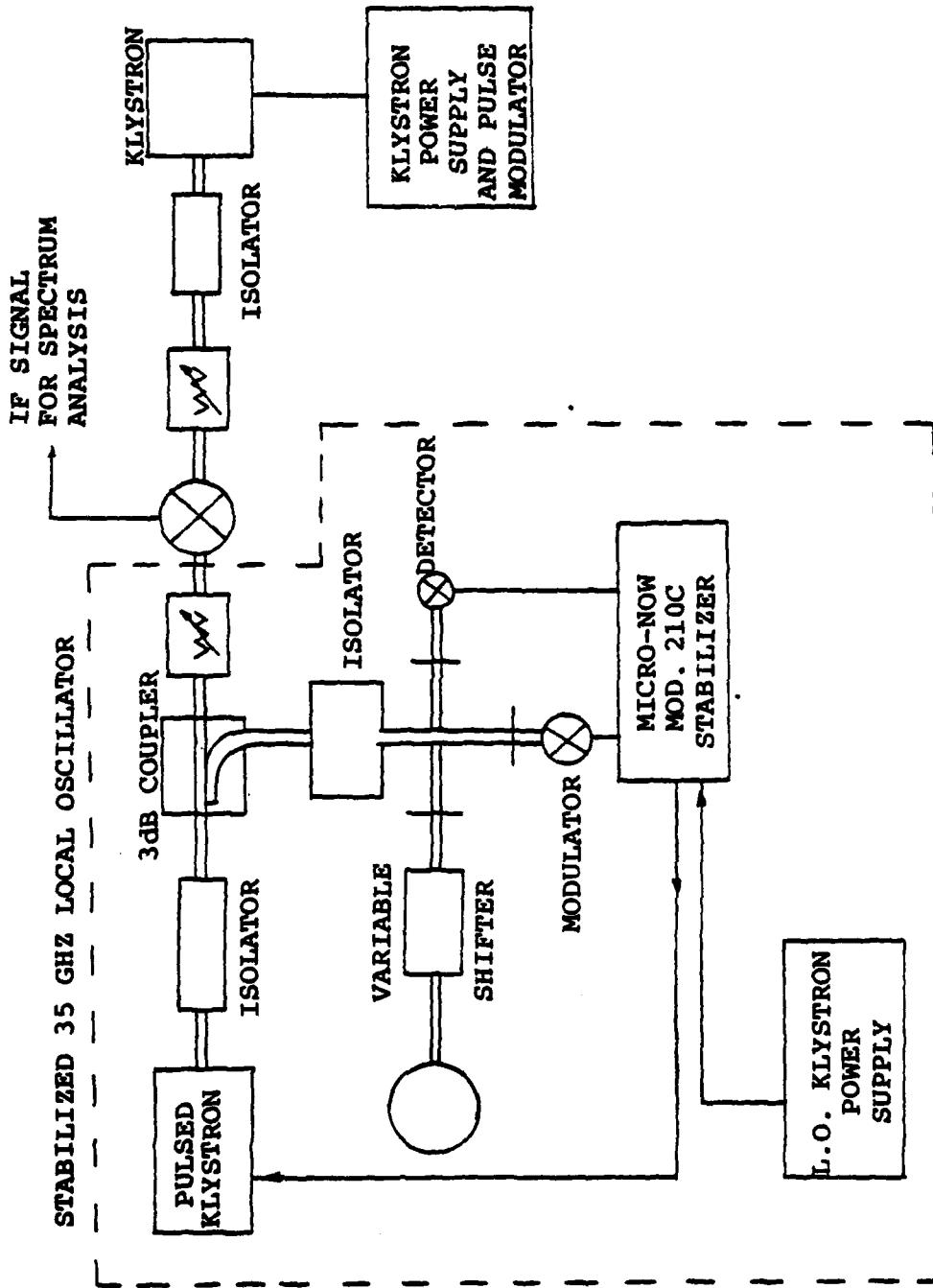


Figure 13. Block diagram of 35 GHz experiments.

Several points should be stressed about these experiments.
Firstly, although the L.O. klystron was stabilized, the pulsed
klystron was not.  In addition to being pulsed on and off, the
original klystron was also subject to whatever random frequency
fluctuations might occur in an unstabilized oscillator.  One
source of instability became evident immediately:  a very small
amount of remanent 60 Hz ripple was found on the klystron re-
peller supply voltage:  0.4V peak to peak out of a DC value
of 2000V, or 0.02%.  This small voltage was enough to cause
several MHz of FM on the signal klystron, which was clearly
visible with the high-resolution 60 MHz Raytheon RAC, as will
be shown.

This posed no major problems for a SAW chirp transform
spectrum analyzer, though, since the 60 Hz ripple just caused
the output spectra of the klystron pulses to jitter a few MHz.
The single shot ability of this transform technique enabled
clear spectra to be obtained merely by photographing single
oscilloscope traces.  Other spectral analysis techniques based
on averaging many pulses together would have had trouble here.

Another point to be mentioned here is that for most of this
series of photographs, an envelope detector was used.  This
tends to produce cleaner looking traces, but the non-linearity
of the detector diode makes the spectrum sidelobes appear smaller
than they really are.

126

A third point is that for most of these photos, the signal
klystron was pulsed on for about 10 μsec, very much longer
than the Fresnel mode pulse width limits for this device.  We
could have looked at the spectrum of the entire pulse by pre-
multiplying the IF with a chirp of the proper slope.  In fact,
we could obtain the effect of that multiplication essentially
for free, merely by sweeping the L.O. klystron at the correct
rate.

However, by simply passing the long IF pulse through a
gating mixer before the RAC, it becomes very easy to look at
the spectrum of a <u>small piece</u> of the signal pulse.  By moving
the gating window around in the IF pulse, <u>one can see how stable</u>
<u>the frequency is as the pulse evolves in time</u>:  whether it chirps
during the turn-on and turn-off transients, whether there may be
several distinct stages of the original pulse, that might be
evident only by looking at its frequency evolution.

That is what was done in this experiment.  The klystron was
pulsed on for 10 μsec, and the IF pulse from the microwave mixer
was further gated with a 2 μsec window which could be moved
anywhere in the pulse.

When the grating window was placed in the center of the 10
μsec klystron pulse, and the oscilloscope was triggered repe-
tively so that the pulse-to-pulse jitter could be seen, traces
like those shown in Figure 14 were obtained.  The lower trace
shows the input pulse to the RAC while the upper trace shows

the RAC output after envelope detection.  Horizontal time
scale is 5 μsec/division, or 1.5 MHz per division in the spec-
tral display.  The pulse frequencies seem to be varying within
a range of ±1.5 MHz, due to the aforementioned 60 Hz ripple
on the klystron repeller.  Changing the oscilloscope triggering,
so that only one trace is photographed, results in the clean-
looking spectra shown in Figure 15.  The sin(x)/x character
evident in these traces is what we would expect for the spectrum
of a 2 μsec rectangular piece gated out of the center of the
10 μsec klystron pulse.

If we move the gating window around in the pulse, we find
that the spectra obtained are of the same form everywhere but
at the very leading edge.  Spectra of the first 2 μsec of the
klystron pulse are shown in Figure 16; now the spectrum is
highly unsymmetrical, due to chirping of the klystron during
this time interval.  The upper traces of the figure shows 10x
expansion of the input pulse to the RAC.  The envelope of this
section of the pulse is closer to rectangular in shape than its
spectrum would suggest, indicating that an appreciable amount
of FM-ing must be occurring within the pulse as well.

Figure 17 shows portions of the spectra obtained when the
klystron is only pulsed on for 1 μsec.  The full spectrum of
this pulse is wider than the 6 MHz bandwidth of the particular
RAC, so not all of it is seen in one trace.  The upper trace
shows some of the lower sidelobes and the majority of the main

128

Figure 14.
LOWER TRACE: 2 μsec CENTER
SEGMENT GATED OUT OF A LONG
KLYSTRON PULSE. HORIZONTAL
SCALE 5 μsec/DIV.
UPPER TRACE: MULTIPLE EXPOSURE
OF SPECTRA OF PULSE SEGMENTS.
HORIZONTAL SCALE 1.5 MHz/DIV.
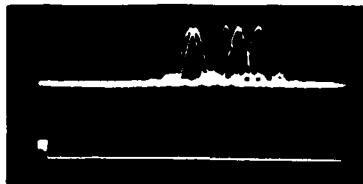


Figure 15.
SINGLE EXPOSURE OF FIGURE 13
DATA.



a)
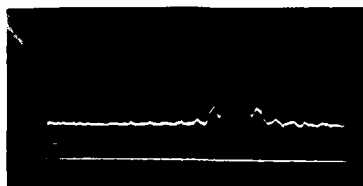
Figure 16.

a) 10x EXPANDED TRACE OF FIRST
   2 μsec SEGMENT OF LONG
   KLYSTRON PULSE.

b) SPECTRUM OF a).
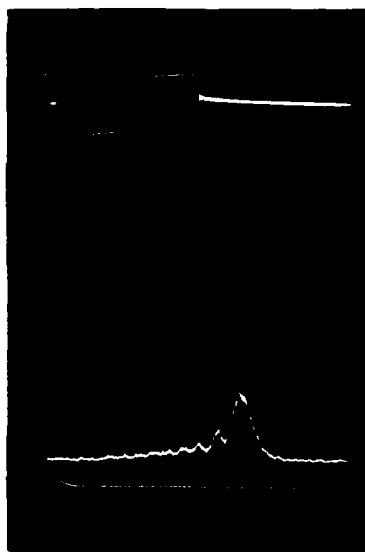
b)
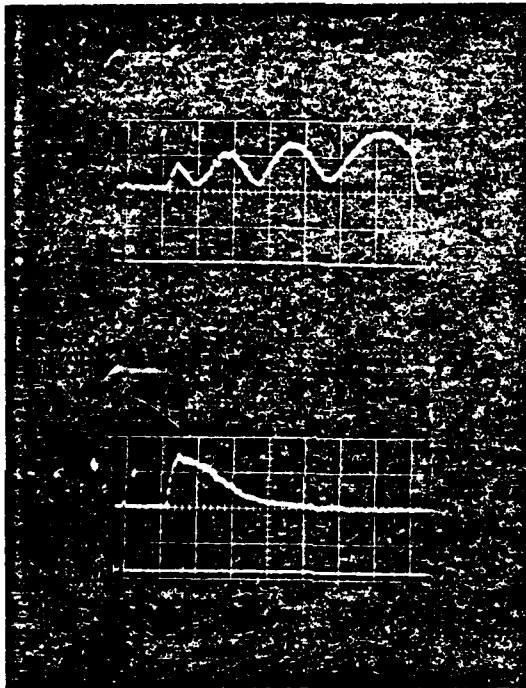
Figure 17. Different segments of the spectra of a 1.0 μsec klystron pulse. Rightmost lobe of upper trace is main lobe of spectrum. Lower trace shows upper hald of main lobe; note absence of upper sidelobes of spectrum, similarity of shape to trace in Figure 15b).

129

130

lobe of the spectrum.  The lower trace shows half of the main

lobe, and the fact that there are no upper sidelobes.  The

shape of this spectrum is therefore very similar to that of

the first two microseconds of the longer klystron pulse.  This

short klystron pulse is essentially all transient.


## References

1.  H. R. Fetterman, et al., "Real-Time Spectral Analysis of
    Far-Infrared Laser Pulses Using a SAW Dispersive Delay Line",
    Appl. Phys. Lett. 34, 123 (1979).

2.  See, for example, A. Yariv, Quantum Electronics, Second
    Edition, (Wiley, New York, 1975) chapter 18.

3.  "Spectrum Analysis ... Pulsed RF", Application Note 150-2,
    Hewlett-Packard Corporation, 1971.

4.  R. C. Williamson and H. I. Smith, "The Use of Surface Elastic
    Wave Reflection Gratings in Large Time Bandwidth Pulse Com-
    pressor Filters", IEEE Trans., MTT-21, 195 (1973).

5.  D. R. Arnesault and P. Das, "SAW Fresnel Transform Devices
    and Their Applications, 1977 IEEE Ultrasonics Symposium
    Proceedings, IEEE Cat. # 77CH1264-1SU, p. 969.

6.  G. R. Nudd and O. W. Otto, "Chirp Signal Processing Using
    Acoustic Surface Wave Filters", 1975 IEEE Ultrasonics
    Symposium Proceedings, IEEE Cat. 3 75 CHO 994-4SU, p. 350.

7.  O. W. Otto, "The Chirp Transform Signal Processor", 1976
    IEEE Ultrasonics Symposium Proceedings, IEEE Cat. # 76 CH
    1120-5SU.

8.  R. C. Williamson, "Reflection Grating Filters" in Surface
    Wave Filters, H. Matthews, ed., (Wiley, NY, 1977), p. 436.

9.  R. V. Pound, "Electronic Frequency Stabilization of Micro-
    wave Oscillators", Rev. Sci. Instru., 17, 490 (1946).

VII.  PERSONNEL ASSOCIATED WITH GRANT AFOSR 76-2988

| | Percent of Time | | |
|---|---|---|---|
| Paul D. Coleman, Professor<br>  Principle Investigator | 10% | 1 February 1976 -<br>15 January  1980 | |
| E. J. Danielewicz<br>  Research Assistant | 50% | 1 February 1976 -<br>20 August    1976 | |
| E. G. Malk<br>  Research Assistant | 50% | 1 February 1976 -<br>5 January   1980 | |
| R. Ziolkowski<br>  Research Assistant | 50% | 1 February 1976 -<br>20 July      1976 | |
| D. Parsons<br>  Visiting Ass't Professor | 50% | 1 June      1977 -<br>30 July      1977 | |
| William Lee<br>  Research Assistant | 50% | 21 May       1976 -<br>5 January   1980 | |
| Joseph Niesen<br>  Research Assistant | 50% | 23 August    1976 -<br>20 September 1977 | |
| | 17% | 21 August    1977 -<br>20 May       1978 | |
| John Leap<br>  Research Assistant | 50% | 1 October   1977 -<br>20 April     1978 | |
| Raymond Chu<br>  Research Assistant | 50% | 21 March     1977 -<br>20 July      1977 | |
| Robert Miller<br>  Research Assistant | 25% | 6 January   1979 -<br>20 May       1979 | |
| | 50% | 21 August    1979 -<br>5 January   1980 | |
| David Kim<br>  Research Assistant | 50% | 21 April     1978 -<br>30 December  1979 | |
| Jimmie Smith<br>  Secretary | 25% | 1 February 1976 -<br>15 January  1980 | |
| Donald S. Fulton<br>  Electronics Technician | 25% | 1 February 1976 -<br>20 May       1979 | |

132

## VIII.  MANUSCRIPTS

1.  E. J. Danielewicz, et al., "Hybrid Output Mirror for Optically Pumped Far IR Laser", Opt. Comm., 13, 366 (1975).

2.  E. J. Danielewicz, et al., "Continuous-Wave $CH_3F$ Waveguide Laser at 496 μm:  Theory and Experiment", IEEE J. Quan. Electron., QE-12, 40 (1976).

3.  E. J. Danielewicz, "Hybrid Metal Mesh-Dielectric Mirrors for Optically Pumped Far IR Lasers", Appl. Opt., 15 (1976).

4.  E. J. Danielewicz, et al.,"High Power Vibration-rotation Emission from $^{14}NH_3$ Optically Pumped Off Resonance", Appl. Phys. Lett., 29 (1976).

5.  E. J. Danielewicz, et al., "Assignments of the High Power Optically Pumped CW Laser Lines of $CH_3OH$", IEEE J. Quan. Electron., QE-13, 485 (1977).

6.  P. D. Coleman, "Present and Future Problems Concerning Lasers in the Far IR Spectral Region", J. Opt. Soc. Am., 67, 894 (1977).

7.  E. G. Malk, et al., "Laser Emission in the 83-223 μm Region from $PH_3$ with Laser Line Assignments", IEEE J. Quan. Electron QE-14, 544 (1978).

8.  W. Lee, et al., "Hot Band Lasing in $NH_3$", IEEE J. Quan. Electron., QE-15, 838 (1979).

9.  K. Kim, et al., "Stimulated Hyper-Raman Scattering in Molecular Lasers", IEEE J. Quan. Electron., QE-16, (1980).

10. K. Kim, et al., "Calculated-Experimental Evaluation of the Gain/Absorption Spectra of Several Optically Pumped $NH_3$ Systems", to be published in IEEE J. Quan. Electron., (1980).

## IX. TECHNICAL MEETING PAPERS

1. "Far IR Guided Wave Optics Experiments in Anisotropic Crystal Quartz Waveguides", Paper MC-2, Topical Meeting on Integrated Optics, Salt Lake City, Utah, January 12-14, 1976.

2. "Assignments of the High Power Optically Pumped CW Laser Lines of $CH_3OH$", Paper M-3-7, Second International Conference of Submillimeter Waves and Their Applications, San Juan, Puerto Rico, December 6-11, 1976.

3. "Present and Future Problems in the Far IR", Invited Paper M-I, Second International Conference on Submillimeter Waves and Their Applications, San Juan, Puerto Rico, December 6-11, 1976.

4. "Far IR Laser Technology", 6th ARPA Tri-Service Millimeter Wave Meeting, Harry Diamond Laboratories, Adelphi, Maryland, November 1977.

5. "Laser Emission in the 83-223 µm Region from $PH_3$ with Laser Line Assignments", Third International Conference on Submillimeter Waves, University of Surrey, Guildord, England, March 1978.

6. "Far Infrared/Submillimeter Wave Technology and Applications", SPIE Technical Symposium, Reston, Virginia, April 1977.

7. "Hyper-Raman Scattering and Related Phenomena", International Conference on Lasers '78, 93-98, Orlando, Florida, December 1978.

8. "A Comparison of the Calculated and Measured Raman and Laser Gain Spectra of Optically Pumped $NH_3$", K. Kim, et al., Paper S-1-9, Fourth International Conference on Infrared and Millimeter Waves, Miami Beach, Florida, December 10-15, 1979.

134

X.   THESIS

M.S. Theses

1.   "Superfluorescent Emission at 12.08 Microns and Off-Resonant
     Emission at 11.46 Microns in Ammonia Optically Pumed by a
     Transverse Excited Atmospheric Carbon Dioxide Laser", E. G.
     Malk, 1977.

2.   "A Phosphine Far Infrared Laser Optically Pumped by a $CO_2$
     TEA Laser", J. W. Niesen, 1978.


Ph.D. Theses

1.   "Far IR Guided Wave Optics Experiments Using a Waveguide
     Laser with a Hybrid Output Mirror", E. J. Danielewicz,
     1976.

2.   "Stimulated Raman and Hyper-Raman Scattering in the FIR
     Region", K. J. Kim, 1979.

3.   "Optically Pumped Frequency Stable Tunable Maser and Infra-
     red-Microwave Double-Resonance Experiments in Ammonia",
     E. G. Malk, 1980.

ILMED

∞